Shear Rheology of Cellulose Nanocrystal (CNC) Aqueous Suspensions

by

SADAF SHAFIEI SABET

B.Sc., Amirkabir University of Technology, Iran, 2005
M.Sc., Amirkabir University of Technology, Iran, 2007

A THESIS SUBMITTED IN PARTIAL FULFILLMENT OF
THE REQUIREMENTS FOR THE DEGREE OF

DOCTOR OF PHILOSOPHY

in

THE FACULTY OF GRADUATE AND POSTDOCTRAL STUDIES

(Chemical and Biological Engineering)

THE UNIVERSITY OF BRITISH COLUMBIA
(Vancouver)

December 2013

Abstract

Scientific and commercial interests in renewable nanomaterials have been receiving increasing attention over the years. Cellulose nanocrystal (CNC) derived from entirely renewable resources promises wide applicability owing to its high strength, chirality, self-assembly and electromagnetic properties. In this thesis the rheology of CNC aqueous suspensions was studied and the rheological behaviour was correlated with their microstructure. It has been found that the CNC aqueous suspensions experience two microstructural transitions by increasing CNC concentration: a transition from isotropic to chiral nematic liquid crystal occurs above a first critical concentration, and by further increasing concentration, the suspensions go through another transition from chiral nematic liquid crystal to gel above a second critical concentration. The viscosity profile of anisotropic suspensions shows a three-region behaviour characteristic of liquid crystals, and after gel formation a single shear thinning is observed over the whole investigated range.

CNC suspensions possessing a higher degree of sulfation have more tendency to form anisotropic chiral nematic structures, and form gels at relatively higher concentration compared to those with a lower degree of sulfation. Sonication up to 1000 J/g CNC, breaks all the aggregates in the system and significantly decreases the viscosity. Although the sonication-induced decrease in viscosity levels off through further sonication (>1000 J/g CNC), it still affects the viscosity of anisotropic suspensions at low shear rates by increasing the size of chiral nematic domains.

The effects of adding NaCl to CNC aqueous suspensions have been evaluated in different concentration regimes: isotropic, anisotropic chiral nematic, and gel. For isotropic samples and gels, the viscosity decreases by the addition of NaCl up to 5 mM. For anisotropic samples, on the other hand, the viscosity at low shear rates increases by addition of NaCl up to 5 mM due to decrease in chiral nematic domain size. However, at high shear rates, where all the domains are broken, the viscosity decreases when adding NaCl. Further addition of NaCl (>5 mM) results in extensive aggregation in suspension, and thus the viscosity increases.

Preface

Financial support for this work was provided by Natural Sciences and Engineering Research Council of Canada (NSERC) and FPInnovations. The CNC used for this research was kindly provided by FPInnovations.

The following journal papers and conference presentations have been published from the research work presented in this dissertation. I am the primary author and Professor Savvas G. Hatzikiriakos and Dr. Wadood Y. Hamad extensively helped with all the aspects of the research work.

Journal Papers

1. **S. Shafiei-Sabet**, W. Y. Hamad, S. G. Hatzikiriakos "Effects of Ionic Strength on Rheology and Microstructure of Cellulose Nanocrystal (CNC) Aqueous Suspensions" (in progress) (This paper is based on the data presented in Chapter 9 of this thesis.)

2. **S. Shafiei-Sabet**, W. Y. Hamad, S. G. Hatzikiriakos "Influence of Degree of Sulfation on the Rheology of Cellulose Nanocrystal Suspensions" Rheologica Acta (2013), 52, 741– 751. (This publication is based on the data discussed in Chapter 8 of this thesis.)

3. **S. Shafiei-Sabet**, W. Y. Hamad, S. G. Hatzikiriakos "Rheology of Nanocrystalline Cellulose Aqueous Suspensions" Langmuir (2012), 28 17124-17133. (This publication is based on part of the data discussed in Chapters 5, 6, and 7 of this thesis.)

Conference Presentations

1. **S. Shafiei-Sabet**, W. Y. Hamad, S. G. Hatzikiriakos “Effects of Degree of Sulfation and Ultrasound Treatment on Rheology and Microstruycture of Cellulose Nanocrystal (CNC) Aqueous Suspensions” The SOR 85th Annual Meeting October 13-17, 2013 Montreal, Quebec, Canada.

2. **S. Shafiei-Sabet**, W.Y. Hamad, S.G. Hatzikiriakos, “Effects of Temperature and Sonication on the Rheology and Microstructure of Cellulose Nanocrystal (CNC) Aqueous Suspensions” The SOR 84th Annual Meeting February 10-14, 2013 Pasadena, CA, USA.

3. **S. Shafiei-Sabet**, W.Y. Hamad, S.G. Hatzikiriakos, “Rheology and Microstructure of NCC Suspensions: Effect of Ultrasound Treatment” 62nd

Canadian Chemical Engineering Conference, October 14-17, 2012, Vancouver, BC, Canada.

4. **S. Shafiei-Sabet**, B. Derakhshandeh, W. Y. Hamad, S. G. Hatzikiriakos "The Rheology of Cellulose Suspensions: Nanocrystalline Cellulose (NCC) and Conventional Wood Pulp Fiber Suspensions" The 82nd Annual Meeting of Society of Rheology, October 24-28, 2010, Santa Fe, NM, USA.

Some data of this thesis work were also used in the following publications in which I am co-author and have performed the experiments regarding polarized optical microscopy and rheometry.

1. N. Noroozi, D. Grecov, **S. Shafiei-Sabet** "Estimation of Viscosity Coefficients and Rheological Functions of NanoCrystalline Cellulose Aqueous Suspensions" Liquid Crystals (2013) (DOI: 10.1080/02678292.2013.834081)

2. B. Derakhshandeh, **S. Shafiei-Sabet**, W. Y. Hamad, G. Petekidis, S. G. Hatzikiriakos "Ageing, Yielding and Rheology of Nanocrystalline Cellulose Suspensions" J. Rheol. (2013), 57, 131-148.

Table of Contents

List of Tables

List of Figures

List of symbols

D	Diameter of nanocrystal (nm)
D	Diffusion coefficient (m/s)
D_t	Translational diffusion coefficient (m/s)
E	Electric field strength (V/m)
G'	Storage modulus (Pa)
G"	Loss modulus (Pa)
K_B	Boltzman constant (m^2Kg/s^2K)
L	Length of nanocrystal (nm)
L/D	Aspect ratio of nanocrystal (-)
P	Pitch size of chiral nematic domain (nm)
T	Temperature (ºC)
v	Velocity (m/s)

Greek Letters

$\dot{\gamma}$	Shear rate (s^{-1})
φ	Particle concentration (vol. %)
ε_r	Dielectric constant of the dispersion medium (-)
ε_0	Permittivity of free space (C^2/Nm^2)
η	Shear viscosity (Pa.s)
η^*	Complex viscosity (Pa.s)
η_r	Relative viscosity (-)
μ_E	Electrophoretic mobility (μm cm/Vs)
ζ	Zeta-Potential (mV)
ω	Angular frequency (rad/s)

Abbreviations

AFM	Atomic force microscopy
BSKP	Black spruce kraft pulp
CNC	Cellulose nanocrystal

DI	De-ionized
DLS	Dynamic light scattering
POM	Polarized optical microscopy
TEM	Transmission electron microscopy

Acknowledgements

My utmost gratitude to my supervisor, Professor Savvas G. Hatzikiriakos, whose sincere support and constant encouragements I will never forget. Without his guidance, this work would never have been done.

It is my pleasure to acknowledge my co-supervisor, Dr. Wadood Y. Hamad, for all of the useful discussions, for his kindness and encouragement.

I gratefully acknowledge Professor Chad P.J. Bennington who passed away unexpectedly on February 14, 2010 for introducing me into the inspiring field of cellulose nanocrystals. He will always be in my thoughts and in my prayers.

I would like to acknowledge my supervisory committee members Professor Dana Grecov and Professor Mark Matrinez for their time and helpful comments.

Working in the Rheology Laboratory has been a privilege and I would like to thank all my past and present colleagues for making this lab an inspiring and enjoyable place to work. I also thank Siham Atifi from FPInnovations for training me in the production of cellulose nanocrystals.

FPInnovation is greatly appreciated for providing the cellulose nanocrystal samples used throughout this work.

I gratefully acknowledge the Natural Sciences and Engineering Research Council of Canada (NSERC) and FPInnovations for the financial support of this research.

From the bottom of my heart, I thank my dear friend Paria Parvizi for her endless emotional support, camaraderie and caring during all these years.

And finally, my most loving thanks to those who matter to me the most, my parents, Minoo and Kianoush, my sister, Sepideh, and my brother, Siavash.

This dissertation is dedicated to:

My parents, my sister and brother;

For their endless love, support and belief in me.

CHAPTER 1: INTRODUCTION

Cellulose is the main constituent in woody plants and the most renewable bioresource and thus development of advanced cellulosic materials is of great interest. In the biosynthesis of wood, intermolecular hydrogen bonds promote parallel association of the cellulose chains which results in substructures termed microfibrils. These primary fibril structures, with cross section dimensions around 2-5 nm (Jakob et al. 1995, Hult et al. 2001, Saito et al. 2007) make up the wall layers and finally, the whole cell wall of the cellulose fiber (see Figure 1-1). These microfibrils have high aspect ratio, and they consist of fully crystalline regions and amorphous less ordered regions.

Strong acid hydrolysis of cellulose fibers, extracts the highly crystalline parts, resulting in rod-like crystallites of colloidal dimension named cellulose nanocrystals (CNC) or nanocrystalline cellulose (NCC) (Marchessault et al. 1959, Marchessault et al. 1961, Revol et al. 1992). The hydrolysis conditions and cellulose source affect the surface chemistry and particle size of isolated cellulose nanocrystals (Dong et al. 1998). Sulfuric acid hydrolysis results in CNC particles with anionic sulfur groups on the surface, leading to electrostatically stabilized CNC aqueous suspensions (Marchessault et al. 1959, Marchessault et al. 1961; Revol et al. 1992, Revol et al. 1994, Dong et al. 1996).

Marchessault et al. (1959) showed that colloidal suspensions of cellulose nanocrystals exhibit nematic liquid crystalline alignment. Nematic ordering is the alignment of rod-like particles in the same direction along a director. Further, it has been found that CNC aqueous suspensions exhibit chiral nematic (cholesteric) ordering above a critical concentration (Revol et al. 1992, Revol et al. 1994, Revol and Marchessault 1994, Beck-Candanedo et al. 2005) and form birefringent gel at even higher concentrations (Liu et al. 2011, Urena-Benavides et al. 2011).

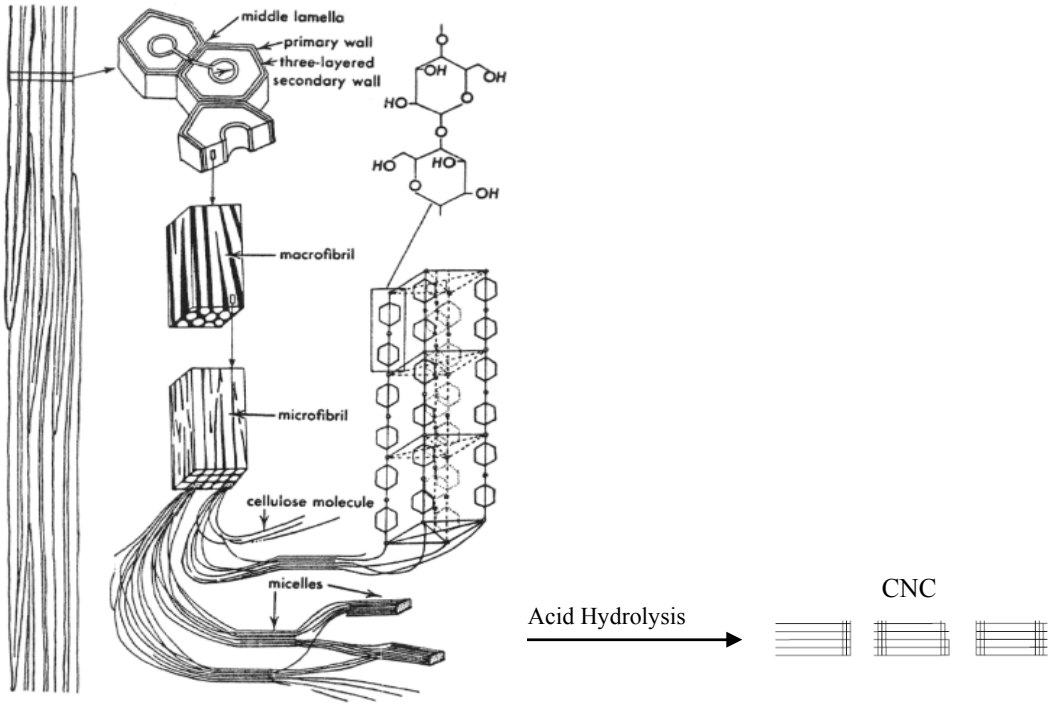

Figure 1-1: The ultrastructure of lignocellulosic fibres (adapted with permission from Hamad 2006)

Chiral nematic ordering, in simple terms can be described as the helicoidal stacking of nematic planes (Orts et al. 1998). Figure 1-2 shows the isotropic phase and the chiral nematic ordering schematically. Rods within a plane are aligned along a director, and these nematic planes are stacked in such way that the angle of the director in each subsequent plane is offset incrementally, which results in spiral staircase packing of nano-rods around a cholesteric axis.

The formation and characteristics of chiral nematic ordered domains in CNC aqueous suspensions is generally governed by basic properties of the nanoparticles, namely, physical dimension, size polydispersity, surface charge and the ionic strength of the system (Onsager 1949, Odjik 1986, Dong et al. 1998, Hamad and Hu 2010).

By casting CNC suspensions, the chiral nematic structure is reserved resulting in cellulose films with optical properties of chiral nematic liquid crystals. Possible applications for these films include optically variable films and ink pigments for security papers and cosmetics (Revol et al. 1998, Fleming et al. 2001). The optical properties of

these films are controlled by the cholesteric pitch size and are affected by CNC suspension concentration, sonication, shear and temperature (Dong et al. 1998, Revol et al. 1998, Pan et al. 2010, Beck et al. 2010).

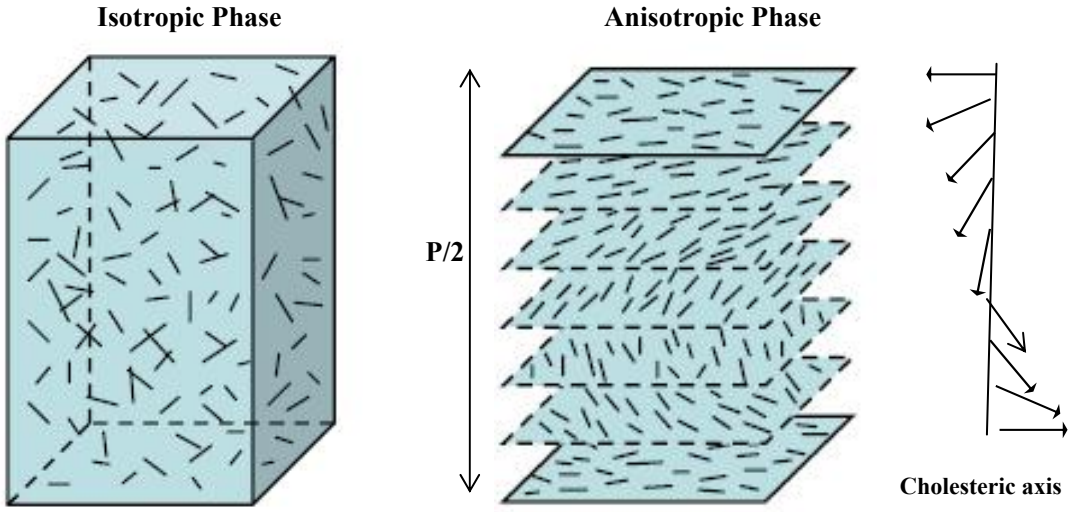

Figure 1-2: Schematic illustration of the isotropic and chiral nematic phase. There is a twisted stacking of nematic planes in a chiral nematic structure. P is the pitch size of a chiral nematic domain.

High aspect ratio (length/diameter), surface area, stiffness and strength are other characteristics of CNC particles, which make them suitable as high performance reinforcement in polymer composites (Favier et al. 1995, Dubief et al. 1999, Grunert et al. 2002, Azizi Samir et al. 2004, Ljungberg et al. 2005, Orts et al. 2005, Liu et al. 2010). Considering the fact that aqueous suspensions of CNC are highly shear sensitive fluids or gels, even at low concentrations, understanding the rheology will be critical for processing CNC suspensions in any application. Due to formation of liquid crystalline ordered domains in these systems, CNC suspensions have a complicated microstructure which controls the macroscopic flow behavior of the material and is sensitive to applied flow fields similar to other systems, such as rod-like virus suspensions (Lettinga et al 2005, Kang et al. 2006, Ripoll et al. 2008). Disruption of ordered domains significantly affects the rheological behaviour of CNC aqueous suspensions. In order to understand the

rheological behaviour of these suspensions, their ability to form an anisotropic phase should be taken into account.

Existing information on the relationship between the microstructure of CNC suspensions and their rheological properties are very limited. Orts et al. (1998) showed that by increasing the shear rate, CNC particles orient in the direction parallel to shear (Orts et al. 1998). A three-region viscosity behaviour, typical of liquid crystal polymer solutions, is observed for CNC suspensions with liquid crystalline structures, while the isotropic suspensions behave as conventional polymer solutions (Bercea and Navard 2000, De Souza Lima and Borsali 2004).

Given the critical role that CNC concentration plays in dictating the rheological response of its suspensions, in this thesis, the rheological properties of CNC suspensions at different concentrations (1 to 15 wt.%) have been studied at a fundamental level in order to gain an in-depth understanding of their behaviour. Using rheometry combined with polarized optical microscopy over a broad range of concentration enabled us to capture both microstructural transitions namely, isotropic to chiral nematic and chiral nematic liquid crystal to gel formation. We will show that the amount of applied ultrasound energy, temperature, degree of sulfation, and ionic strength significantly affect the microstructure of CNC suspensions and thus their rheological behaviour. This work ultimately aims to provide a deeper understanding of (i) the microstructural formation in CNC aqueous suspensions, and (ii) the inter-relationship of microstructure with rheological properties. This should help provide better decision-making for process design and optimization of CNC extraction and subsequent handling.

CHAPTER 2: LITERATURE REVIEW

2.1. Structure and chemistry of cellulosic fibres

The native cellulose molecule consists of linear glucan chains with repeating (1→4)-β-glucopyranose units. Cellobiose is the dimer of cellulose and the repeating unit of the cellulose polymer chain (see Figure 2-1).

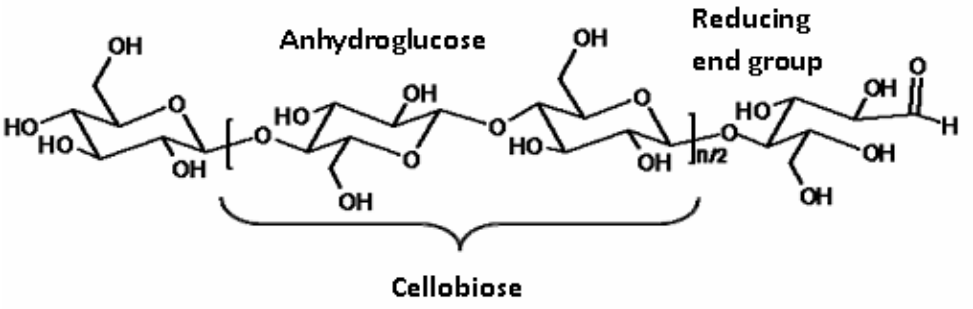

Figure 2-1: Structure of cellulose (reprinted from Kontturi et al. 2006 with permission of The Royal Society of Chemistry).

The degree of polymerization is determined by the number of single anhydroglucose units, and changes depending on the origin of cellulose. The complex supramolecular structure of cellulose has been the subject of debate for decades. Although four different polymorphs of cellulose are known, (cellulose I, II, III, and IV), in living plants cellulose occurs in fibres mostly in the crystalline form cellulose I and in less ordered amorphous regions (O'Sullivan 1997).

In the biosynthesis of wood, parallel association of cellulose chains results in substructures termed microfibrils. These fibrils have high aspect ratio, and consist of fully crystalline regions and less ordered amorphous regions. The smallest fibril unit has been shown to be 2-5 nm in diameter and up to a few micrometers in length (Jakob et al. 1995, Hult et al. 2001, Saito et al. 2007). The microfibrils aggregate further and form larger fibril bundles and finally the cellulosic fibres. Figure 2-2 shows the composition of wood cell wall and a cellulose microfibril schematically.

The cell wall of wood fibres consists of cellulose microfibrils which are surrounded by an amorphous matrix of hemicelluloses and lignin. The cell wall can be divided into different layers: middle lamella, primary cell wall, secondary cell wall and warty layer. These layers differ from one another in terms of structure and chemical composition (Sjöström 1993). The middle lamella consists mainly of lignin. The primary wall consists mainly of amorphous hemicelluloses and lignin, but also some pectin, proteins and cellulose are present. The secondary wall which is further divided into S_1, S_2, and S_3 layers, contains most of the cellulose, especially in the S_2 layer. The warty layer is located in the inner surface of the cell wall in softwoods and in some hardwoods, and its chemical composition is still unknown.

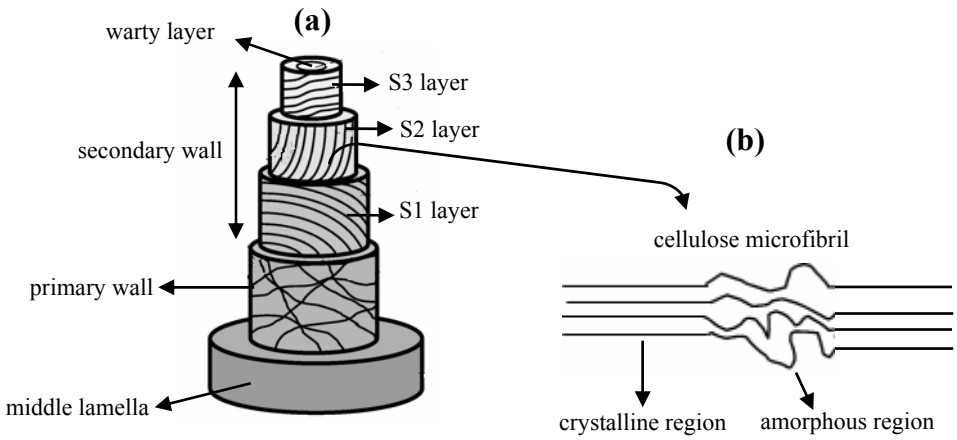

Figure 2-2: (a) Composition of the wood cell wall. The cell wall is divided into middle lamella, primary wall, secondary wall and watery layer. The secondary wall is further divided into S1, S2, and S3 layers. (b) A schematic illustration of a cellulose microfibril consisting of crystalline and amorphous regions.

2.2. Preparation and applications of cellulose nanocrystals (CNC)

As mentioned, a high aspect ratio (L/D ~ 20) and specific surface area (~400 m^2/g, measured and reported by FPInnovations) combined with high strength are characteristics of cellulose nanocrystals. Functional hydroxyl groups in cellulose also enable chemical modifications for further applications. These nanomaterials are biocompatible and non-toxic which makes them useful in biochemical and biomedical applications. All these

features provide them with high potential for different applications. The preparation and applications of cellulose nanocrystals are described in the following sections.

2.2.1. Preparation of CNC

Cellulose fibers can be disintegrated into substructures by strong acid hydrolysis. When native cellulose is treated with strong acids, the amorphous regions of cellulose microfibrils are preferentially attacked and the resulting material is a colloidal suspension of cellulose crystallites (Ranby 1951, Marchessault et al. 1959, Marchessault et al. 1961, Revol et al. 1992, Revol et al. 1994, Dong et al. 1996, Lima and Borsali 2004). These rod-like crystallites, termed cellulose nanocrystal (CNC), are shorter and stiffer than the native microfibrils and they are sometimes referred to as whiskers or nano-rods.

Hydrolysis with sulphuric acid is commonly used, and this results in particles with anionic sulfur ester groups on the surfaces, which leads to electrostatically stabilized CNC aqueous suspensions (Revol et al. 1992, Revol et al. 1994, Dong et al. 1996, Dong et al. 1998, Orts et al. 1998). Hydrochloric acid has also been used in the hydrolysis, resulting in nanocrystals with no surface charge, which therefore tend to aggregate (Wagberg et al. 1987, Araki et al. 1998, Araki et al. 2000).

In addition to wood fibres, cellulose nanocrystal suspensions have been prepared from many other cellulose sources, namely, cotton (Revol et al. 1994, Dong et al. 1996, Dong et al. 1998), bacterial cellulose (Araki and kuga 2001, Grunert and Winter 2002, Hirai et al. 2009) and sea animals (Heux et al. 2000, Azizi Samir et al. 2004).

Besides CNC, there are other cellulose nanomaterial such as microfibrillated cellulose (MFC) and cellulose nanofibrils (CNF). MFC is produced through homogenization process of wood pulp fiber (Turbak et al. 1983) and CNF is produced by a combination of enzymatic or chemical pre-treatment followed by mechanical disintegration of cellulosic fibers (Paakko et. al. 2007, Saito et al. 2007)

Having longer length, less crystallinity and thus more flexibility (lower rigidity), the properties of cellulose micro- or nano-fibrils differ greatly from those of CNC suspensions. MFC and CNF suspensions consist of interconnected cellulose fibrils and

form a gel like, highly viscous network at very low concentrations (i.e. 2 wt.% aqueous suspensions). The formation of anisotropic liquid crystalline phases is also a unique characteristic of CNC, which does not occur in the case of other cellulosic nanostructures such as MFC and CNF.

2.2.2. Effects of preparation condition

Preparation of cellulose nanocrystals is central to its further development and processing into high value-added materials. The preparation parameters affect the resulting nanocrystal properties (size, aspect ratio, degree of sulfation (surface charge), and the ability of formation of the chiral nematic liquid crystalline ordered phase) and thus their potential applications (Dong et al. 1998, Beck-Candanedo et al. 2005, Hamad and Hu 2010). The acid hydrolysis of wood fibers is a heterogeneous process which involves the penetration of acid into the cellulose fibers, and the subsequent cleavage of glycosidic bonds. These steps both depend on the acid species, acid concentration, time and temperature of the hydrolysis reaction, and possibly other factors. For instance, CNC can be produced using different acid species (sulphuric acid, hydrochloric acid and phosphoric acid) but only the suspensions hydrolysed by sulphuric acid are able to form a chiral nematic ordered phase above a critical concentration (Dong et al. 1998).

2.2.3. Applications of CNC

The cellulose nanocrystals are able to form chiral nematic liquid crystalline ordered phases in concentrated suspensions (Marchessault et al. 1959, Revol et al. 1992, Revol et al. 1994, Dong et al. 1996, Revol et al. 1997, Araki et al. 1998, Dong et al. 1998, Araki et al. 2000, Fleming et al. 2000, Lima and Borsali 2004). By casting films from CNC suspensions, cellulose films with the optical properties of chiral nematic liquid crystals can be prepared. Changing the hydrolysis condition (which affects the properties of resulted CNC), the salt content of the suspension, and the amount of applied ultrasound energy, the films can be tailored to give different colours of reflected light (iridescent films). These films can have important applications, such as security paper, including bank notes, passports, and certificates. They can also be used to produce novel pigments for optically variable coatings and inks, whose colours depend on the viewing angle

(Revol et al. 1998, Fleming et al. 2001). The CNC, due to its high strength and modulus, can be used as reinforcement in nanocomposites of various polymer matrices (Favier et al. 1995, Dubief et al. 1999, Grunert et al. 2002, Azizi Samir et al. 2004, Ljungberg et al. 2005, Orts et al. 2005). Other applications include pharmaceutical tablets and food production additives, such as stabilizers, texturing agents and fat replacers (Fleming et al. 2001). It is noteworthy that although cellulose nanocrystals have potential for many applications, the number of established commercial products is still very limited. Further research in this area and specifically understanding the rheology of this novel material could lead to introduction of new commercial applications for CNC in the near future, i.e. coating, composites, rheology modifier in food and gas industry.

2.3. Optical and orientation properties of CNC suspensions

Cellulose nanocrystals, being rigid rod-like particles, have a strong tendency to align along a vector director. As a result of the strong birefringence of the native cellulose, this rod alignment creates a macroscopic birefringence that can be directly observed through crossed polarizers. Marchessault et al. (1959) have observed and reported this birefringent character of the CNC suspensions for the first time. CNC particles in dilute suspensions (low concentration) are randomly oriented, forming an isotropic phase. As the concentration increases, for example by water evaporation, the suspension phase separates and an anisotropic phase is formed which is characterized by the self-orientation of the CNC rods in the same direction along a vector director, resulting in a nematic liquid crystalline alignment. By further increasing concentration, the suspension reaches a critical concentration at which the nanocrystals can form a chiral nematic ordered phase, displaying optical characteristics of a typical cholesteric liquid crystal (Marchessault et al. 1959, Marchessault et al. 1961, Revol et al. 1992, Revol et al. 1994, Dong et al. 1996). The chiral nematic ordering in CNC suspensions is due to the intrinsic chiral interaction between cellulose nanocrystals. Straley (1976) hypothesised that the source of this chiral interaction is directly attributed to the packing of screw-like rods. Orts et al. (1998), using small angle neutron scattering, found that the cellulose nano-rods pack tighter along the cholesteric axis than in the nematic planes perpendicular to it, which supports Straley's hypothesis. Figure 2-3 shows that threaded rods can be packed

more tightly when their main axes are offset such that their threads fit within the each others' grooves (Straley 1976).

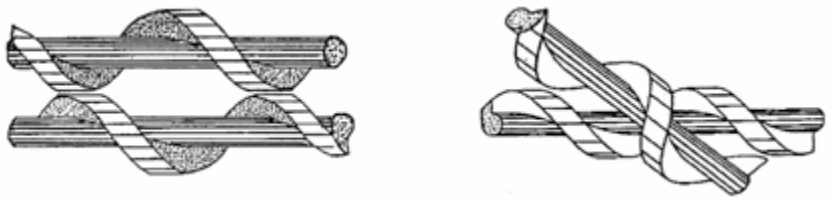

Figure 2-3: Representations of the tighter packing achievable by the chiral interaction of twisted rods. The upper rod can approach the lower one most closely when their principle axis are offset; thus they pack with the thread of one rod fitting into the groove of its neighbour instead of packing with axes parallel to each other (reprinted with permission from Straley 1976).

The pitch of chiral nematic structure, which is the distance required for the pseudo-layers to complete one full rotation, affects the optical properties. When the pitch is in the order of the wavelength of visible light it will reflect the polarized light (deVries 1951). The wavelength of this selectively reflected light changes with the viewing angle, leading to an iridescent appearance. It has been shown that these chiral nematic orders can be retained after evaporation of the solvent (generally water), leaving iridescent films (Revol et al. 1998, Pan et al. 2010). The pitch size, which controls the reflected colour, can be affected by concentration, temperature (Pan et al 2010), the ionic strength of the suspension (Revol et al. 1994, Dong et al. 1996, Dong and Gray 1997, Revol et al. 1998), ultrasound energy (sonication) (Beck et al. 2010) or applying an electromagnetic field (Nishio et al. 1998, Pan et al. 2010).

2.4. Phase separation properties of CNC suspensions

Pan et al. (2010) studied the chiral nematic phase formation of CNC films and the effects of different parameters on CNC ordering behaviour. Based on some previous studies on cellulose molecular structure (Witter et al. 2006) and chiral nematic phase formation (Orts et al. 1998, Lima and Borsali 2004), they have presented a structural model of CNC at the molecular, rod and liquid crystal level (see Figure 2-4).

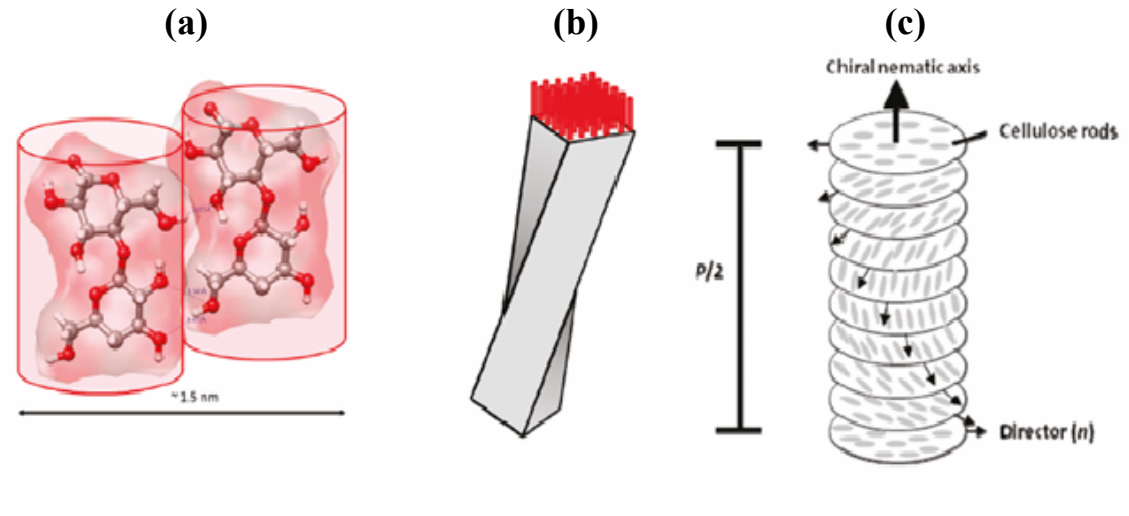

Figure 2-4: The three levels of structure in CNC films (reprinted with permission from Pan et al. 2010): (a) Model of two cellulose I chains in crystalline domains, based on the findings of Witter et al. (2006). (b) A cellulose nanocrystal (grey rod) which consists of a number of cellulose chains (shown in red). As reported by Orts et al. (1998) and by Lima and Borsali (2004), these rods are helically twisted along their length. (c) The rods come together in layers to form the chiral nematic phase of CNC.

Pan et al. 2010 examined the effects of ionic strength, temperature, suspension concentration and exposure to magnetic field on CNC at a molecular level as well as CNC at the chiral nematic phase level and showed that increasing electrolyte concentration (increasing ionic strength), as well as increasing temperature, will increase the critical concentration required for anisotropic phase formation which consequently leads to decreased pitch and volume fraction of the anisotropic phase in the biphasic cellulose suspension. On the other hand, increase in suspension concentration promotes the formation of a proportionately more anisotropic phase and as the volume fraction of the anisotropic phase increases, the pitch of the chiral nematic phase will also increase. They have also demonstrated that the chiral nematic pitch increases in the presence of a magnetic field and that the pitch increases with increasing exposure time (Pan et al. 2010). Their data supports the results of Dong et al. (1996) for CNC suspensions prepared from cotton filter paper, who showed that by increasing the ionic strength of the

system, the electrical double layers of the particles are suppressed and the chiral interaction becomes stronger, leading to an anisotropic phase with shorter pitch.

The phase separation and chiral nematic texture of cellulose nanocrystal suspensions for wood (Revol et al. 1992, Revol et al. 1994, Beck-Candanedo et al. 2005), cotton (Dong et al. 1996, Dong et al. 1998) and bacterial cellulose (Araki and Kuga 2001, Hirai et al. 2009) have been reported in the literature considering the effects of different parameters. Dong et al. (1996) studied the effects of the ionic strength on the isotropic to chiral nematic phase transition of suspensions of cotton cellulose nanocrystals; the volume fraction of the chiral nematic phase decreased from 0.56 to 0.05 as the concentration of the added electrolyte (HCl, NaCl, or KCl) increased from 0 to 2.4 mM. The presence of electrolyte decreased the chiral nematic pitch, due to reduction of effective diameter and apparent volume of the charged rods in the presence of salt, thus the chiral interaction becomes stronger; the stronger the interaction, the smaller the pitch. Araki and Kuga (2001) also reported a decreased in the volume of anisotropic phase for bacterial cellulose nanocrystals in the presence of an electrolyte (0 to 1.0 mM). A detailed examination of the phase separation behaviour of bacterial cellulose nanocrystals (L/D ~44-73) have been carried out by Hirai et al. (2009) who found that without NaCl addition the volume fraction of the chiral nematic phase increases with the total cellulose concentration. They also investigated the effects of added NaCl on the phase separation behaviour of aqueous suspensions of bacterial cellulose nanocrystal, discussing the changes in the liquid crystalline textures upon the addition of salt. By adding NaCl, the volume fraction of the chiral nematic phase decreased up to the addition of 1 mM NaCl and then increased. Hirai et al. (2009), using polarized microscopy, showed that the domain size of the anisotropic phase decreased with an increase in the NaCl concentration from 0 to 1 mM and the chiral nematic region vanished at 5.0 mM NaCl. Figure 2-5 shows the schematic illustration of the observed effects of added NaCl on the phase separation behaviour of the cellulose nanocrystal suspensions prepared from bacterial cellulose studied by Hirai et al. (2009).

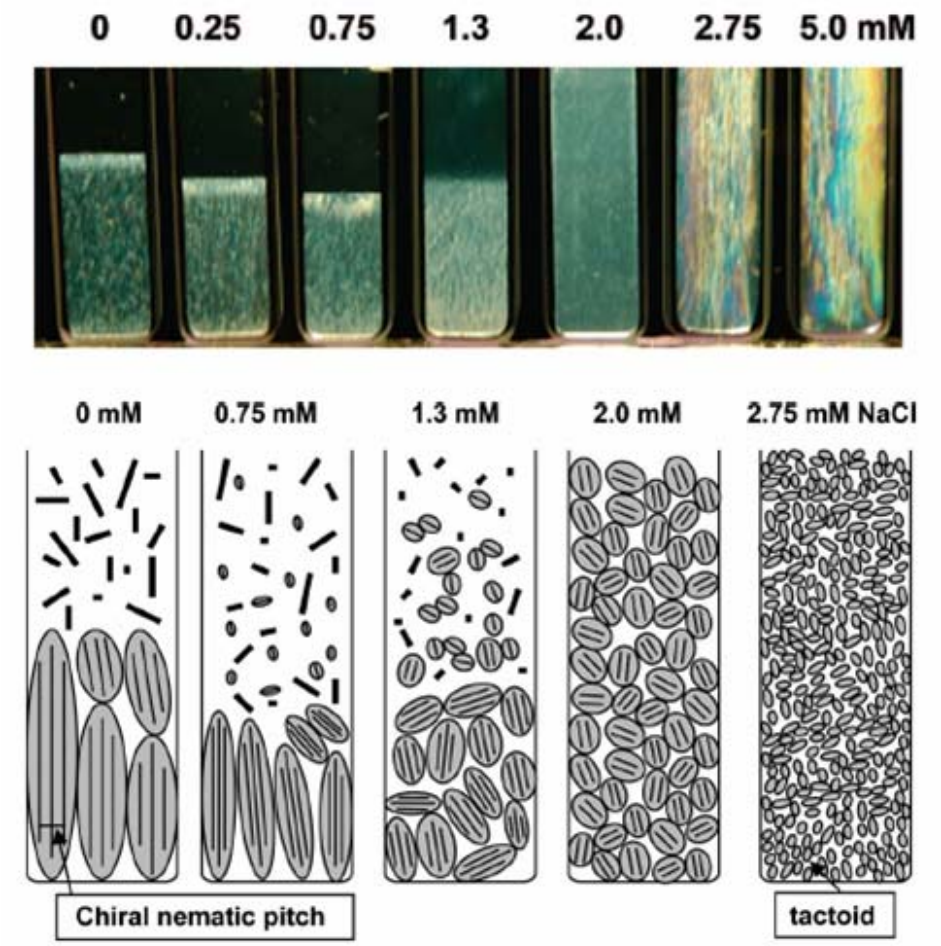

Figure 2-5: Effect of added NaCl on the phase separation behaviour of suspensions of CNC extracted from bacterial cellulose for a fixed total CNC concentration of 3 wt % after 25 days of standing (top) and schematic illustration of the effects of added NaCl on the phase separation behaviour of suspensions of CNC extracted from bacterial cellulose for a fixed CNC concentration (bottom) (reprinted with permission from Hirai et al. 2009).

Dong and Gray (1997) reported a detailed study on the effects of counter-ions (H_3O+, Na+, K+ and Cs+) on the phase separation and stability of suspensions of CNC isolated from Whatman No. 1 filter paper (with average L/D~16). They reported that chiral nematic phases formed for all the suspensions with different counter-ions, but the critical concentration for the anisotropic phase formation is different and depends on the counter-ion associated to the surface of cellulose nanocrystals. The change in volume fraction of

chiral nematic phase with concentration in the presence of different inorganic counter-ions are shown in Figure 2-6. As can be seen in Figure 2-6, the proportion of anisotropic chiral nematic phase decreases in the order H+ > Na+ > K+ > Cs+. The acid-form suspension has the greatest tendency to form ordered phase and thus, yields the highest volume of the anisotropic phase at any given total suspension concentration.

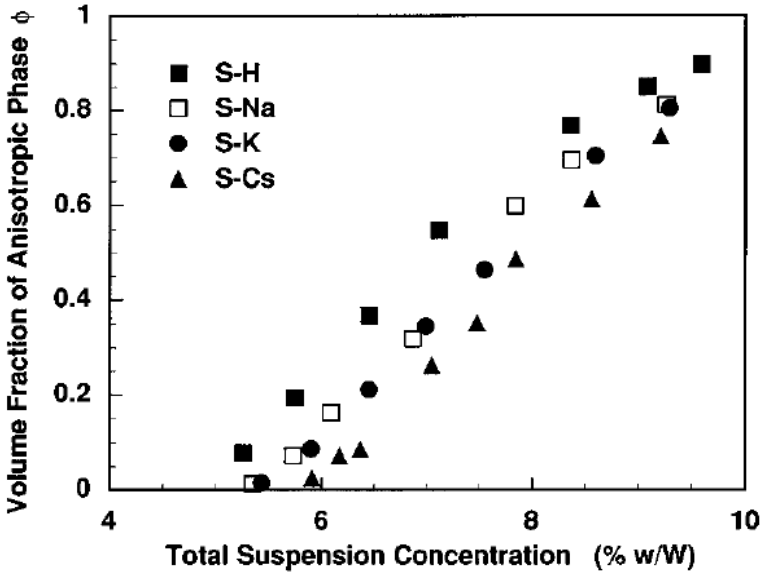

Figure 2-6: The relationship between the volume fraction of the anisotropic phase with the total CNC concentration in the suspension in the presence of different inorganic counter-ions (reprinted with permission from Dong and Gray 1997).

By measuring the translational diffusion coefficients (D_t) of suspensions with different counter-ions, they found that the effective particle size of the polyelectrolyte is reduced as the atomic number of the inorganic counter-ions increases. The diffusion coefficient increased in the order H+ <Na+ < K+ < Cs+, confirming that the hydrodynamic volume of the particles decreased from H+ to Cs+. The changes in mobility (change in D_t) for different counter-ions confirms the change in isotropic/anisotropic phase equilibrium observed in Figure 2-6. As the particle size decreases, their excluded volume is reduced, and a higher suspension concentration is required to form an ordered phase. The critical concentration should thus increase with the atomic number of the counter-ions.

Urena-Benavides et al. (2011) studied the phase behaviour of cellulose nanocrystals isolated from cellulose cotton powder (L/D ~ 12). Figure 2-7 shows the cross-polarized optical microscopy images of these suspensions at different concentrations. As can be seen in Figure 2-7, the suspensions are biphasic up to 10 vol.% and the fraction of liquid crystalline phase increases by concentration until it becomes entirely liquid crystalline at 12.1 vol.% (when a "fingerprint texture", characteristic of chiral nematic structure appears) and finally forms a gel at 14.5 vol.% (a random texture with bright colours).

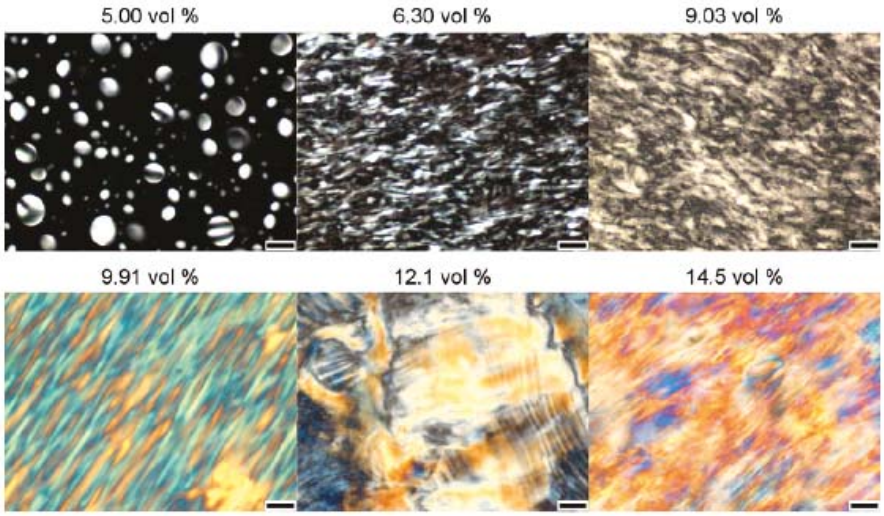

Figure 2-7: Polarized light microscopy of CNC suspensions of various concentrations at 25 ºC. Scale bars: 50 µm (reprinted with permission from Urena-Benedevise et al. 2011).

Urena-Benavides et al. (2011) reported the effects of temperature on the phase behaviour of CNC suspensions, showing that for biphasic CNC suspensions at a given concentration, by increasing temperature, the fraction of liquid crystal phase decreases at 40 ºC (see Figure 2-8). Dong and Gray (1997) had also reported a decrease in volume fraction of liquid crystalline phase by increasing temperature, especially near 40 ºC (see Figure 2-9).

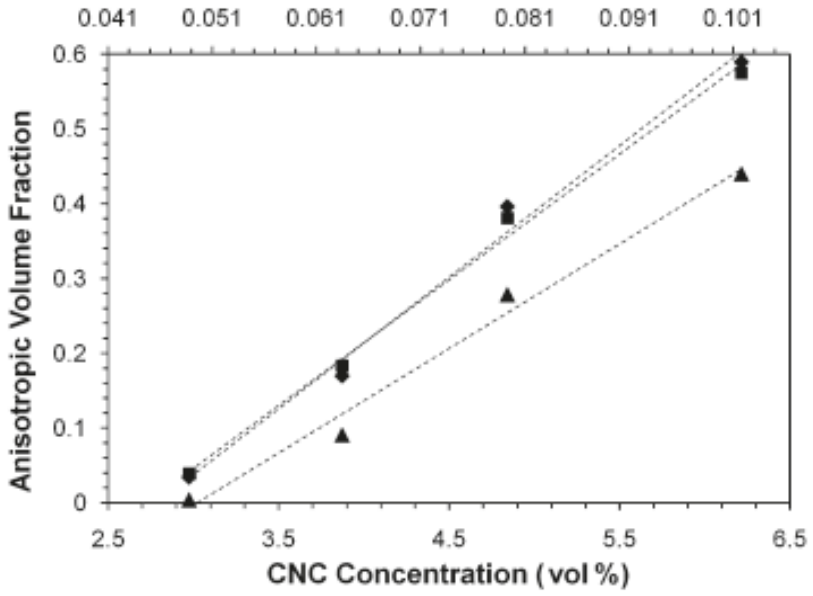

Figure 2-8: Amount of liquid crystalline (anisotropic) phase as a function of CNC concentration at 4ºC (diamonds), 20ºC (squares), and 45ºC (triangles) (reprinted with permission from Urena-Benedevise et al. 2011).

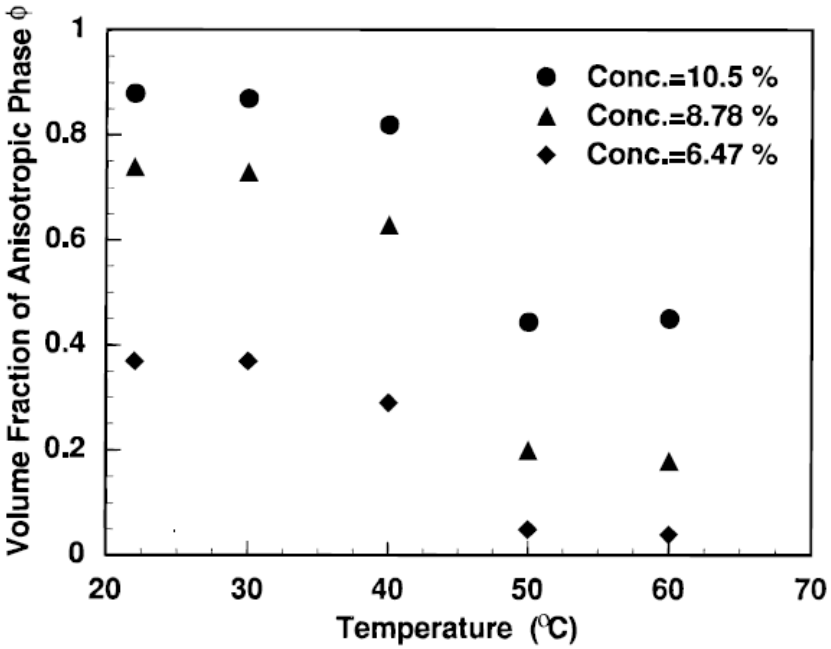

Figure 2-9: Volume fraction of anisotropic phase, ϕ, as a function of temperature for acid-form suspensions with concentrations as indicated in the figure (reprinted with permission from Dong and Gray 1997).

2.5. Rheological behaviour of CNC suspensions

As previously discussed, CNC suspensions are able to form ordered liquid crystalline phases. The alignment of these nano-rods is strongly influenced by the shear rate, which makes them good models to study the rheological behaviour and the ordering phenomenon in long rigid rods. Marchessault (1961) carried out the first investigation in this field, demonstrating that the hydrodynamic properties of the nanocrystals are directly related to the size and the length distributions of these particles in suspension. Onogi and Asada (1980) showed a typical rheological behaviour for liquid crystalline polymers in solutions for which the shear-dependent viscosity profile showed three distinct regions. The first one (region I) appears at low shear rates, which represents a constant decrease of viscosity. The second region (region II) appearing at intermediate shear rates, is characterized by a plateau. The third region (region III), appears at higher shear rates, which represents again a constant decrease of the viscosity. This behaviour is characteristic of liquid crystals and has rarely been observed in a single system, probably because of the limited experimentally accessible shear rate window (Lima and Borsali 2004). Using small angle neutron scattering (SANS), Orts et al. (1998) studied the liquid crystalline ordering of cellulose nanocrystals isolated from black spruce bleached Kraft pulp (with L/D ~30-45) and its effect on rheology. They have shown that there are three different regions in the shear-dependent viscosity profile. The first region was observed at very low shear rates and corresponds to the shear thinning, where the domains begin to flow. As the shear rate is increased the domains are broken up, inducing the existence of a plateau in the flow curve. At higher shear rates there is a further shear thinning with the alignment of individual rods. In other words, as shear disrupts the chiral nematic phase, nano-rods exhibit nematic ordering, with their axis aligned parallel to the flow direction. In this SANS investigation the most rapid ordering behaviour of the cellulose nanocrystals occurred in regime II, indicating that the order reaches a plateau in the shear-thinning regime (see Figure 2-10). To study the effect of particle size on the shear-induced orientation, Orts et al. (1998) plotted the order parameter, S, versus shear rate in the same figure (Figure 2-10), which shows that the longer rods reached higher order parameter due to having higher axial ratio, L/D. Figure 2-10 shows that there are correlations between the two parameters determined by the two very different techniques,

namely the viscosity, which reflects a bulk property of the system, and SANS, which measures order on the macromolecular/inter-particle scale.

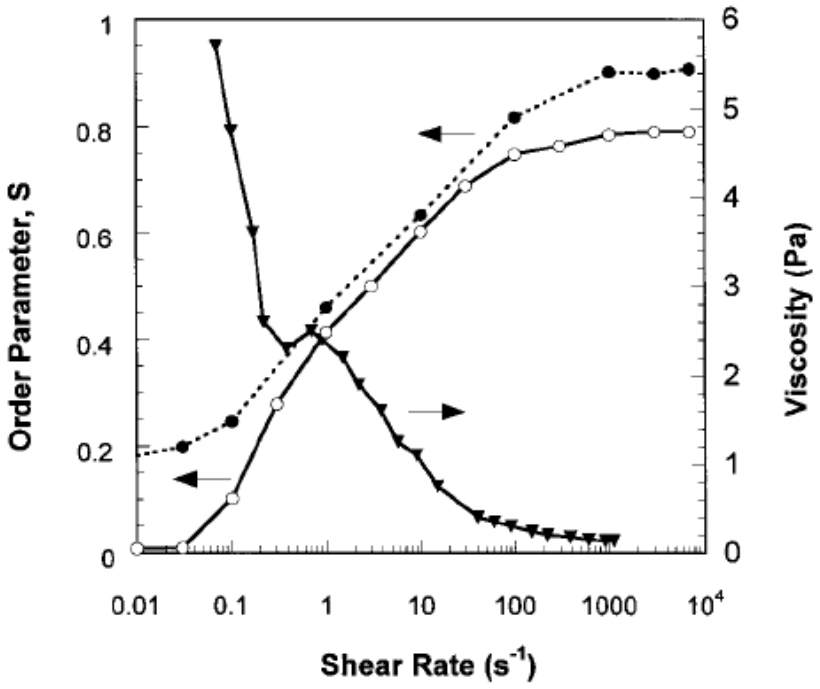

Figure 2-10: Shear rate dependence of the order parameter, S, for the cellulose nanocrystals of L= 280 nm (●) and L=180 nm (○), and the viscosity profile of the suspensions of nanocrystals with L=280 nm as a function of shear rate (▼) (reprinted with permission from Orts et al. 1998).

Lima and Borsali (2004) have obtained similar results on the cotton linter cellulose nanocrystals (L/D ~17). Figure 2-11 illustrates this behaviour, where three distinct regions can be observed. At low shear rates, one can observe the first shear thinning region (region I). At intermediate shear rates, the second region appears (region II), a plateau indicating that these domains are aligned in the flow direction. At higher shear rates, a second shear thinning region (region III) is observed, because of the breaking down of these domains giving rise to individual alignment of the nanocrystals.

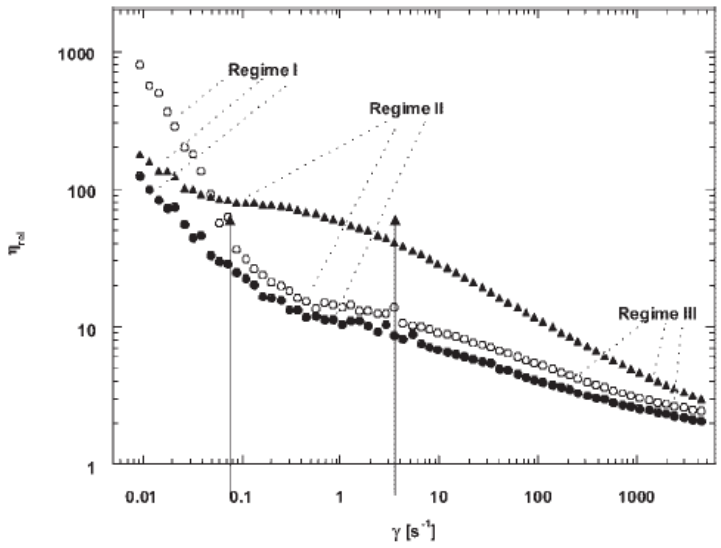

Figure 2-11: Relative viscosity versus shear rate for cellulose nanocrystals from cotton linter at concentrations of 1.2 wt% (●), 1.7 wt% (○), and 2.7 wt% (▲). Here the shear thinning region (regime I), a plateau (regime II) and a second shear thinning region (regime III) can be seen (reprinted with permission from Lima and Borsali 2004).

Bercea and Navard (2000) have studied the shear dynamics of aqueous suspensions of micrometer length CNC derived from tunicate (L/D ~140) at two different concentration regimes, isotropic-at-rest (0 to 0.85 wt.%, which comprises the dilute and semi-dilute regimes) and anisotropic-at-rest (1 to 3.5 wt.%, which is in the concentrated regime). Figure 2-12 shows the viscosity versus shear rate curves of both regimes.

The main characteristic of the isotropic-at-rest regime is that the viscosity versus shear rate curves have two plateaus, one at low shear rates and another one at high shear rates. The low shear rate plateau is the true Newtonian viscosity regime, where the rods keep a random orientation. The plateau at high shear rates indicates that the rods are oriented in a steady state manner. In other words, nanocrystals are well oriented in this region, where increase of shear rate does not change the mean rod orientation and thus does not change the viscosity.

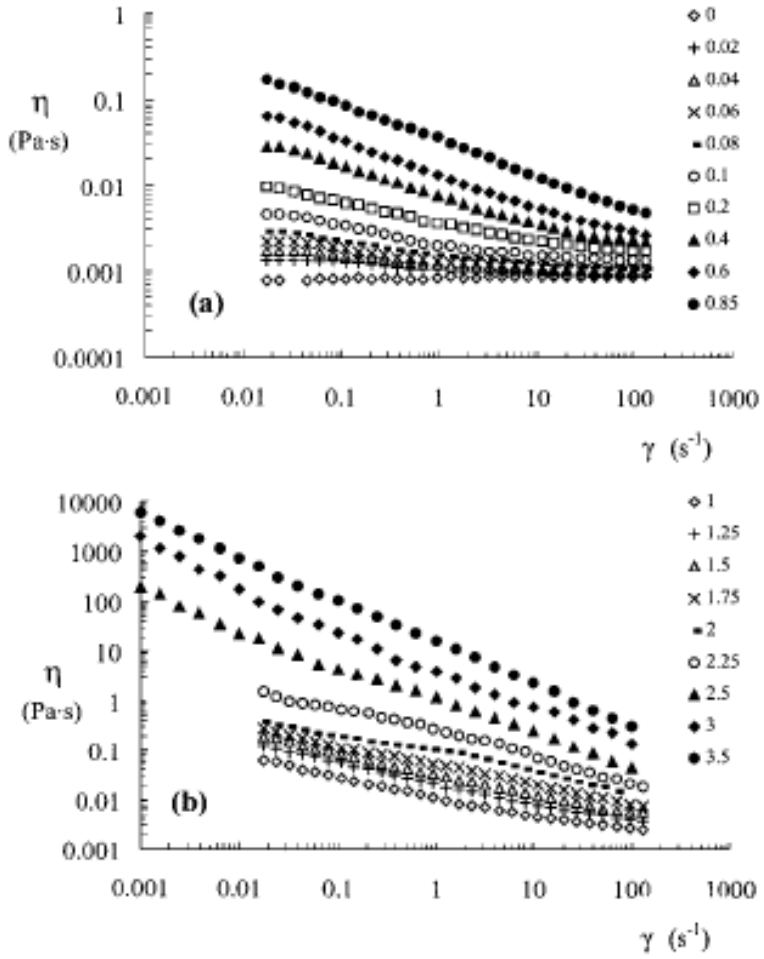

Figure 2-12: Viscosity versus shear rate for suspensions of cellulose nanocrystal derived from tunicate, at different concentrations (wt %) (reprinted with permission from Bercea and Navard 2000).

The concentration dependence of viscosity in these low and high shear rate plateaus is shown in Figure 2-13. The viscosity of the high shear rate plateau is linearly proportional to concentration and is much lower than the one for the Newtonian plateau. Orientation of the rods in the flow direction, as shown by neutron scattering (Orts et al. 1998), decreases the drag force and reduces the viscosity of the suspension at higher shear rates.

According to Figure 2-13, the suspensions are in the semi-dilute regime when studied at rest or below a shear rate lower than the inverse of the rotational relaxation time. The suspensions are in the dilute regime above a second critical shear rate, which marks the

beginning of the high shear rate plateau, since the interactions between oriented rods occur at a much higher concentration than when they are randomly oriented.

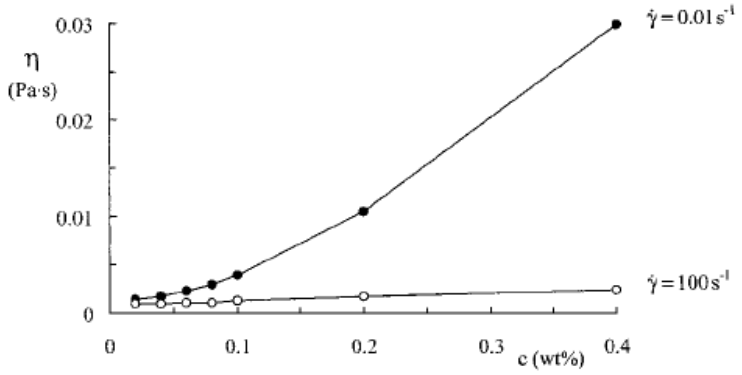

Figure 2-13: Viscosity as a function of rod concentration for shear rates of 0.01 and 100 s^{-1} (reprinted with permission from Bercea and Navard 2000).

On the other hand, suspensions in the anisotropic-at-rest regime (c >1 wt.%) show a plateau (or a weak shear thinning zone) surrounded by two shear thinning regions. This behaviour is characteristic of liquid crystal polymer solutions (Onogi and Asada 1980, Noel and Navard 1991). These suspensions also showe a sudden small reduction of viscosity upon the appearance of a liquid crystalline phase (at the critical concentration of transition) followed by a monotonic increase in viscosity with concentration (see Figure 2-14). Although this is the case for many polymeric lyotropic suspensions, where the low shear viscosity versus concentration goes through a maximum in the biphasic region, and the magnitude of this maximum decreases with increasing shear rate (Larson 1999), the steady shear viscosity does not go through a maximum with increasing concentration for some CNC (Urena-Benavides et al. 2011).

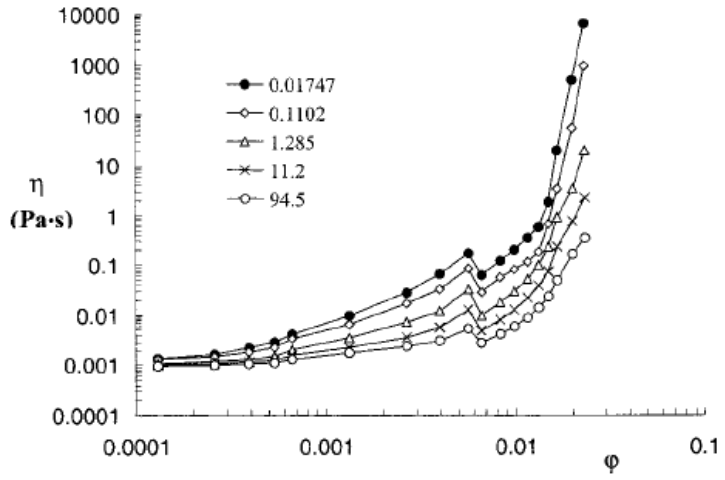

Figure 2-14: Viscosity, η, versus volume fraction, ϕ, at the indicated shear rates (s^{-1}) (reprinted with permission from Bercea and Navard 2000).

Araki et al. (1998) have comparatively studied H_2SO_4- and HCl-hydrolyzed CNC suspensions to investigate the effect of preparation method on the rheological behaviour of these suspensions. Although both H_2SO_4-hydrolyzed and HCl-hydrolyzed particles showed similar size and shape when observed under the electron microscope (Figure 2-15), the viscosity of H_2SO_4-hydrolyzed suspension showed no time dependence, while the HCl-hydrolyzed suspension was thixotropic at concentrations > 0.5 % (w/v) and anti-thixotropic at concentration < 0.3% (w/v) (see Figure 2-16).

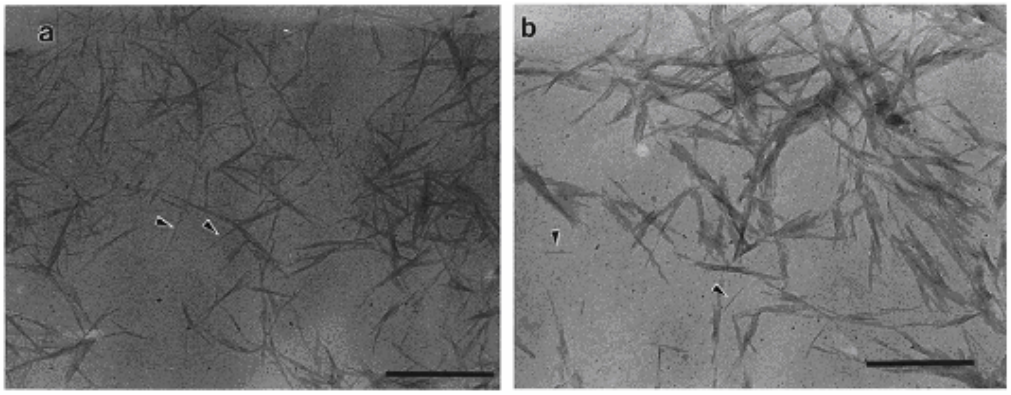

Figure 2-15: TEM micrographs of cellulose nanocrystals prepared by (a) H_2SO_4 and (b) HCl hydrolysis. Typical individual nanocrystals are shown by arrowheads. Scale bars show 500 nm (reprinted from Araki et al. 1998 with permission from Elsevier).

H_2SO_4 hydrolysis introduces sulfuric half-ester groups on the surface of cellulose nanocrystals that contribute to the electrostatic stability of the CNC colloidal suspension (Marchessault et al. 1959, Marchessault et al. 1961, Revol et al. 1992, Revol et al. 1994, Favier et al. 1995, Dong et al. 1996). In the case of HCl-hydrolyzed suspensions, due to lack of surface charge, there is a significant inter-particle aggregation which forms at static conditions and breaks under shear (Mewis and Spaull 1976, Mewis 1979). At very low concentration on the other hand, the inter particle distances are large so that the contribution of aggregation to thixotropy is reduced and the interaction between particles increases as shear aligns them, which results in anti-thixotropy behaviour observed for the low concentration suspensions (Araki et al. 1998). However, both suspensions showed shear thinning behaviour, which was steeper in the case of HCl-hydrolyzed sample because of breakdown of the flocculation.

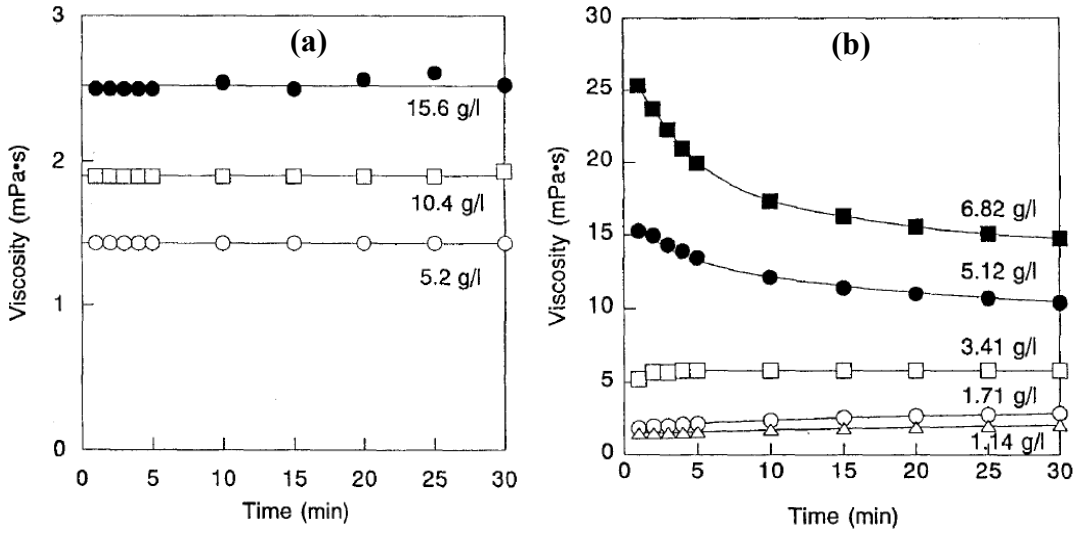

Figure 2-16: Time dependence of the viscosity of CNC suspensions prepared by H_2SO_4-hydrolysis (a), and HCl-hydrolysis (b) (reprinted from Araki et al. 1998 with permission from Elsevier).

Araki et al. (1998) also reported the relative viscosity, η_{rel} of H_2SO_4- and HCl-hydrolyzed CNC suspensions as a function of concentration, φ, and from the inclination of the curves and using Einstein's viscosity equation and Simha's formula, calculated the aspect ratio (L/D) of the samples:

$\eta_{rel} = 1+\varphi\nu$, Einstein's viscosity equation (Adamson 1990)

Where φ is particle concentration and ν is the coefficient which can be calculated by

$$\nu = \frac{(L/D)^2}{15(\log 2(L/D) - 3/2)} + \frac{(L/D)^2}{5(\log 2(L/D) - 1/2)} + \frac{14}{15} \quad \text{(Simha 1940)}$$

The estimated L/D was in good agreement with the axial ratio obtained from TEM micrographs for H_2SO_4-hydrolyzed samples, but not for HCl-hydrolyzed ones, which they argued as the anomalous viscosity behaviour of the latter due to flocculation.

Recently, Boluk et al. (2011) measured the intrinsic viscosity for CNC suspensions to characterize the shape factor (L/D) of CNC particles by correcting the contribution of the effects of electro-viscous interactions for the first time. The calculated shape parameter (L/D ~41) was verified by using AFM and dynamic light scattering (DLS). The shape parameter that resulted from AFM was 30±14.

Figure 2-17 shows the viscosity of CNC suspensions prepared from commercial softwood, at different concentrations, reported by Boluk et al (2011), where shear thinning non-Newtonian behaviour was only observed for the sample with the highest concentration (1 g/dl). They also investigated the effect of NaCl electrolyte concentration and the resulting double layer interactions in CNC suspensions on the low-shear viscosity. Figure 2-18 shows the decrease in viscosity due to addition of an electrolyte to the system.

Other studies also showed that the low-shear viscosity of charged particles are higher than those of un-charged ones, as a result of electro-viscous effects (Russel 1978, Wierenga and Philipse 1997). When the charged Brownian particles are sheared, the deformation of the double layer around the particles, and also the overlapping of double layers under the shear flow, contribute to the low-shear rate viscosity (Conway and Dobry-Duclaux 1960). These electro-viscous contributions to suspension viscosity is reduced as the ionic strength increases; NaCl compresses the double layer and thus the distortion of a thinner double layer by shear is small and at the same time overlapping

and interactions between the compressed double layers will be less, both effects resulting in lower viscosity at higher ionic strength.

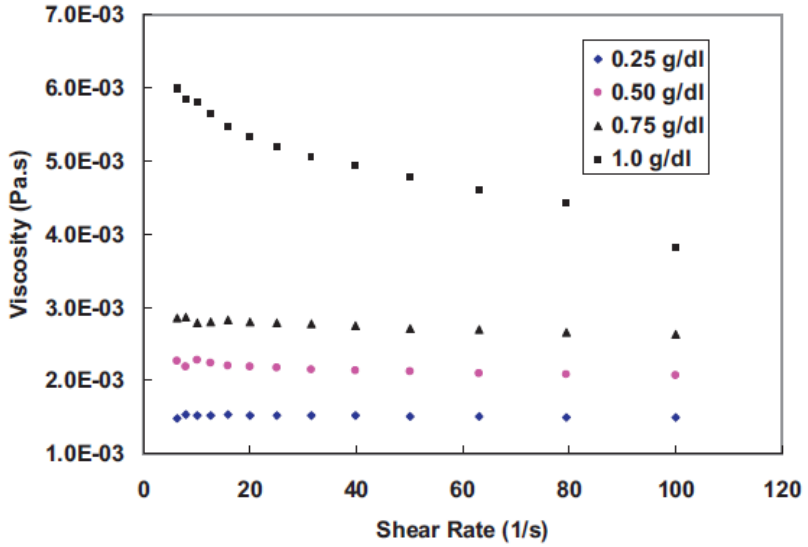

Figure 2-17: Shear rate dependence of viscosity of CNC suspension at various concentrations without electrolyte addition (reprinted from Boluk et al. 2011 with permission from Elsevier).

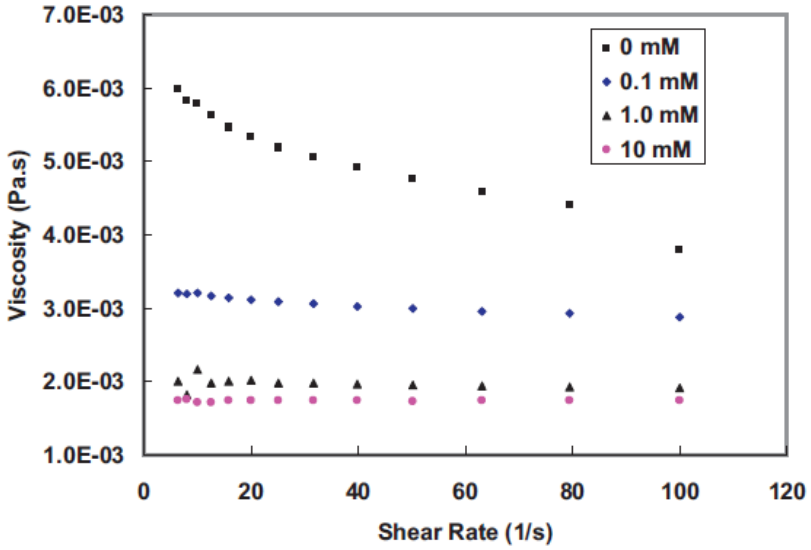

Figure 2-18: Shear rate dependence of viscosity of 1.0 g/dl CNC suspension with various NaCl concentrations (reprinted from Boluk et al. 2011 with permission from Elsevier).

Recently, Urena-Benavides et al. (2011) studied the rheology of concentrated (3-17 vol.%) aqueous suspensions of cellulose nanocrystals isolated from cellulose cotton powder (L/D ~ 12). In order to study the effects of temperature-induced microstructure changes, they have measured the steady shear viscosity for the predominantly isotropic 3.07 vol % sample, the predominantly liquid crystalline 6.99 vol % sample, and the liquid crystalline 12.1 vol % sample; data are shown in Figure 2-19. The 3.07 vol % (Figure 2-19 a) had a large Newtonian plateau at all measured temperatures with the inception of a shear thinning at 30 s^{-1} at 10 and 25 ºC. As the sample was isotropic, the decrease in viscosity with increasing temperature as expected. In the case of the biphasic 6.99 vol % sample (Figure 2-19 b), the viscosity showed three-region behaviour at all three temperatures tested. The viscosity generally decreased with increasing temperature, but little effect was observed in region I. For the 12.1 vol % sample the viscosity was independent of temperature between 10 and 35 ºC, but there was a marked viscosity increase at 40 ºC, being more significant at low shear rates. The viscosity increase at 40 ºC was thought to be due to changes in the microstructure or the relative fractions of isotropic and liquid crystalline regions, which was confirmed by hot stage optical microscopy revealing an increase in isotropic domains between 35 and 40 ºC.

They have also studied the linear viscoelastic properties of CNC suspensions and showed that the CNC suspensions behaved as viscous fluids (G"> G') up to concentration of 10 vol % and that an elastic behaviour (G"<G') was observed for higher concentrations.

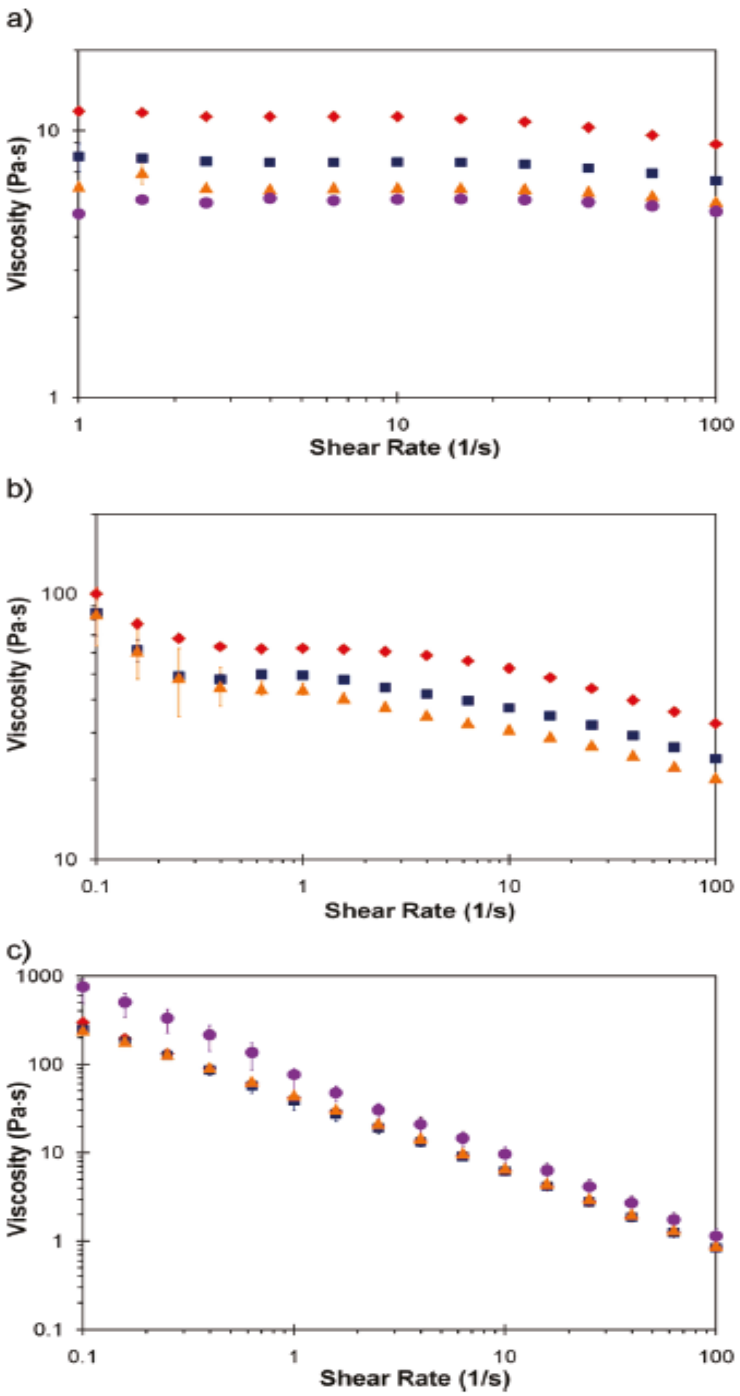

Figure 2-19: Steady shear viscosity versus shear rate at 10 (red diamonds), 25 (blue squares), 35 (orange triangles), and 40 ºC (purple circles) of CNC suspensions with concentrations of (a) 3.07, (b) 6.99, and (c) 12.1 vol.% (reprinted with permission from Urena-Benedevise et al. 2011).

The rheology of cellulose nanocrystals fabricated from chemical and homogenization treatments of microcrystalline cellulose powder (L/D~10 to 15) was recently studied by Liu et al. (2011). They have reported the viscosity versus shear rate for CNC suspensions at different concentrations (see Figure 2-20). They attributed the shear thinning to breakage of the network constructed by strong hydrogen or ionic bonding interactions among nanocrystals and the upturn in viscosity at high shear rates to rearrangement of the nanocrystals to form an ordered network.

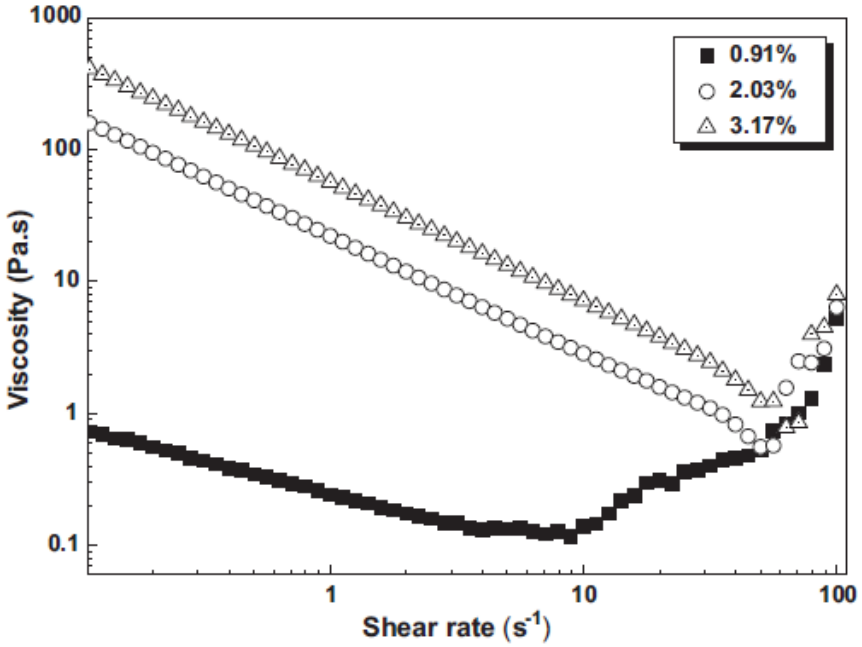

Figure 2-20: Viscosity as a function of shear rate for the CNC suspensions at different concentrations (reprinted from Liu et al. 2011 with permission from Elsevier).

CHAPTER 3: THESIS OBJECTIVES AND ORGANIZATION

3.1. Thesis objectives

Considering the previous discussion, rheology has been proven to be a powerful tool that can be used to monitor structural changes. Exploring the relationships between macromolecular structure and bulk rheology is critical in developing optimum processing conditions for CNC suspensions as novel cellulosic nano-materials. The scope of this thesis is to conduct a careful experimental study of the rheological behaviour of different cellulose nanocrystal aqueous suspensions over a broad range of concentrations and experimental conditions (temperature and shear rates) and to correlate the rheological properties with the microstructure of these suspensions.

This thesis focuses on addressing the following objectives:

A. To characterize the microstructure of the CNC suspensions under various flow conditions i.e. to study flow-induced structure development.

B. To study the effects of ultrasound treatment on the rheology and microstructure of CNC aqueous suspensions.

C. To study the effects of the degree of sulfation (surface charge) on the microstructure and rheology of CNC aqueous suspensions.

D. To study the effects of electrolyte concentration (ionic strength of the system) on the microstructure and rheology of CNC aqueous suspensions.

3.2. Thesis organization

This thesis is organized as follows. Chapter 1 briefly describes the introduction and motivation of this study. The literature review on CNC suspensions related to the present study is provided in chapter 2. The objectives and the organization of this thesis is presented in chapter 3. Chapter 4 describes the material and methodology used in this study to characterize the physico-chemical properties of CNC suspensions. The experimental and methodology to evaluate the shear-induced structure development of CNC aqueous suspensions using rheo-optics, are also discussed in detail in this chapter.

In chapter 5, the shear rheology of CNC aqueous suspensions at different concentrations are studied and correlated to the microstructure of the system. Chapter 6 discusses the effects of ultrasound energy on the physico-chemical properties of CNC. The changes in the microstructure and rheology of CNC suspensions by increasing degree of sonication are also discussed in this chapter. In chapter 7, the effects of temperature on the microstructure and rheological properties of CNC aqueous suspensions are presented. Chapter 8 discusses the effects of the degree of sulfation on the microstructural transitions of CNC aqueous suspensions and their rheological behaviour. Chapter 9 discusses the results regarding the effects of ionic strength (addition of NaCl) on the microstructure and rheology of CNC aqueous suspensions in three different concentration regimes, namely, low concentration (isotropic), medium concentration (anisotropic chiral nematic), and high concentration (gel). In chapter 10, the concluding marks and the contributions of this thesis to knowledge are described. Finally, recommendations for future research are summarized in Chapter 11.

CHAPTER 4: EXPERIMENTAL

4.1. Material and preparation procedure

Freeze dried CNC powder and also CNC suspensions with different degree of sulfation have been kindly provided by FPInnovations throughout this study. All these samples have been prepared in FPInnovations and the material and CNC extraction process is described in this section.

4.1.1. Material

A fully bleached commercial softwood kraft pulp was used as cellulose source. Prior to acid hydrolysis, the pulp was milled to pass through a 0.5 mm screen in a Wiley mill (Thomas-Wiley Lab mill, Model 4, Thomas Scientific, Philadelphia, PA) to ensure particle size uniformity and increase surface area. Concentrated sulfuric acid (98%) (Fisher Scientific) was diluted to 64 wt.% solutions, by adding the concentrated acid under magnetic stirring to deionised (DI) water cooled in an ice bath. The specific gravity of the diluted solutions measured by a hydrometer gave the value of 1.5421 for 64 wt.% solution at 20 ºC.

4.1.2. Extraction of cellulose nanocrystals

Milled pulp (about 50 g) was hydrolysed with 64 wt.% sulfuric acid aqueous solution, with acid/pulp ratio of 8.75 ml/g (Dong et al. 1998, Hamad and Hu 2010), unless otherwise mentioned, for 25 min. The sulfuric acid solution was heated to the desired temperature (45 ºC), added to the pulp in an Erlenmeyer flask in a hot water bath heated to the same temperature, and allowed to hydrolyse the pulp under vigorous stirring for 25 min. To stop the hydrolysis reaction, the mixture was immediately diluted with cold DI water (10 folds), and allowed to settle overnight. The clear top layer was decanted off and the remaining white cloudy layer was centrifuged at 4000 rpm for 15 min (Beckman J6-HC). The clear, top layer after centrifugation was decanted off, and DI water (same volume as that which had been decanted) was added and mixed with the remaining thick white suspension and then centrifuged again. This procedure was repeated 3-4 times. The precipitate, after the last centrifugation and decanting of the clear top layer, was placed in dialysis membrane tubes (Fisher Scientific) having a molecular weight cut off of 12000–

14000 and dialysed against slow running DI water for 1–4 days. The procedure was continued until, when the pH of DI water became constant over a period of 1 h. The suspension from the membrane tubes was dispersed by subjecting it to ultrasound treatment for 10 min at 60% power. Since H-form CNC can not easily be re-dispersed in water, the suspensions were then titrated with 0.1 M NaOH to replace the hydrogen ions on the surface of the CNC spindles[1] with sodium ions; this step is necessary to ensure that the suspension has reached the right pH (~7). The suspensions were then freeze-dried (VirTis adVantage freeze dryer), and perfectly re-dispersed in deionized DI water to prepare CNC suspensions at different concentrations.

4.2. Preparation of cellulose nanocrystals suspensions

Suspensions of different concentrations have been prepared by dispersing the appropriate amount of freeze-dried CNC in DI water followed by sonication (Joules of ultrasound energy/ g of CNC in the sample.)

In order to study the effect of degree of sulfation on the structure and rheology of CNC suspensions, two different sets of CNC were synthesized and provided by FPInnovations. The production conditions of these two sets of CNC are summarized in Table 4-1. Post-hydrolysis processing was controllably modified to produce these CNC suspensions with different sulfur contents, or degrees of sulfation.

In order to study the effects of electrolyte concentration on the structure and rheology of CNC suspensions, 15 wt.% CNC suspensions in NaCl solutions with different NaCl concentrations (0 mM to 15 mM NaCl solution) were prepared followed by sonication. These suspensions were then diluted to different CNC concentrations with the corresponding NaCl solution and have been further studied.

[1] Spindles are a more precise description of the geometry of CNC particles. However, rods and whiskers have commonly been used as well. We will use the term rods throughout this thesis to denote the approximate CNC geometry.

Table 4-1: Hydrolysis conditions for two different sets of CNC suspensions possessing different degree of sulfation.

Property / Sample	Pulp Source	Pulp Consistency (%)	Acid/Pulp (ml/g)	Reaction Temperature (ºC)	Reaction Time (min)	Final Sample wt.%	Yield (%)
CNC-A	BSKP	96.6	8.75	45	25	1.98	21
CNC-B	BSKP	96.4	6.00	45	25	3.80	32

4.3. Ultrasound treatment (sonication)

Ultrasonic processor model VCX-130 (Sonics & Materials Inc.) with a 6 mm probe was used to apply ultrasound energy (in Joules per gram of CNC) to suspensions at different concentrations in order to disperse the CNC particles. Ultrasound treatment was carried out in an ice bath to avoid overheating, since the surface charge of CNC particles is heat-sensitive and an increase in temperature can cause de-esterification of the sulfate groups on the surface of the crystals (Beck-Candanedo 2005).

4.4. Elemental analysis

The exact amount of sulfur has been measured using elemental analysis (in a gas chromatography unit, Carlo Ebra 1106) and the number of anionic sulfate ester groups on the surface of CNC has been found based on the formula of $C_6H_{10}O_5\text{-}(SO_3)_n$ and calculated from the equation $S(\%) = 100n*S / [6C + 10H + (5 + 3n)*O + nS]$, as described in Hamad and Hu (2010).

4.5. Zeta potential measurements

Malvern Instruments Zetasizer (ZEN 3600) was used to characterize the size and zeta-potential of CNC particles suspended in water. Zetasizer uses the dynamic light scattering technique to measure the size of the particle; This technique measures the diffusion of particles moving under Brownian motion and converts this to size, using the Stokes-Einstein relationship ($D= K_BT/6\pi\eta R$, where D is diffusion constant, K_B is Boltzmann's constant, T is the absolute temperature, η is solvent viscosity and R is the radius of equivalent spherical particle). Knowing that CNC particles are rod-like and Stokes-

Einstein equation is for diffusion of spherical particles, the size of CNC particles measured by zetasizer technique does not represent the exact particle size and shape, but only gives an equivalent hydrodynamic size of the particle. Therefore, the results of size measurements from zetasizer are only used for comparison between different CNC samples, and not as an exact size measurement in this thesis.

When an electric field is applied across the suspension, charged particles move with constant velocity (v) which is dependent on the strength of the electric field (E), the dielectric constant (ε), the viscosity of the medium (η), and the zeta potential (ζ). The velocity of a particle in an electric field is referred to as its electrophoretic mobility (μ_E = v/E) and is directly measured by zetasizer using laser Doppler micro-electrophoresis. Zeta-potential cannot be measured directly but it can be calculated using theoretical models and an experimentally-determined electrophoretic mobility. For CNC aqueous suspensions the mobility values were converted to ζ-potentials using the Smoluchowski equation.

$$\mu_E = \varepsilon_r \varepsilon_0 \zeta / \eta \qquad \text{(Smoluchowski Equation (1903))}$$

Where ε_r is the dielectric constant of the dispersion medium (being water here), ε_0 is the permittivity of free space ($C^2\ N^{-1}\ m^{-2}$), η is the dynamic viscosity of the dispersion medium (Pa.s), and ζ is the zeta potential. This equation is valid for thin double layers (smaller than the radius of the particle) which applies for most aqueous systems since the double layers are a few nanometers in water.

It should be noted that the technique used in zetasizer to measure the electrophoretic mobility requires dilution of the sample which sometimes affect the properties of the sample and change the zeta-potential. The calculated zeta-potential is sensitive to the degree of dilution and also to the ionic strength of the sample. Therefore, the results of zeta-potential have been used only for comparison of different CNC samples in this thesis and may not be considered to indicate the exact value of the CNC surface charge.

All the reported values in this thesis are an average of 10 measurements.

4.6. Transmission electron microscopy (TEM)

TEM images of the CNC crystallites were obtained using an FEI Tecnai G2 200 kV. To image the individual CNC crystallites, 1mL drop of very dilute (~0.005 wt.%) CNC suspension was deposited on a TEM grid immediately after sonication and dried under ambient conditions. Image J software has been used to measure the physical dimensions of CNC particles.

4.7. Polarized optical microscopy (POM)

Photomicrographs of CNC suspensions were taken using a polarized light microscope (Mitutoyo microscope set up equipped with Lumenera LU 165 color CCD camera and polarizer). In a typical experiment, CNC suspensions were placed in the space between two glass plates of the rheometer (parallel-plate geometry), and the microstructure was observed under crossed-polarizer. Since this microscope set-up is coupled with the rheometer, it enables the investigation of local shear-induced effects in liquid crystals. Images were taken during rheological testing and also at rest, during the drying process, close to the edges of the samples.

Polarized light microscopy is generally utilized to distinguish between optically isotropic and optically anisotropic materials. Anisotropic substances, such as liquid crystals, generate interference effects in the polarized light microscope, which results in differences of color and intensity in the image. Figure 4-1 shows a schematic of the polarized microscope used in this study. The direction of the polarizer and analyzer of this set up can be manipulated to take images of the sample while the polarizer and analyzer being parallel (maximum transmission) or perpendicular to each other, crossed-polars, (maximum extinction). By rotating the analyzer and changing the angle between polars from 90 to 0 º, no change in the observed structure occurs but the image becomes brighter which is expected (see Figure 4-2).

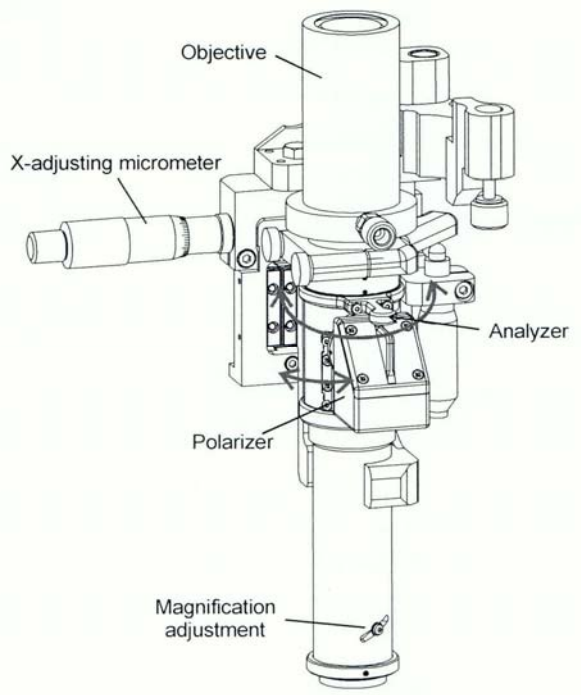

Figure 4-1: The schematic of polarized microscope used in this study.

In order to capture the microstructural transition from isotropic to chiral nematic liquid crystal in the sample, cross-polars at 90 º has been used here, with the initial polarization in flow direction and the analyzer perpendicular to flow. The emitted light is polarized by the polarizer and the reflected light is detected through a second polarizer which is used as the analyzer. Under cross-polars, the images of isotropic samples are dark and chiral nematic liquid crystal domains show colored fingerprint patterns.

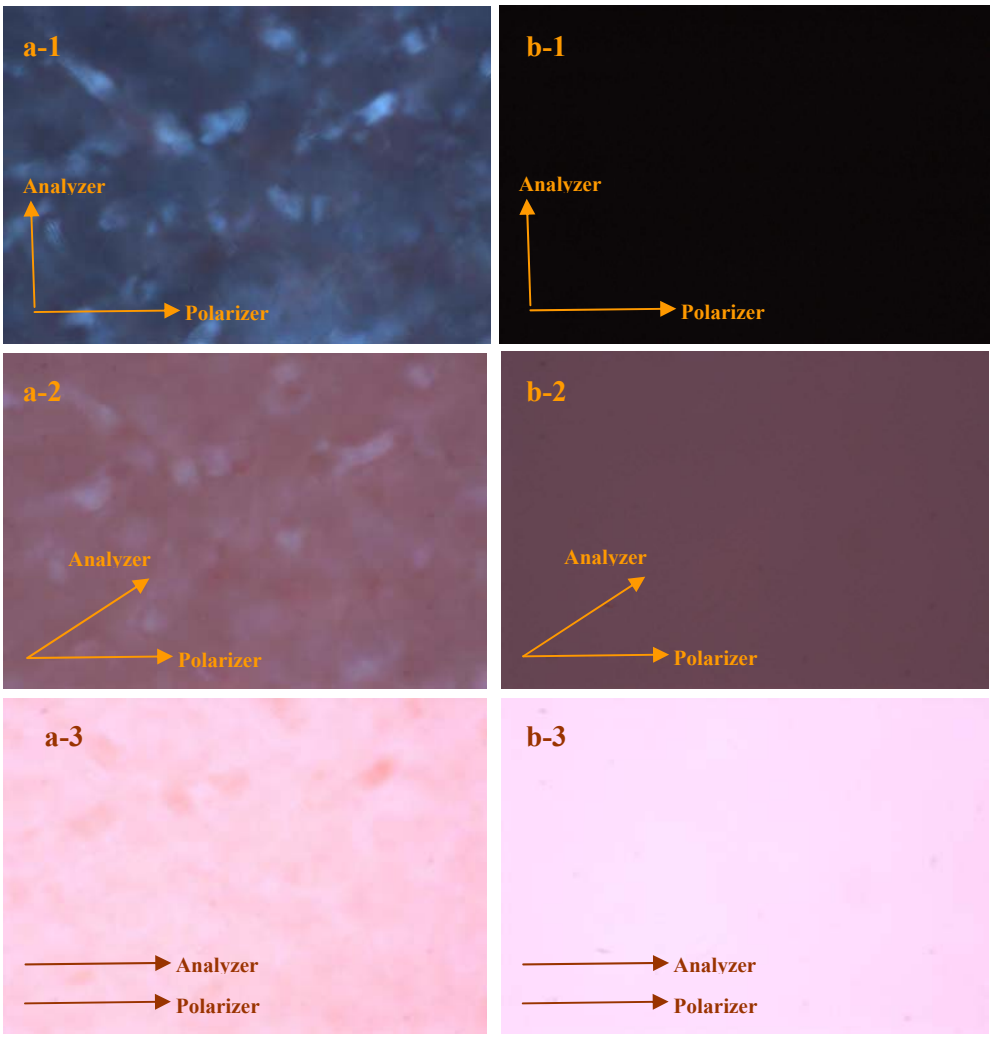

Figure 4-2: Polarized optical micrographs of (a) anisotropic chiral nematic sample and (b) an isotropic sample taken at different angles of polarizer and analyzer to get maximum extinction (a-1 and b-1) or maximum transmission (a-3 and b-3).

We have also tried to capture images by rotating the sample which are shown in Figure 4-3 for both isotropic and chiral nematic structures. As can be seen in Figure 4-3, for an isotropic CNC suspension, the image is black at 90 degree and no change occurs by rotating the sample from 90 to 0º. This is also the case for anisotropic samples at high shear rates where the liquid crystal structures are broken and single particles are aligned in shear direction. For all the POM micrographs presented in this thesis, the initial polarization is in the flow direction and the analyzer is perpendicular to flow.

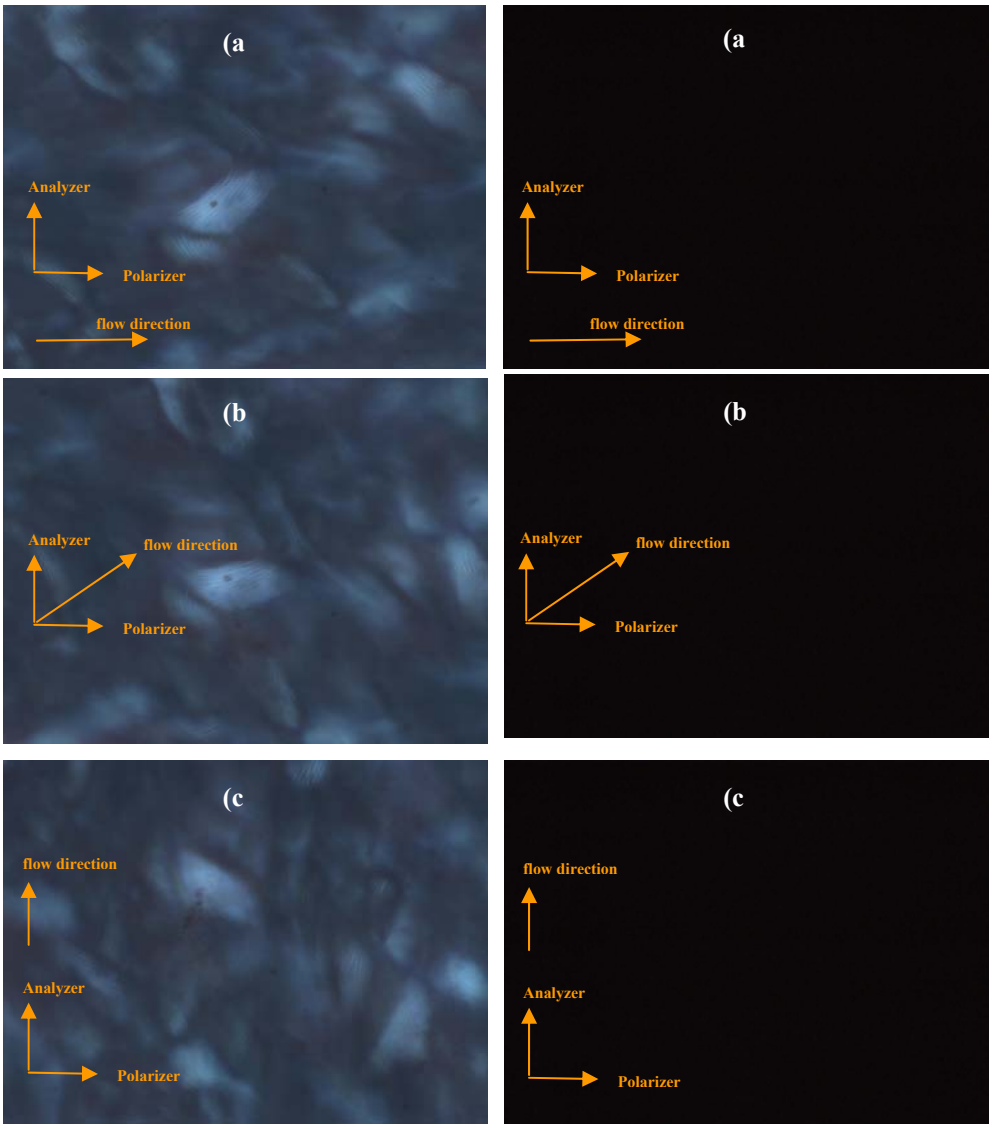

Figure 4-3: Cross polarized microscopy images of an anisotropic chiral nematic (left), and an isotropic (right) CNC suspension, rotated from 0° to 90°.

4.8. Rheological measurements

The rheological measurements were performed using a rotational rheometer (MCR 501 Anton Paar Physica) with a parallel plate glass geometry of 43 mm diameter. The steady state shear viscosity versus shear rate curves were generated for all samples for shear rates in the range from 0.01 to 100 s^{-1}. For each sample, the time required to reach steady state at 0.01 s^{-1} was determined by a transient test; the sampling time used to generate the flow curves was decreased with increasing shear rate. Each data point in the viscosity

versus shear rate curves is the average of 3 measurements. The viscosity of several samples were measured at different gap sizes (0.5, 1, 1.5, and 2 mm) and the results showed no gap dependency (see Figure A1 in Appendix) ensuring that there is no slip for these samples, consistent with previous literature (Marchessault et al. 1959, Orts et al. 1998, De Souza and Borsali 2004). The gap size of 0.5 mm was used for performing all the rheological tests presented in the thesis. For several samples, two different geometries (parallel plate glass geometry with diameter of 43 mm and cone and plate geometry with cone angle 1º and diameter of 40 mm) were used to ensure no experimental artifacts were present. The error bars were smaller than the size of the symbols in most cases and are not included in plots, for the sake of clarity.

Isothermal dynamic frequency sweeps were performed to determine the linear viscoelastic properties over the whole accessible frequency range. The strain amplitude used was 1-5 % during all small amplitude oscillation tests, where the samples have shown linear viscoelastic behaviour determined by performing amplitude sweep experiments at a frequency of 1 Hz. To avoid evaporation, a small amount of silicone oil was placed on the periphery of samples together with an evaporation blocker. All rheological measurements were performed at the temperature of 25 °C unless otherwise mentioned. To follow the microstructural changes during shear and to investigate the effect of different shear conditions on CNC alignment, a polarized optical microscope set up (refer to section 4.6.) has been coupled with the rheometer. This rheo-optic set up consists of Anton-Paar Physica MCR 501 rheometer, P-PTD 120 Glass Plate (transparent parallel plate geometery), a microscopy holder with adjusting mechanism and a light source (Dolan-Jenner MI-150 Illuminator).

CHAPTER 5: SHEAR RHEOLOGY OF CNC SUSPENSIONS[2]

As discussed before, the main aim of this research is to understand the rheological behaviour of CNC aqueous suspensions due to its significance in optimizing various process of these novel materials that involve flow. As a first step, we prepared CNC aqueous suspensions at different concentrations and characterized their physico-chemical properties and rheological behaviour which will provide a base line for further rheological studies of these suspensions.

5.1. Characterization of CNC suspensions

As discussed before, the liquid crystalline behaviour in CNC aqueous suspensions is governed by the dimensions, aspect ratio and the surface properties of CNC particles. Therefore, a thorough characterization of the physico-chemical properties of the particles is crucial in understanding their flow behaviour. The surface properties of CNC, obtained by elemental analysis, ζ-potential measurements and transmission electron microscopy (TEM) are summarized in Table 5-1.

Table 5-1: Dimensions and surface characteristics of CNC suspensions prepared and studied in this work.

	Equivalent Hydrodynamic Particle Size (nm) (from Zetasizer)	Electrophoretic Mobility (μm cm/(V.s))	ζ-potential (mV)	Sulfur Content (%)	OSO_3H / 100 anhydro-glucose units	Nanocrystal Dimensions (nm) (from TEM)
CNC	35±2 nm	-2.46	-31.50	0.66	3.39	100× 7

To measure the degree of sulfation on the surface of studied CNC suspensions, elemental analysis was performed. The elemental analysis of the CNC particles has shown that they contain 0.66 wt.% of sulfur, which results in 3.39 SO_3^-/100 glucose units (Hamad and Hu 2010). The degree of CNC sulfation determines the surface charge density of cellulose nanocrystals, which in turn affects the stabilization of the suspension. The magnitudes of

[2] Part of this chapter is published: Shafiei-Sabet, S., Hamad, W. Y., and Hatzikiriakos, S. G. Langmuir, 28, 2012.

ζ-potential of these CNC (-31.50 mV) confirms that these CNC particles are negatively charged and their suspension is stable.

A typical TEM image that shows the high aspect ratio (L/D ~ 13-20) of these CNC particles is shown in Figure 5-1. The concentration of the suspension used for the TEM analysis was 0.005 wt.%. Different samples were prepared starting from CNC suspensions at different concentrations (3, 5 and 7 wt.%) and diluted to 0.005 wt.%, then sonicated (1000 J/g of CNC), and deposited on TEM grids and were analyzed. The results were reproducible; i.e., independent of the starting concentration of CNC suspensions. The CNC micrograph shown in Figure 5-1 indicates average nanocrystal dimensions of 100±8 nm × 7±3 nm.

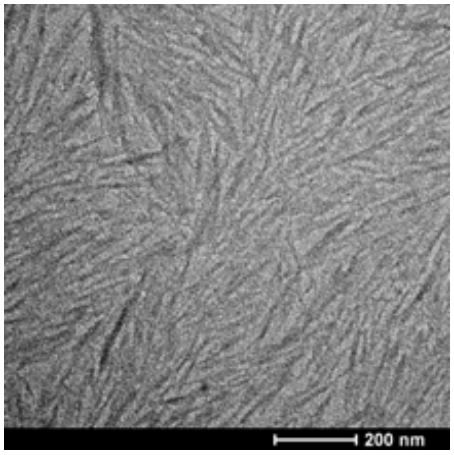

Figure 5-1: TEM micrograph of CNC suspensions sonicated at 1000 J/g CNC.

5.2. Shear rheology of CNC aqueous suspensions at different concentrations

Aqueous suspensions of CNC of concentration in the range from 1 to 7 wt.% have been prepared and the steady-state shear viscosities were measured. Figure 5-2 depicts the shear viscosity of these suspensions at different concentrations. The 1 and 2 wt.% samples exhibit a Newtonian plateau at low shear rates followed by a shear thinning region at intermediate shear rates and another plateau at high shear rates, typical of an isotropic sample. For samples of 3 and 4 wt.%, the three-region viscosity profile, typically associated with lyotropic polymer liquid crystals (Onogi and Asada 1980), is observed confirming the occurrence of isotropic to liquid crystalline phase transition. For

these concentrations (above the critical concentration for transition), the viscosity profile consists of three different regions; namely, a shear thinning at low shear rates (region I) due to the alignment of the chiral nematic liquid crystal domains; a plateau region at intermediate shear rates (region II), where the domains have all been oriented along the shear direction; and finally a second shear thinning region (region III) at high shear rates, where the shear stress is high enough to destroy the liquid crystal domains and make it possible for the individual rods to be oriented along the shear flow direction. However, these three distinct regions are not observed at higher concentrations of 5 and 7 wt.%, where a single shear thinning behaviour is only observed over the whole investigated shear rate range. Since the suspensions are not sonicated, this single shear thinning viscosity profile is attributed to aggregation and gel formation at higher concentration, which breaks by application of shear. This gelation inhibits the formation of chiral nematic ordered phases (Liu et al. 2011, Urena-Benavides et al. 2011).

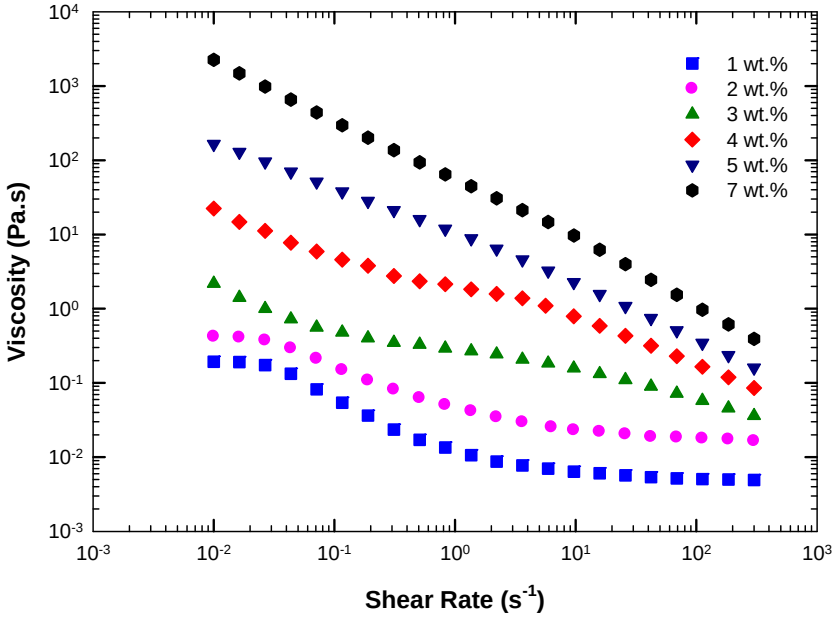

Figure 5-2: Steady state viscosity versus shear rate for unsonicated CNC suspensions with concentrations varying from 1 to 7 wt.%.

To follow changes in the microstructure of these suspensions under shear, polarized optical microscopy has been used on-line with a rheometer to capture in situ POM

micrographs at various shear rates. Typical micrographs of 1 wt.%, 4 wt.% and 7 wt.% unsonicated samples at different shear rates are shown in Figures 5-3, 5-4 and 5-5, respectively. These three concentrations were chosen as they have shown different viscosity profile in Figure 5-2. For the 1 wt.% CNC aqueous suspensions, where the sample is in isotropic state, Figure 5-3 shows that the POM micrographs (under crossed polarizer at 90º) are dark and show no indication of existence of anisotropic ordered phases, no matter what is the magnitude of the applied shear.

Figure 5-3: Polarized optical micrographs of unsonicated 1 wt.% CNC aqueous suspension during steady shear tests, at shear rates of (a) 0.01 s^{-1}, (b) 0.1 s^{-1}, (c) 10 s^{-1}. The scale bar is 50 µm.

In the case of 4 wt.% sample, which showed a three-region viscosity profile (refer to Figure 5-2), typical of liquid crystal polymer solution, the existence of chiral nematic ordered phases are represented as fingerprints in the corresponding POM micrograph (see Figure 5-4-a). By increasing the shear rate, the suspension goes through three distinct microstructural changes. The first shear thinning region, represented by micrographs a-c in Figure 5-4, where the viscosity decreases due to deformation and re-alignment of chiral nematic domains; the plateau region (micrographs d-e in Figure 5-4), where all domains become aligned along the shear direction; and eventually break down of all ordered domains represented by the micrograph in Figure 5-4-f. This last dark micrograph shows that the liquid crystal domains are broken and are no longer present in the suspension at higher shear rates. It is important to note that the individual rods essentially align themselves in this shear rate region (typically higher than10 s^{-1}).

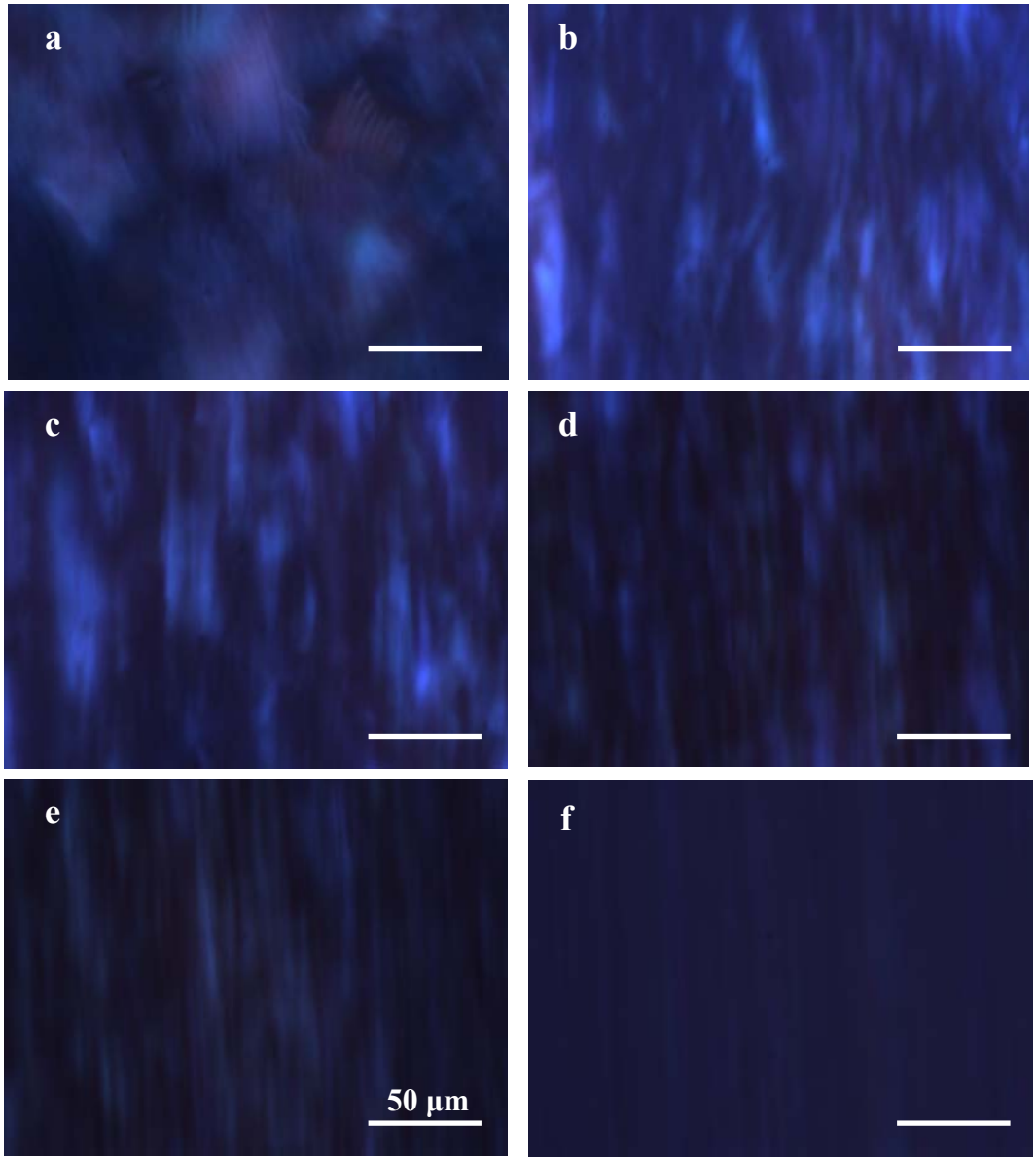

Figure 5-4: Polarized optical micrographs of 4 wt.%, unsonicated CNC aqueous suspension during steady shear test, at shear rates of (a) 0.01 s^{-1}, (b) 0.05 s^{-1}, (c) 0.1 s^{-1}, (d) 0.5 s^{-1}, (e) 1 s^{-1}, and (f) 10 s^{-1}. The scale bar is 50 µm.

Figure 5-5 shows the microstructure changes under shear for 7 wt.% sample. According to Figure 5-5-a, sample shows the structure of a birefringent gel at 0.01 s^{-1}. By increasing the shear rate, the applied shear breaks the gel structure and frees the ordered domains to become oriented along the shear direction. The observed shear thinning in viscosity profile of this sample (shown in Figure 5-2) is attributed to a combination of two different

mechanisms: gel breakage and domain deformation (micrographs b-e in Figure 5-5). At even higher shear rates, breakage of any ordered region leads to the orientation of individual CNC particles parallel to the shear direction (micrograph f in Figure 5-5).

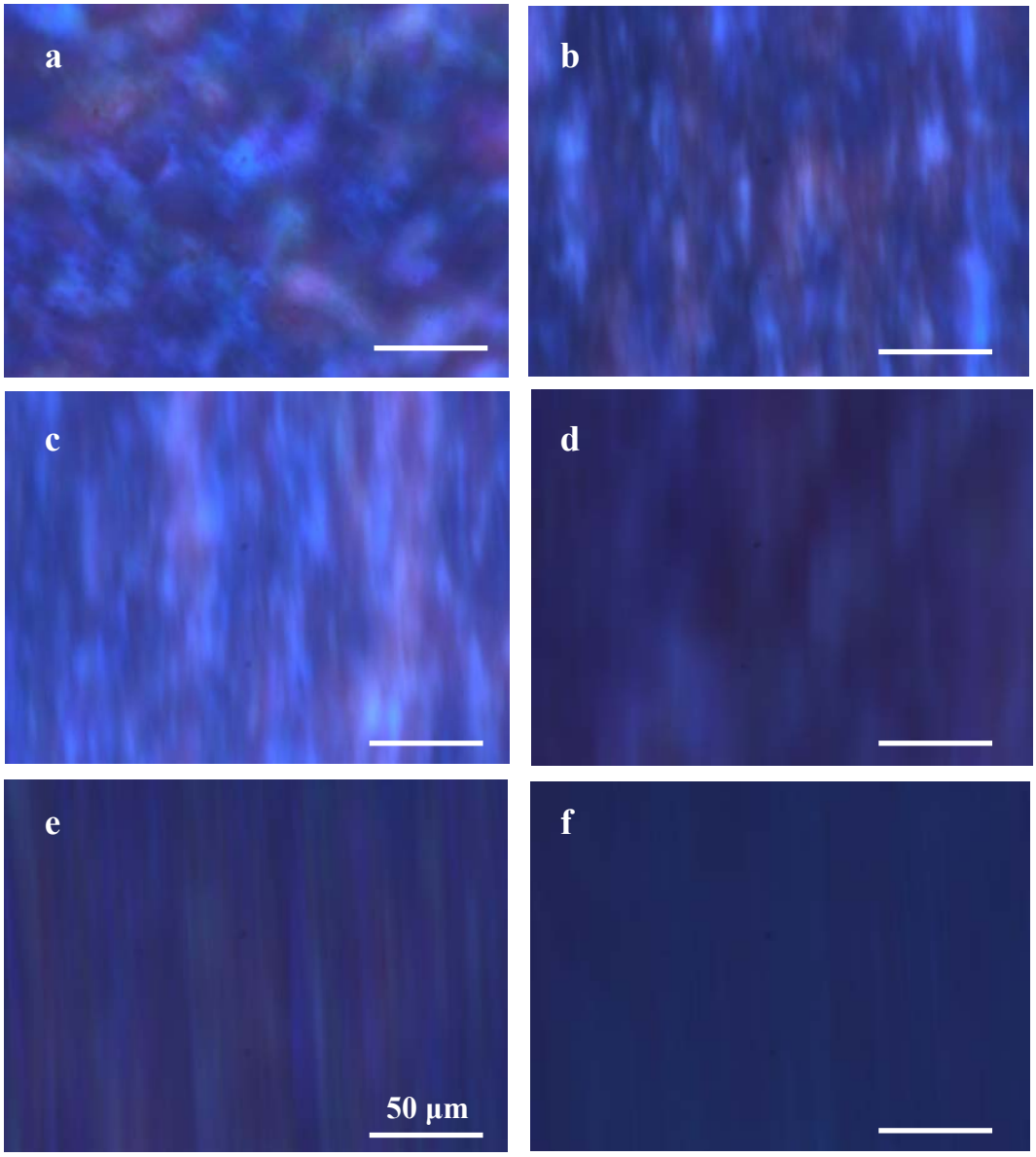

Figure 5-5: Polarized optical micrographs of 7 wt.%, unsonicated CNC aqueous suspension during steady shear test, at shear rates of (a) 0.01 s^{-1}, (b) 0.05 s^{-1}, (c) 0.1 s^{-1}, (d) 0.5 s^{-1}, (e) 1 s^{-1}, and (f) 10 s^{-1}. The scale bar is 50 µm.

5.3. Summary

Based on the results and discussion presented in this chapter, it can be concluded that the CNC particles prepared here contain anionic sulfur ester groups on the surface and their aqueous suspensions are stable (ζ-potential value being -31.5). These nanocrystals are rod-like with length of 100±8 nm and diameter of 7±3 nm, obtained by TEM. The suspensions form chiral nematic liquid crystal phase above a critical concentration, and when observed under the polarized optical microscope, reveal fingerprint patterns indicative of the chiral nematic phase. Disappearance of the fingerprint patterns at high shear rate will provide evidence that as shear disrupts the chiral nematic phase, CNC particles exhibit nematic ordering with their axis aligned parallel to the flow direction. The transition from isotropic to chiral nematic anisotropic phases can also be obtained by measuring the suspension rheology and characterizing the shape of their viscosity profile. The biphasic suspensions, when subjected to increasing shear rate, go through three different microstructural changes which have been captured by using polarized light microscopy while performing the steady shear tests.

CHAPTER 6: EFFECTS OF ULTRASOUND TREATMENT (SONICATION) ON THE MICROSTRUCTURE AND RHEOLOGY OF CNC AQUEOUS SUSPENSIONS[3]

Ultrasound treatment (sonication) is commonly used to disperse CNC particles in suspensions (Dong et al. 1996), which in general causes a decrease in their viscosity (Marchessault et al. 1961, Dong et al. 1998). Although the sonication-induced viscosity change is usually significant, detailed studies on the effect of sonication on rheology and flow behaviour of CNC suspensions do not exist. The amount of sonication applied to the suspension usually is reported by sonication duration (Dong et al 1998, Boluk et al. 2011) which is not very accurate since it depends on the concentration and the volume of the sample being sonicated. Beck et al. (2010) evaluated the effect of ultrasound energy on the optical properties of solid films prepared from CNC suspensions by applying ultrasound energy as J/g of CNC which is a better approach in preparing our CNC aqueous suspensions.

In order to study the effect of sonication on the rheology of CNC aqueous suspensions, we have prepared CNC samples at different concentrations of 1 to 7 wt.% and sonicated them for 1000 J of ultrasound energy per each gram of CNC in the sample (~277 kw h/ton). The steady-state shear viscosity versus shear rate of these sonicated samples are shown in Figure 6-1-a. This can be compared with the viscosity of unsonicated samples shown in Figure 6-1-b. Comparing the viscosity profiles in Figure 6-1-a and b, it can be seen that for all concentrations studied here, the viscosity decreases significantly with sonication. However, decrease in viscosity due to sonication is more significant for higher concentration samples. This decrease is about 3 orders of magnitude for 7 wt.%, which becomes a decrease by a factor of about 2 at the lowest concentration of 1 wt.% (see Figure 6-2). The other interesting observation is that a three-region viscosity profile, resembling those seen in liquid crystalline systems, is observed for the high concentration sample (7 wt.%) after the application of 1000 J/g of CNC sonication. This sample have shown a gel-like rheological behaviour before sonication. This shows that application of

[3] A version of this chapter is published: Shafiei-Sabet, S., Hamad, W. Y., and Hatzikiriakos, S. G. Langmuir, 28, 2012.

ultrasound energy can break the gel structure and disperse the nanocrystals in the system so that the transition from isotropic to chiral nematic liquid crystal can occur in the system.

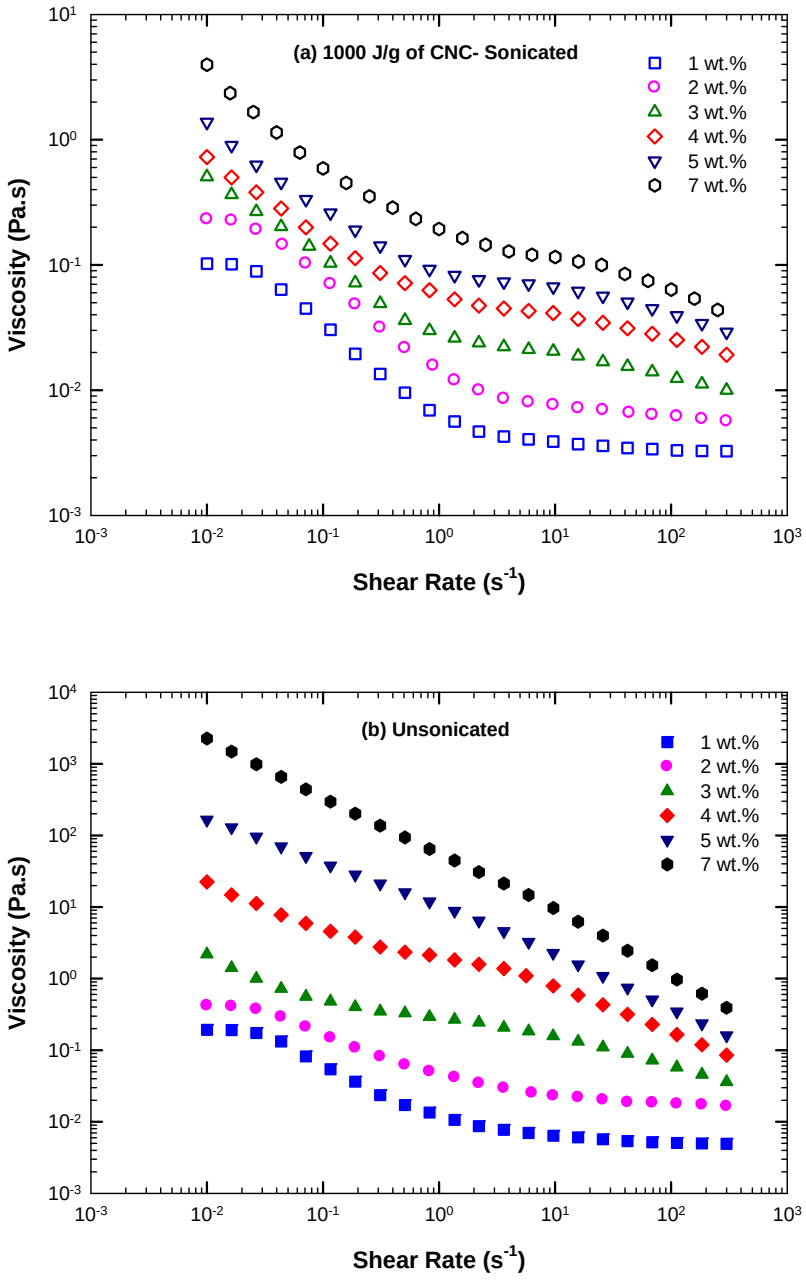

Figure 6-1: Steady-state viscosity versus shear rate for (a) CNC suspensions sonicated at 1000 J/g of CNC, and (b) unsonicated CNC suspensions with concentrations varying from 1 to 7 wt.%.

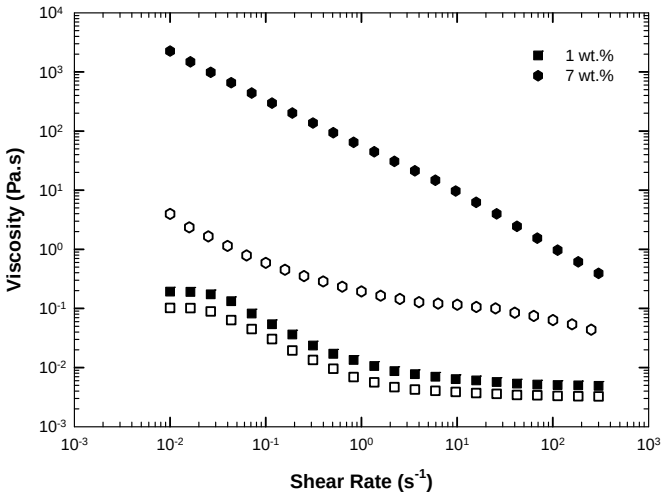

Figure 6-2: Steady-state viscosity versus shear rate of 1 wt.% (■), and 7 wt.% (●) CNC suspensions before sonication (solid symbols) and after sonication at 1000 J/g CNC (open symbols).

To further study the observed changes in rheological behaviour of CNC samples before and after sonication, polarized optical microscopy has been used to follow the microstructure changes of sonicated and unsonicated samples under applied shear. Typical micrographs of a 5 wt.% unsonicated and 1000 J/g CNC sonicated suspensions are shown in Figures 6-3 and 6-4, respectively. For the unsonicated sample, the micrograph at 0.01 s^{-1} shows a birefringent gel structure (micrograph a in Figure 6-3). Shear breaks the gel and ordered domains orient along the shear direction. This microstructure change can be seen in micrographs d-e of Figure 6-3 which results the shear thinning observed for this sample in Figure 6-1-b. Finally at very high shear rates, all the ordered structures are broken and individual CNC particles align parallel to the shear direction (darkening of micrograph f in Figure 6-3). On the other hand, for the sonicated 5 wt.% sample (Figure 6-4), starting from the presence of chiral nematic ordered domains in the system (micrograph a in Figure 6-4), by increasing shear rate the liquid crystal domains deform and align themselves in shear direction (first shear thinning region in corresponding viscosity profile, refer to Figure 6-1-a). The domains become all aligned above a critical shear rate, resulting in a plateau in the viscosity profile which is

imaged in micrographs d-e in Figure 6-4. Eventually, above a second critical shear rate (~10 s^{-1}) shear becomes strong enough to break all the ordered domains resulting in the second shear thinning observed in the viscosity profile of this sample and represented by micrograph f in Figure 6-4. This is where chiral nematic domains are no longer present in the suspension but the individual CNC rods essentially align themselves in this high shear rate regime.

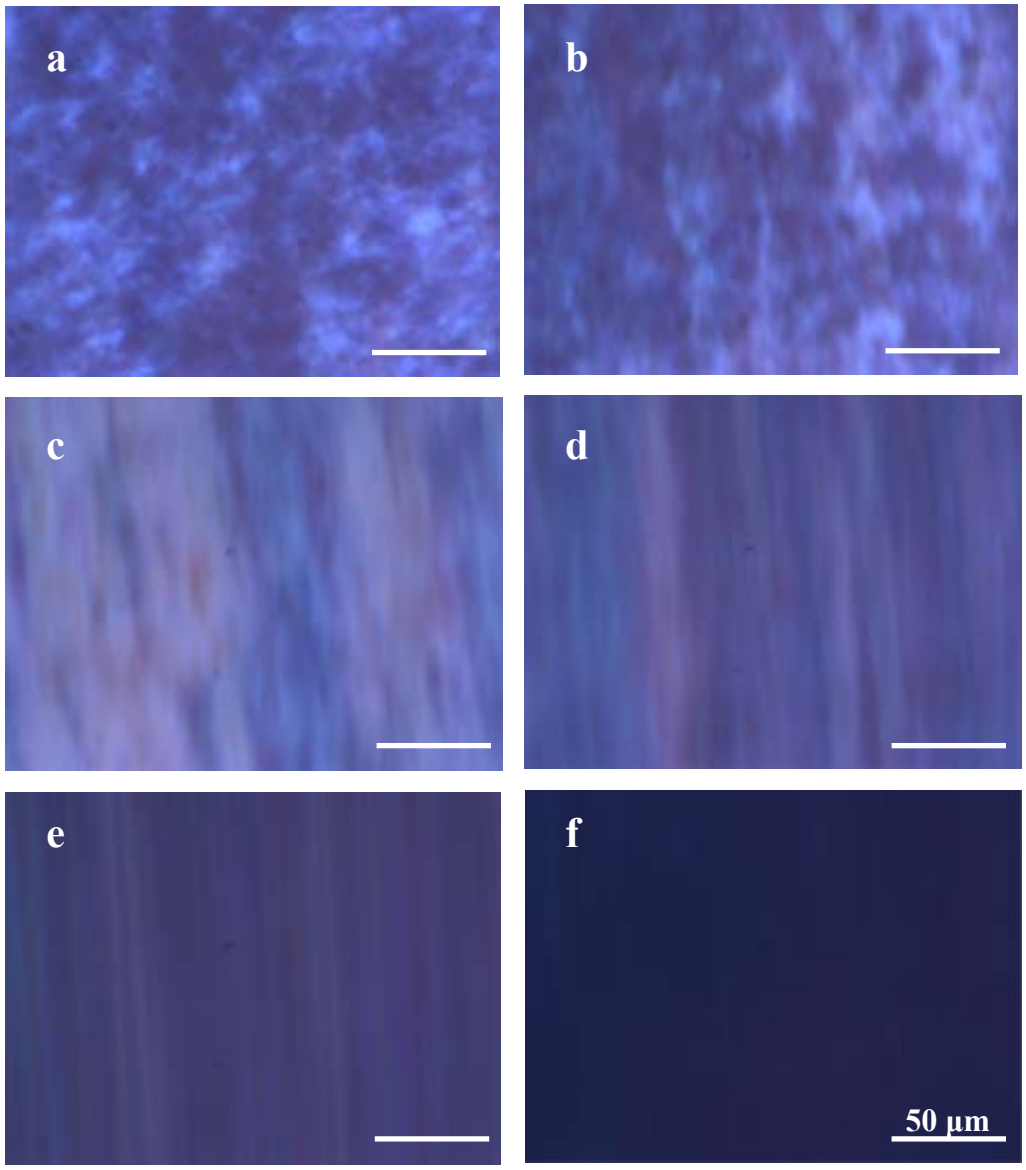

Figure 6-3: Polarized optical micrographs of 5 wt.% unsonicated CNC suspension during steady shear tests, at shear rates of (a) 0.01 s^{-1}, (b) 0.05 s^{-1}, (c) 0.1 s^{-1}, (d) 0.5 s^{-1}, (e) 1 s^{-1}, and (f) 10 s^{-1}.

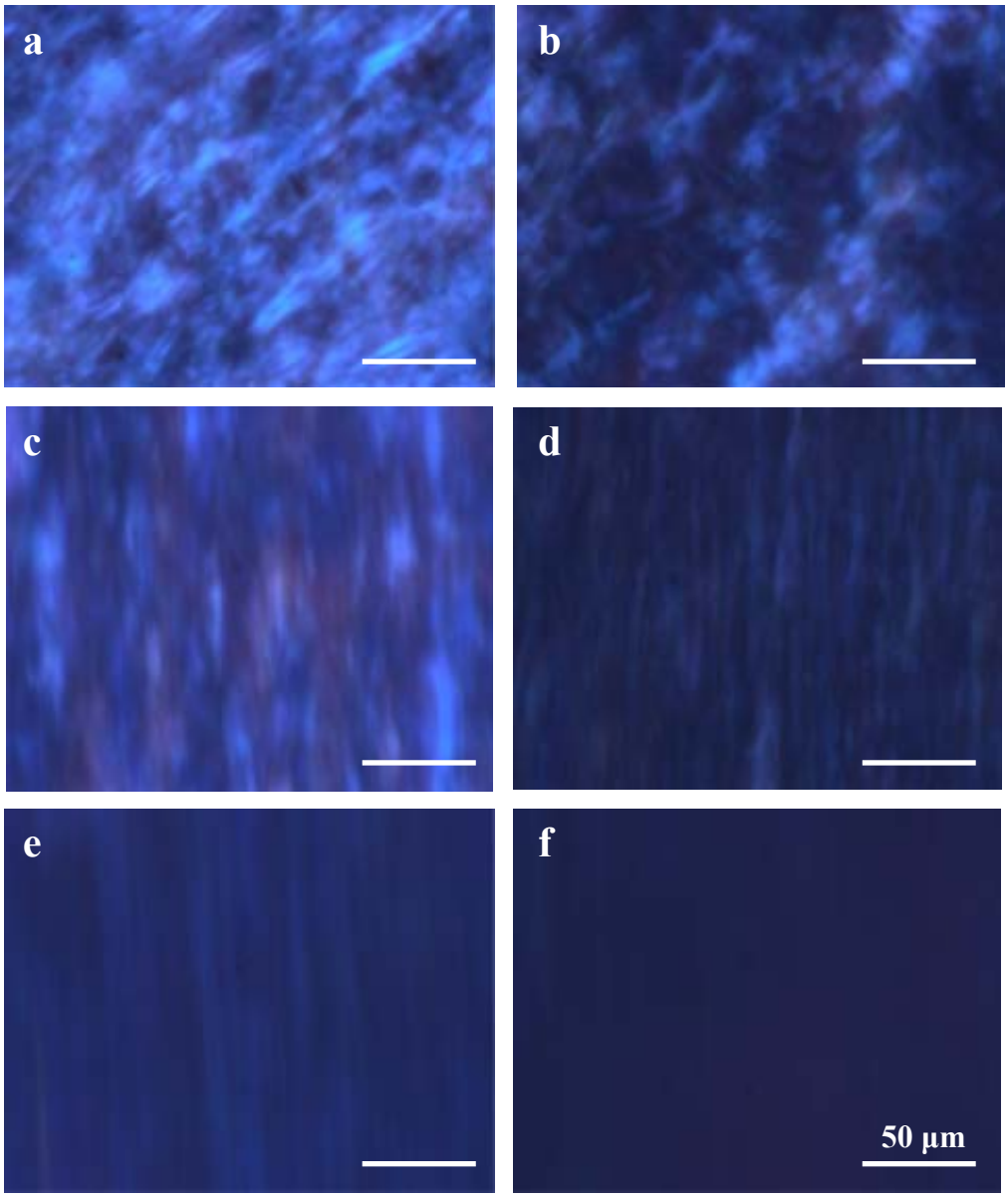

Figure 6-4: Polarized optical micrographs of 5 wt.% CNC suspension, 1000 J/g of CNC sonicated, during steady shear tests, at corresponding shear rates of (a) 0.01 s^{-1}, (b) 0.05 s^{-1}, (c) 0.1 s^{-1}, (d) 0.5 s^{-1}, (e) 1 s^{-1}, and (f) 10 s^{-1}.

Based on these primary observations on the effect of sonication on the rheological behaviour of CNC aqueous suspensions, a systematic study of this effect is needed which is covered in the following sections of this chapter.

6.1. Effects of sonication on surface properties and dimension of CNC particles

6.1.1. Effects of sonication on the surface properties of CNC particles

To study the effect of sonication on the physico-chemical properties of CNC particles, ζ-potential measurement has been performed on samples sonicated with different amounts of ultrasound energy and the data are summarized in Table 6-1.

Table 6-1: Dimensions and surface characteristics of CNC suspensions prepared and studied in this work.

Property \ Sample	Unsonicated (0 J/g NCC)	Sonicated (1000 J/g NCC)	Sonicated (3000 J/g NCC)
Size (nm)	74	38	36
ζ -potential (mV)	-30.70	-32.3	-35.9
Electrophoretic mobility (μm cm/Vs)	-2.41	-2.52	-2.8
Conductivity (mS/cm)	0.32	0.45	0.57

Electrophoretic mobility and conductivity of samples increase with increasing the ultrasound energy input, which suggests that sonication affects the surface charge of the CNC particles and releases some ions into the surrounding media. This will be further discussed in section 6.2 of this chapter, and more specifically in Figure 6-8.

6.1.2. Effects of sonication on the dimension of CNC particles

According to Table 6-1, the hydrodynamic size of nanocrystals, obtained from Zetasizer measurements, decreases drastically as the CNC suspension is sonicated from 0 to 1000 J/g of CNC. However, no significant change is seen by increasing the sonication energy input to 3000 J/g of CNC. We have also measured the hydrodynamic size of samples subjected to higher amounts of ultrasound energy, confirming that the hydrodynamic size does not change any further (a size value of 35 nm was measured for a sample with 5000 J/g of CNC sonication). The particle size measured by zetasizer is expressed in terms of

equivalent spherical diameter and in case of rod-like CNC particles, the measured equivalent hydrodynamic size does not give any information about the particle shape factor and the results can only be used for comparison.

To further study the effect of sonication on the dimension of CNC particles, TEM analysis has been performed on two different samples sonicated with different amounts of ultrasound energy input (see Figure 6-5). According to the TEM micrographs shown in Figure 6-5, the dimension of CNC rods in a suspension sonicated for 1000 J/g of CNC (Figure 6-5-a) is practically the same as that for the one sonicated for 3000 J/g of CNC (Figure 6-5-b). This shows that CNC rods do not break during sonication, which confirms the results presented by Beck et al. (2010). They found that the energy applied using typical ultrasound treatment (less than 5000 J/g of CNC) is insufficient to break the covalent sulfate ester-cellulose bonds at room temperature. Therefore, the size change observed from Zetasizer measurements (Table 6-1) can be attributed to breakage of aggregates, but not the individual rods themselves.

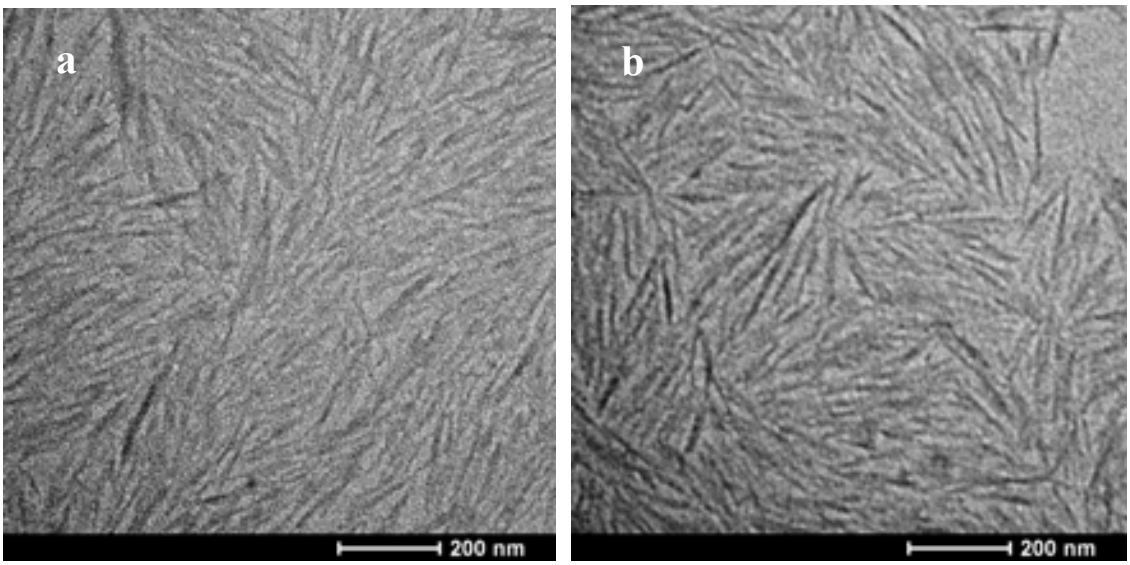

Figure 6-5: TEM micrographs of CNC suspensions sonicated at 1000 J/g CNC (a), and 3000 J/g CNC (b).

6.2. Effects of sonication on shear rheology

To study the effect of ultrasound energy input on the rheological behaviour of CNC suspensions, ultrasound energy in the range from 0 to 5000 J/g of CNC has been applied to various suspensions and their steady-state shear viscosity has been measured. Figure 6-6 depicts the results for 5 wt.% (Figure 6-6-a), and 7 wt.% (Figure 6-6-b) CNC aqueous suspensions. As seen in Figure 6-6, samples before sonication behave like a gel and exhibit shear thinning over the whole shear rate range investigated; by applying ultrasound energy the viscosity drops significantly and its profile changes to one exhibiting three distinct regions, a rheological behaviour typical to that of a lyotropic liquid crystal polymer (Onogi and Asada 1980). Sonication breaks up the gel structure of these high concentration samples, and disperses the individual CNC nano-rods. Thus, the liquid crystal phase formation is not inhibited by gelation anymore, and the samples show liquid crystalline behaviour, namely exhibiting all three distinct regions in their viscosity profiles.

The viscosity decrease is more significant at lower ultrasound energy inputs (levels of sonication). In fact, the viscosity values of the unsonicated samples differs more than two orders of magnitude compared to those of the sample sonicated at 500 J/g of CNC (smallest level used). According to Figure 6-6, although the decrease in viscosity begins to level off at higher energy inputs, it is still significant in the first shear thinning region of the viscosity profiles. This suggest that applying a higher amount of ultrasound energy still affects the structure and size of chiral nematic liquid crystalline domains, which are responsible for the rheological behaviour of shear thinning in the first flow region.

ζ-potential measurements listed in Table 6-1 showed that sonication lowers the hydrodynamic size of CNC particles. However, sonication levels above 1000 J/g of CNC does not significantly change the particle size (Figure 6-5), while still decreasing the viscosity of the sample which has been also reported by Dong et al. (1998) who found that sonication treatments longer than 5 min did not further decrease the CNC particle size, although it did affect the liquid crystal behaviour of the CNC aqueous suspensions. We have also observed change in viscosity due to application of higher amounts of ultrasound energy, which is more significant in the first region of the viscosity profile

(low shear rates). This is clearly attributed to changes in the size and structure of chiral nematic domains.

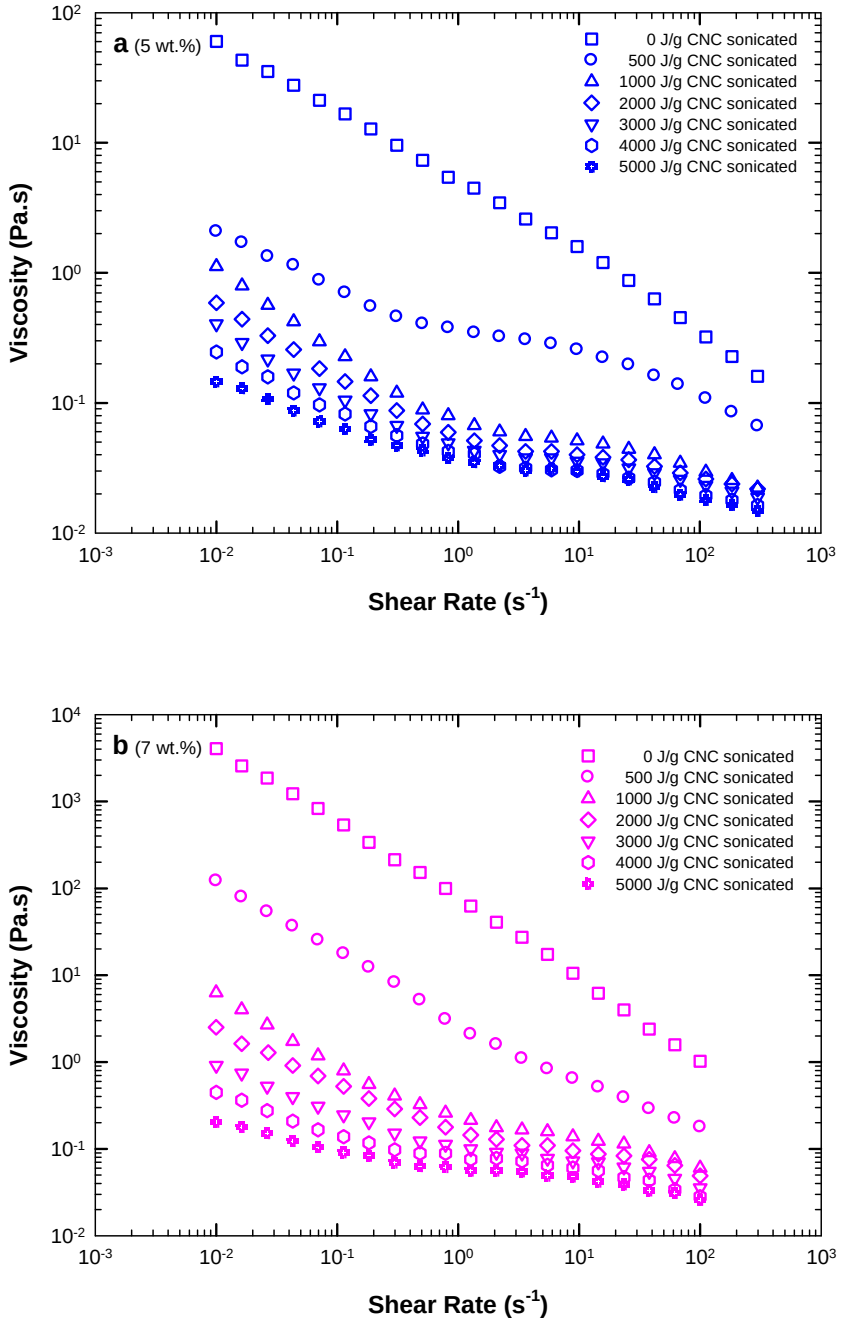

Figure 6-6: Effects of ultrasound energy input (level of sonication) on the viscosity material function of (a) 5 wt.%, and (b) 7 wt.% CNC aqueous suspensions.

To further investigate this, we used polarized optical microscopy. Micrographs of samples at various levels of sonication are shown in Figure 6-7. The micrograph of unsonicated 7 wt.% CNC sample (Figure 6-7-a) shows a birefringent gel. By applying 500 J/g of CNC ultrasound energy, the gel breaks and some liquid crystal domains with fingerprint textures, characteristic of chiral nematic structure, are detectable (Figure 6-7-b). It can be seen that by further increasing the amount of energy input, the size of chiral nematic domains becomes larger with larger pitch, and hence shearing of these larger domains with weaker chiral interactions is easier. This consequently causes a decrease in viscosity. Increase in the pitch of the chiral nematic domains with increasing levels of sonication has been also reported in CNC solid films (Beck et al. 2010). The mechanism proposed for this increase in chiral nematic domain size, has been evaluated to be electrostatic in nature. In other word, applied ultrasound energy ejects the remaining excess ions from the layer around the CNC charged particles, thereby expanding the electrical double layer which results in a weaker chiral interaction between particles. Therefore, the chiral nematic ordering uncoils and ordered domains with larger size and having larger pitch will be formed in the suspension.

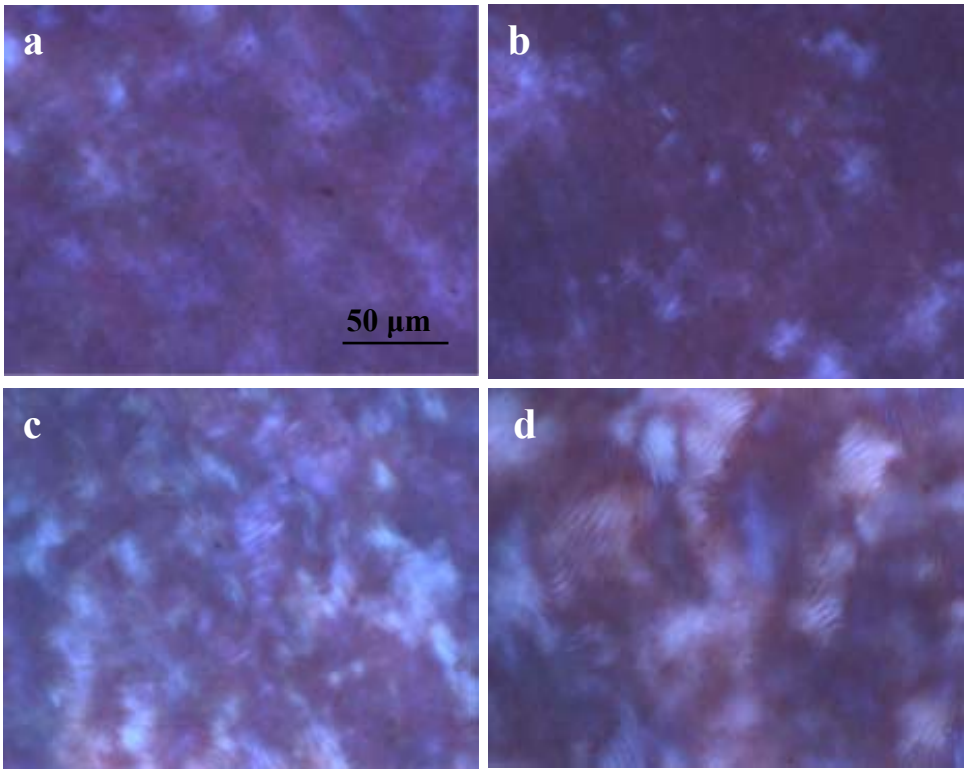

Figure 6-7: Polarized optical micrographs of 7 wt.% CNC aqueous suspensions at rest; (a) unsonicated sample, (b) sample sonicated at 500 J, (c) sample sonicated at 1000 J, and (d) sample sonicated at 2000 J energy applied per gram of CNC in suspension.

A schematic showing the mechanism by which sonication may affect the CNC properties and the resulted liquid crystalline structure is shown in Figure 6-8. According to Beck et al. (2010), there are some excess ions around CNC particles suspended in water. These ions are originated from acid hydrolysis process that have not been removed during the purification steps. These ions screen the electrical double layer of particles in the suspension, and thus decreasing the electrostatic repulsions between particles. Application of ultrasound energy ejects the ions into the bulk suspension, resulting in a larger electrical double layer and stronger repulsive interaction.

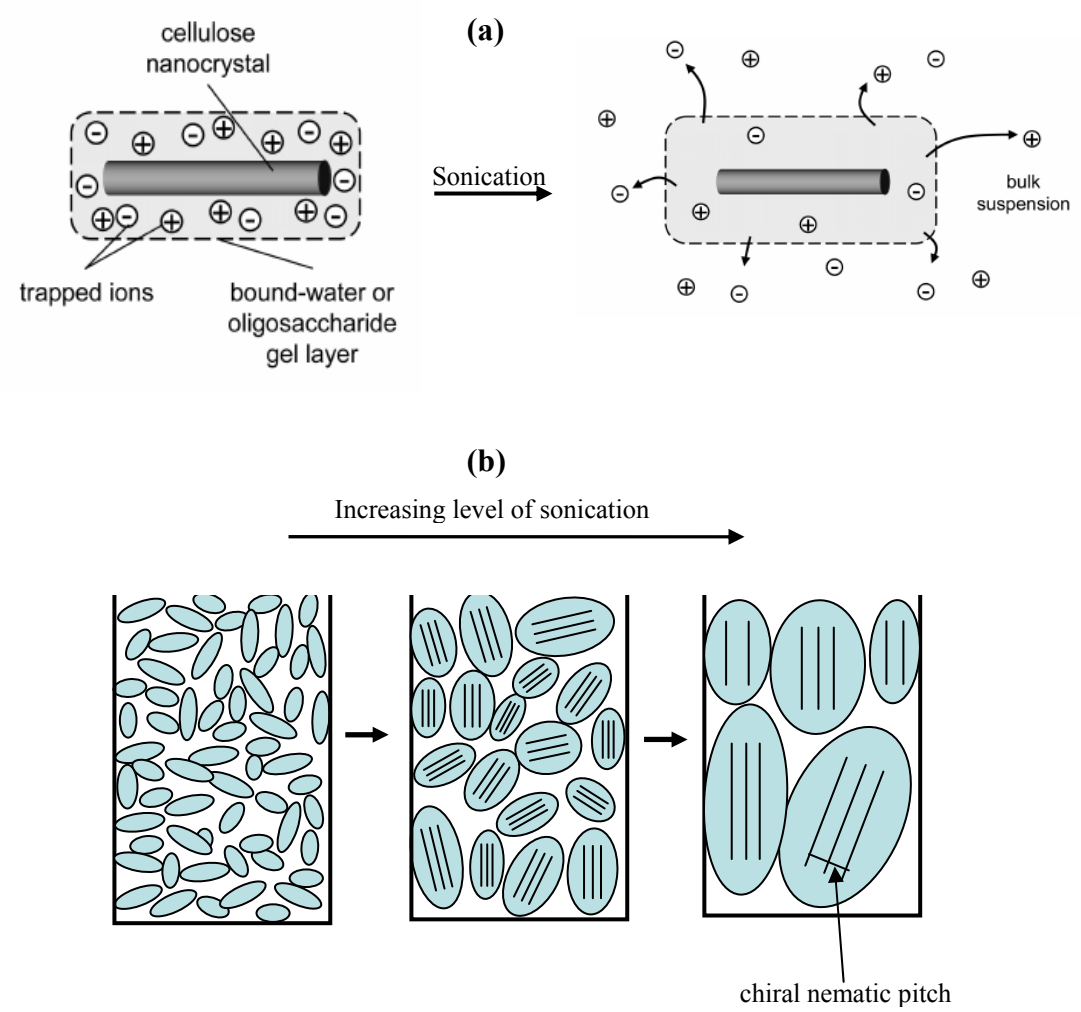

Figure 6-8: Schematic illustration of (a) the mechanism by which sonication affects the surface properties of CNC particles (adapted from Beck et al. 2010), and (b) the resulting chiral nematic liquid crystal ordered domains in CNC aqueous suspensions.

6.3. Effect of sonication on viscoelastic properties

Isothermal dynamic frequency sweep measurements have been done for CNC suspensions before and after sonication and the results are shown in Figure 6-9 for four different concentrations, namely 3, 5, 7, and 10 wt.%. The behaviour of the 3 wt.% CNC suspension (Figure 6-9-a) is typical of a viscoelastic liquid-like material before and after sonication, as can be concluded from the storage modulus, G', and loss modulus, G" (G">G' over the whole investigated frequency range). For 5 wt.% CNC suspensions (Figure 6-9-b), the behaviour of the material is gel-like, where G' and G" overlap over an

extended range of frequency, before sonication, and changes to viscoelastic liquid-like after sonication. In the case of 7 wt.% and 10 wt.% CNC suspensions (Figure 6-9-c and d), the behaviour of unsonicated samples resembles that of a viscoelastic solid, where the G′ is independent of frequency and significantly higher than G″ over the whole investigated frequency domain. The corresponding sonicated samples exhibit gel-like behaviour. As can be seen in Figure 6-9, the frequency range is shortened after sonication (less points at high frequencies) particularly for lower concentration samples. The reason is, due to inertia effect, the rheometer fails to measure the complex viscosity above a critical frequency. This critical frequency is lower for samples with lower viscosities (Schrag 1997). Sonication decreases the viscosity of suspension, which lowers the angular frequency up to which valid data can be obtained.

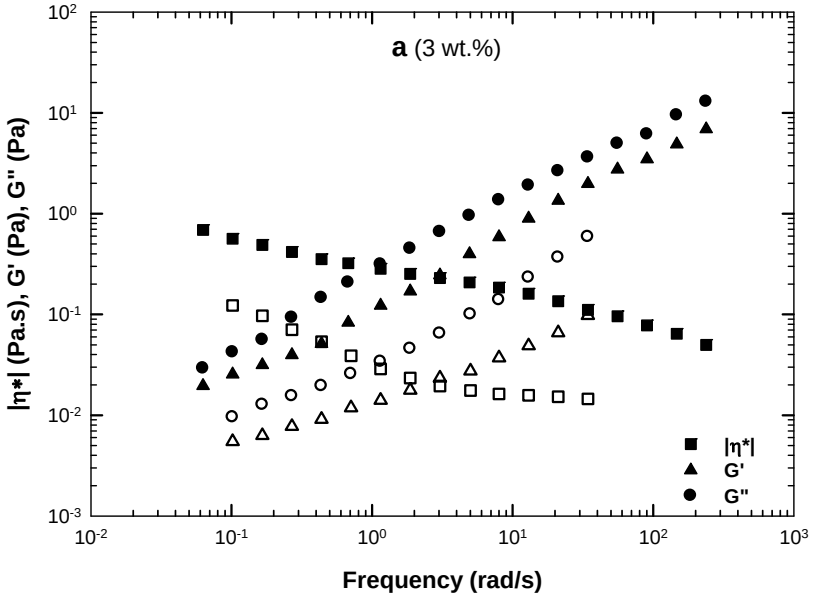
a (3 wt.%)
|η*| (Pa.s), G' (Pa), G'' (Pa)
Frequency (rad/s)
|η*|
G'
G''

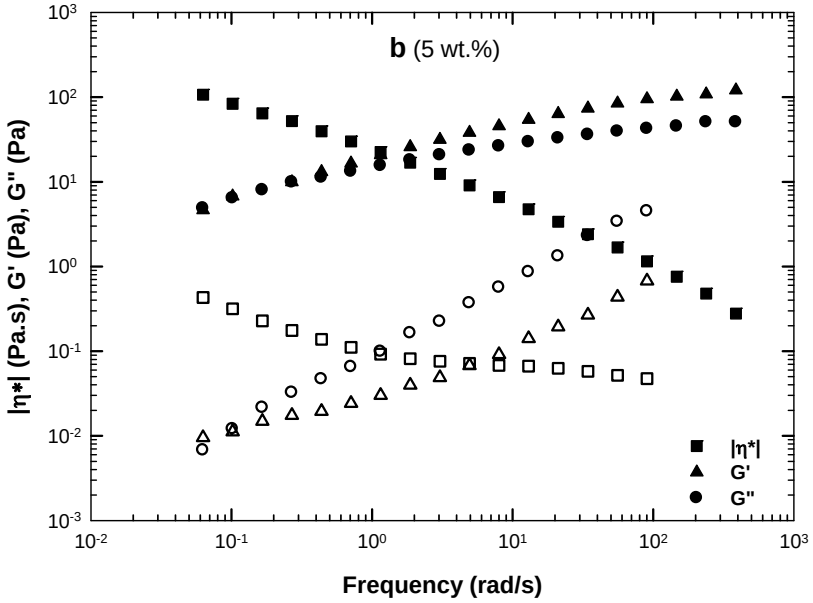
b (5 wt.%)
|η*| (Pa.s), G' (Pa), G'' (Pa)
Frequency (rad/s)
|η*|
G'
G''

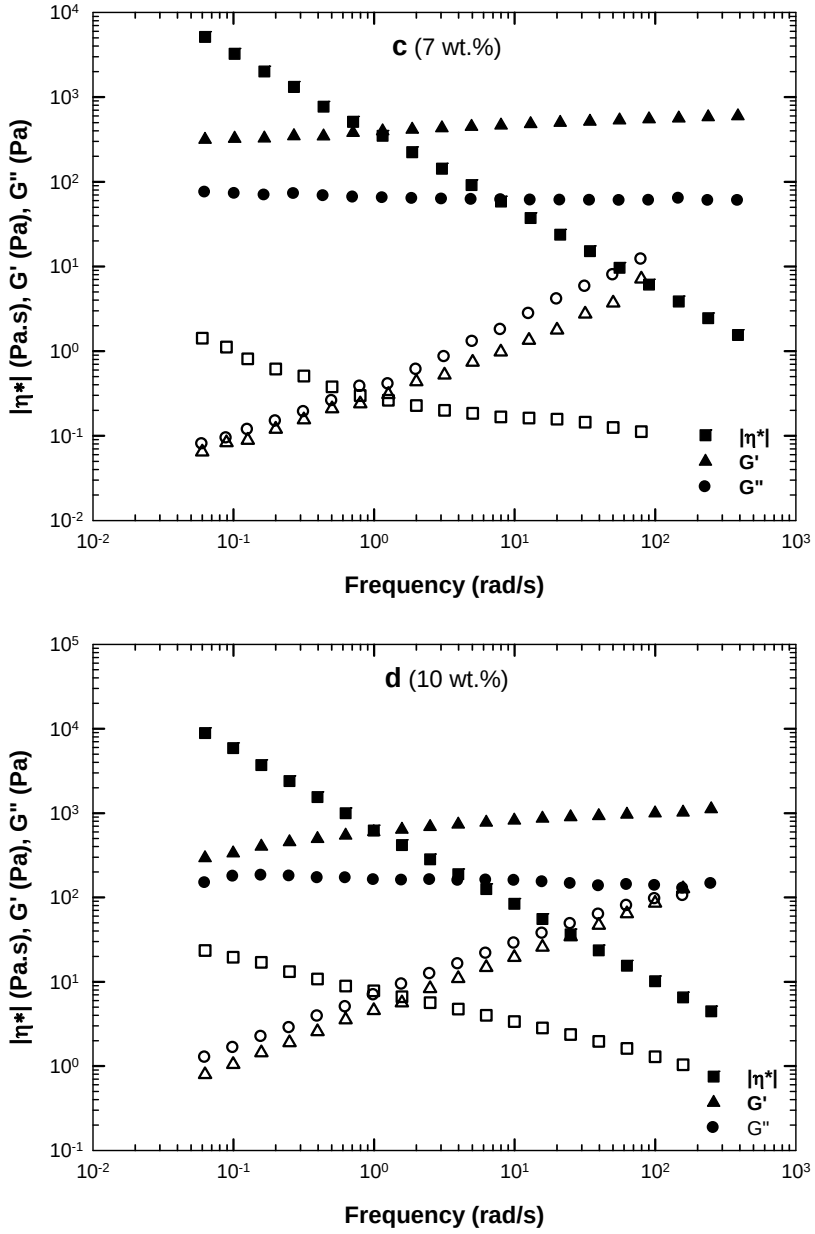

Figure 6-9: Complex viscosity $|\eta^*|$ (■), storage modulus G' (▲), and loss modulus G" (●) versus angular frequency of unsonicated (solid symbols) and sonicated at 1000 J/g of CNC (open symbols) of (a) 3 wt.%, (b) 5 wt.%, (c) 7 wt.%, and (d) 10 wt.% of CNC aqueous suspensions.

6.4. Effects of sonication on the applicability of Cox-Merz rule

One of the rheological characteristics of lyotropic liquid crystals and gels is that the Cox−Merz rule is not obeyed; i.e., the steady-state viscosity $|\eta(\dot{\gamma})|$ and complex viscosity $|\eta^*(\omega)|$ are not equal when compared at the same shear rate $\dot{\gamma}$ and frequency ω (Davis et al. 2004, Urena-Benavides et al. 2011). To study the applicability of the Cox−Merz rule, the complex and steady shear viscosities of CNC suspensions at different concentrations for unsonicated and sonicated (1000 J/g of CNC) samples were compared and plotted in Figure 6-10-a and b, respectively. For unsonicated samples (Figure 6-10-a), at low concentrations (1−3 wt %), where the system is more isotropic, the Cox−Merz rule nearly applies. This shows that there is minimal structural formation at these levels of concentration, which is in agreement with the results from polarized microscopy. At higher concentrations, significant deviations from the Cox−Merz rule is observed, which is clearly attributed to gel-like structural development due to the existence of aggregates in the unsonicated samples. Shear flow breaks these aggregates and affects the structure, and therefore, the dynamic low strain data do not follow the steady-state shear data. In the case of sonicated samples (Figure 6-10-b), applied ultrasound energy breaks the gel structure and the deviation from Cox−Merz rule decreases especially for higher concentrations. The higher concentration samples (5 and 7 wt %) deviate from this rule, which can be attributed to the existence of ordered domains in the system that are sensitive to shear flow. This is consistent with the viscoelastic properties and also polarized microscopy images of the corresponding samples.

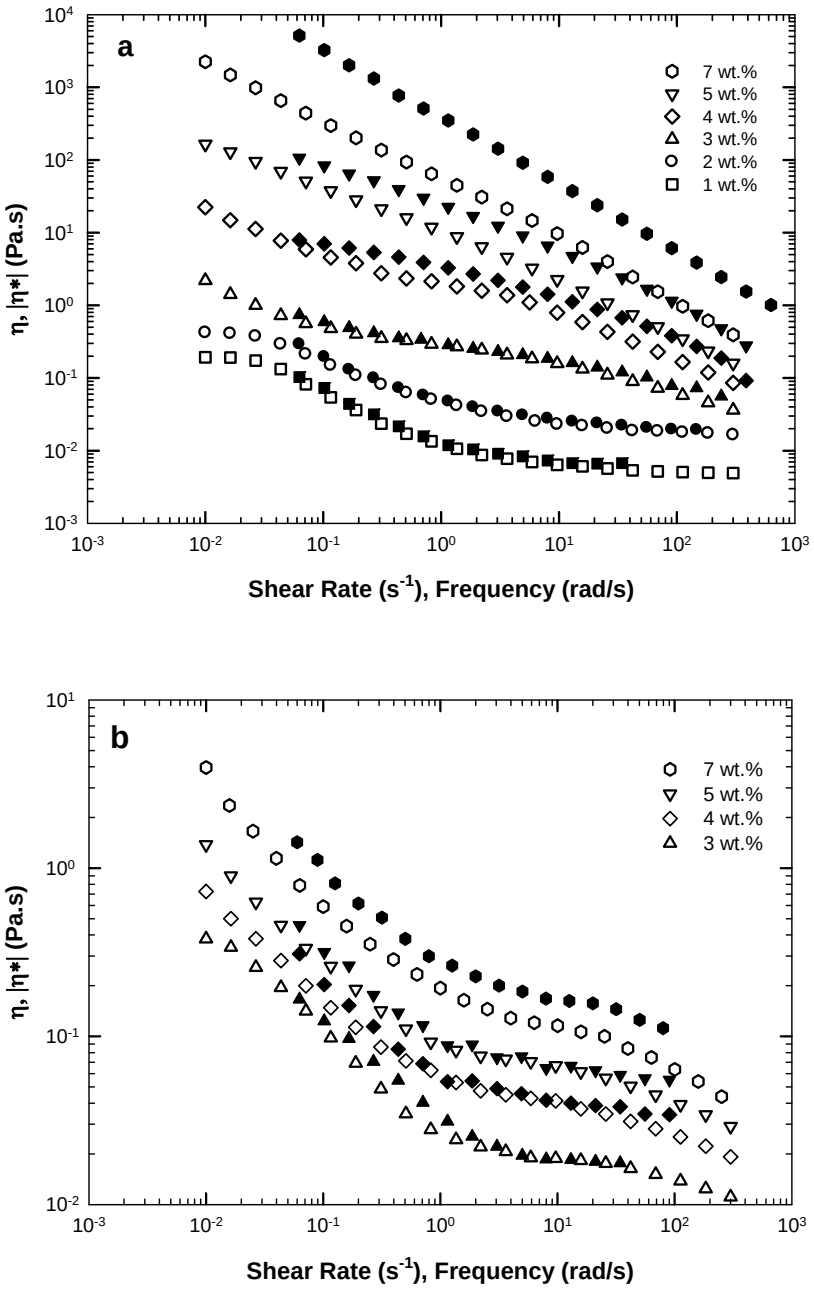

Figure 6-10: Cox-Merz rule comparison of (a) unsonicated and (b) sonicated at 1000 J/g of CNC samples at different concentrations. The open symbols represent the steady shear viscosity, and the solid symbols represent complex viscosity. Failure of this rule indicates significant structural formation.

6.5. Summary

Based on the results and discussion in this chapter, it can be concluded that, for concentrated CNC aqueous suspensions, application of ultrasound energy breaks the aggregates in the system and disperses CNC particles thoroughly. By further sonication, larger chiral nematic ordered domains with larger pitch size are formed. The sonication-induced microstructure changes, been confirmed here by polarized microscopy experiments, result in changes in rheological behaviour of CNC suspensions. To obtain the optimum condition of sonication prior to experimental testing, ultrasonic treatment has been done at different ultrasound energy levels and the variation of viscosity as a function of shear rate has been measured for same samples subjected to different amounts of sonication. The shear viscosity of the samples has shown a significant decrease after sonication comparing to that before sonication. The optimum condition was determined as that for which the same variation of viscosity with shear rate was obtained. Based on the reported results, we chose the 1000 J/g of CNC sonication to be an optimum level of sonication for further rheological evaluation, since this level of energy input was shown to be sufficient for breaking any aggregate in the system and beyond this level of energy the viscosity profile of samples does not change its shape especially at intermediate and high shear rate regions.

CHAPTER 7: EFFECTS OF TEMPERATURE ON THE MICROSTRUCTURE AND RHEOLOGY OF CNC AQUEOUS SUSPENSIONS[4]

7.1. Effects of temperature on rheology of CNC suspensions

Knowing that any change in the microstructure of the sample directly affects its rheological behaviour, the rheological properties of CNC suspensions have been measured at different temperatures in this thesis work in order to study the effects of temperature on the microstructure of these suspensions. The results of steady shear viscosity at different temperatures (10 to 50 ºC) for concentrations of 3, 5, 7, and 10 wt.% CNC are presented in Figures 7-1, 7-2, 7-3 and 7-4, respectively. For 3 wt % CNC suspension (Figure 7-1), the viscosity decreases with increasing temperature at all shear rates. This is expected for a low-concentration suspension that contains a very small amount of ordered domains and can be considered as predominantly isotropic. For 5 and 7 wt % CNC suspensions (Figures 7-2 and 7-3), where the amounts of ordered domains increase and suspensions become predominantly anisotropic, a three-region behaviour is apparent at all tested temperatures. By increasing the temperature from 10 to 50 ºC, the viscosity of the sample decreases in regions II and III. However, in region I (low shear rates) the viscosity of the sample decreases as the temperature increases from 10 ºC to 30 ºC, but surprisingly, a sudden increase in the viscosity is observed at 40 °C. This change in the viscosity at the first shear-thinning region is thought to be due to changes in the microstructure (which will be further discussed in the next section of this chapter). For the 10 wt % CNC suspension (Figure 7-4), the viscosity is independent of temperature between 10 and 40 °C suggesting that the temperature does not affect the mesogen rearrangement up to 40 °C. However, a marked increase in viscosity is observed at 50 °C, particularly at low shear rates. The origin for this temperature-induced viscosity increase for the high-concentration samples is thought to be due to formation of more packed chiral nematic domains with lower pitch size at higher temperature, which has been previously reported by Pan et al. (2010) for CNC solid films. Our results at intermediate

[4] A version of this chapter is published: Shafiei-Sabet, S., Hamad, W. Y., and Hatzikiriakos, S. G. Langmuir, 28, 2012.

and high shear rates are in agreement with those reported by Urena-Benavides et al. (2011) although they have not reported any data at lower shear rates.

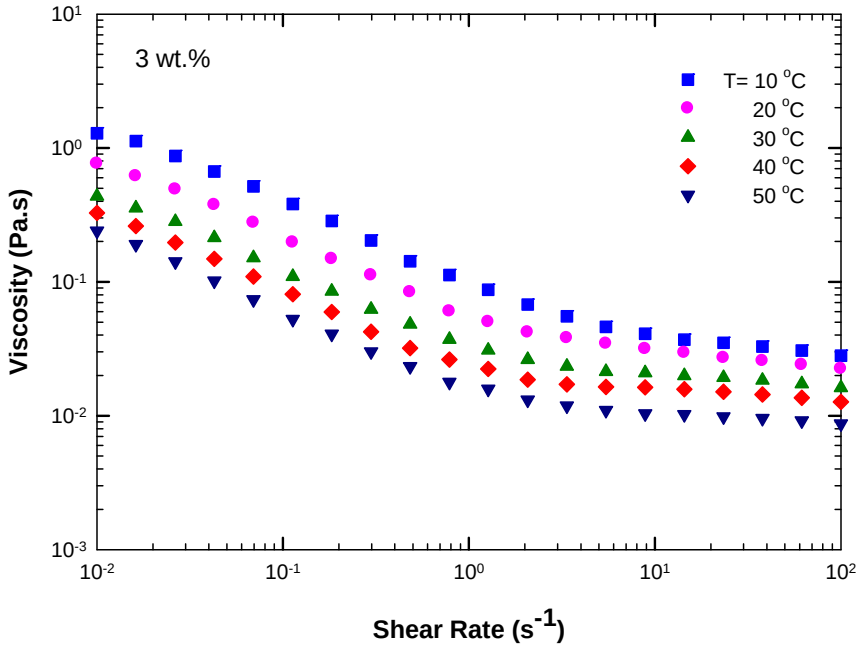

Figure 7-1: Steady shear viscosity versus shear rate of 3 wt.% CNC aqueous suspensions, sonicated at 1000 J/g of CNC, at various temperatures from 10 to 50 °C.

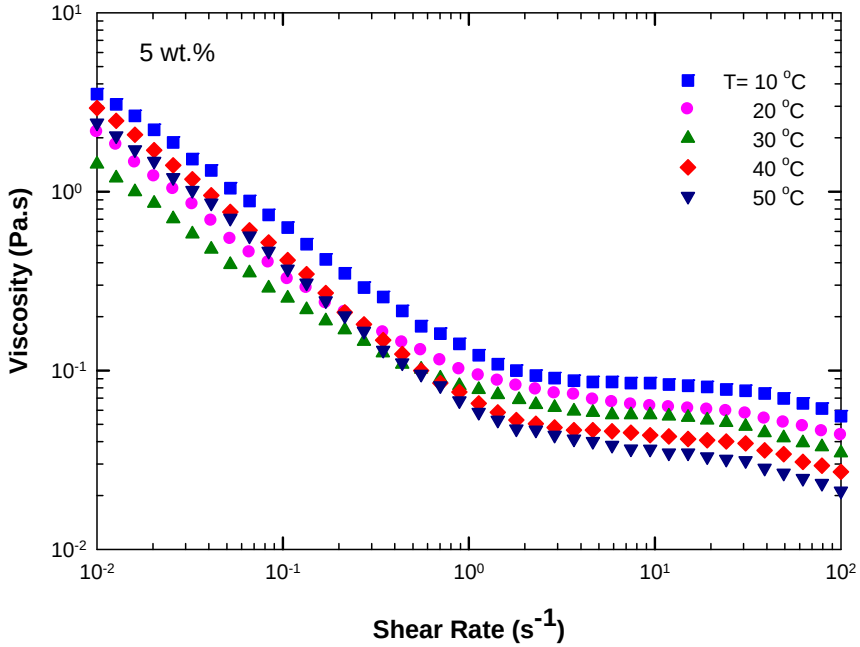

Figure 7-2: Steady shear viscosity versus shear rate of 5 wt.% CNC aqueous suspensions, sonicated at 1000 J/g of CNC, at various temperatures from 10 to 50 °C.

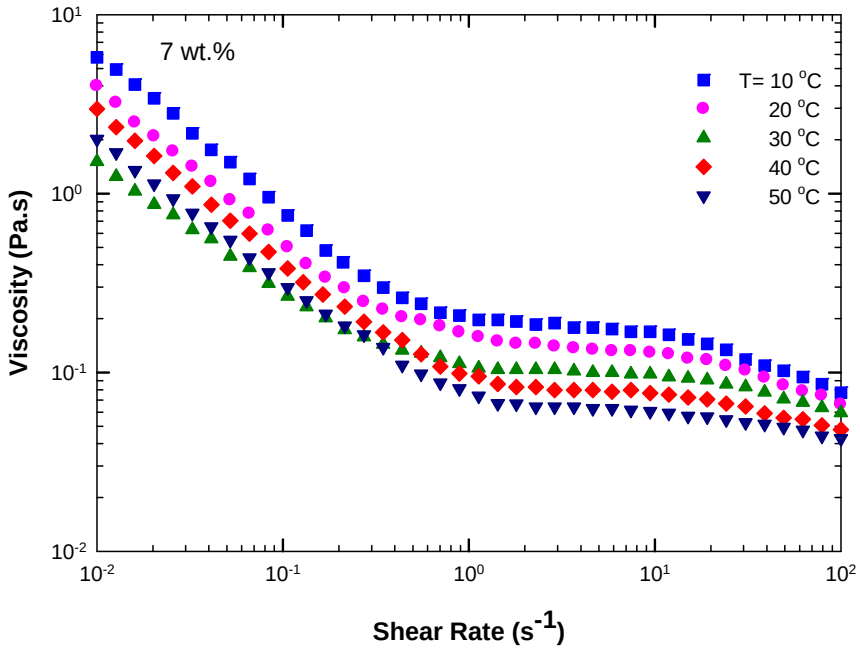

Figure 7-3: Steady shear viscosity versus shear rate of 7 wt.% CNC aqueous suspensions, sonicated at 1000 J/g of CNC, at various temperatures from 10 to 50 °C.

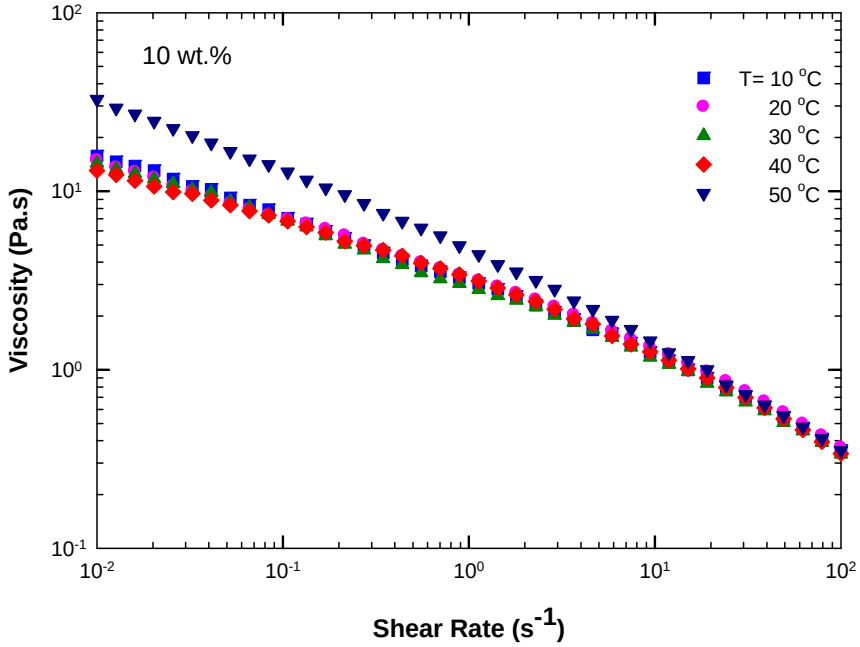

Figure 7-4: Steady shear viscosity versus shear rate of 10 wt.% CNC aqueous suspensions, sonicated at 1000 J/g of CNC, at various temperatures from 10 to 50 °C.

As mentioned before, increase of temperature resulted in a sudden increase in the viscosity of biphasic suspensions at the first shear thinning region (low shear rates). To further study this observation, dynamic temperature sweep tests were performed at constant shear rates. Figure 7-5 shows the results for 5 wt.% CNC suspension, as this concentration has already shown to be biphasic and have chiral nematic ordered structure. According to Figure 7-5, at low shear rates of 0.1, 0.3, and 0.5 s^{-1}, the viscosity decreases with increasing temperature up to 30 °C. It subsequently exhibits an upturn between 30 and 40 °C, and then decreases again with further increase in temperature. For higher shear rates (1 and 10 s^{-1}), no inflection is observed and viscosity decreases in the whole investigated temperature range. This is consistent with the results indicated in Figures 7-2 and 7-3.

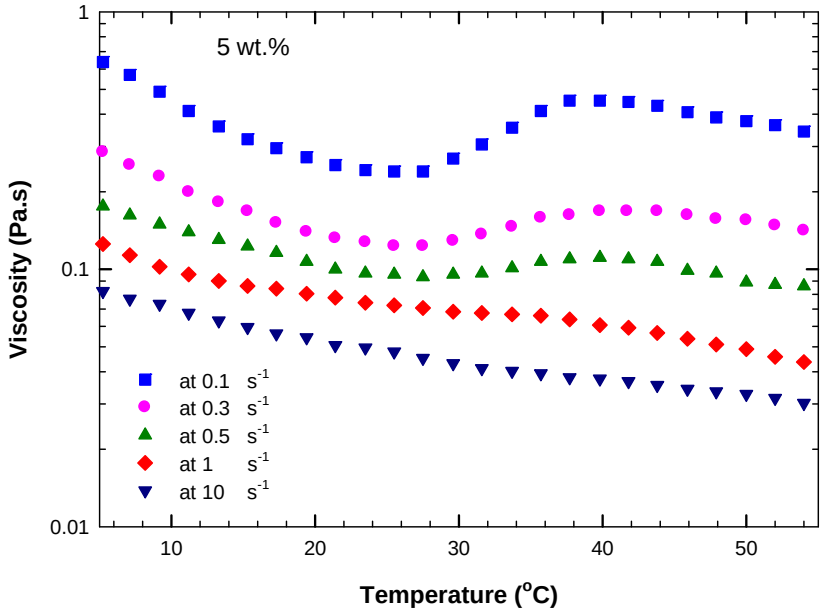

Figure 7-5: Effect of temperature on shear viscosity for a 5 wt.% CNC suspension (sonicated at 1000 J/g of CNC) at different shear rates.

The change in complex viscosity versus temperature for 3, 5, 7, and 10 wt % CNC suspensions are plotted in Figure 7-6. For the 3 wt % CNC sample, the complex viscosity decreases continuously with temperature. For higher concentrations, the complex viscosity decreases with increasing temperature up to a critical value, where the viscosity starts increasing again. This critical temperature occurs at about 42 °C for the 10 wt % CNC suspension, and goes down to about 27 °C for the 5 wt %; a similar value can be obtained from Figure 7-5 for lower shear rates for the 5 wt % CNC suspension. The origin of this minimum can be attributed to microstructural changes; more specifically, a sudden increase in the number of isotropic regions at a specific temperature causes an increase in viscosity (see further discussion in next section).

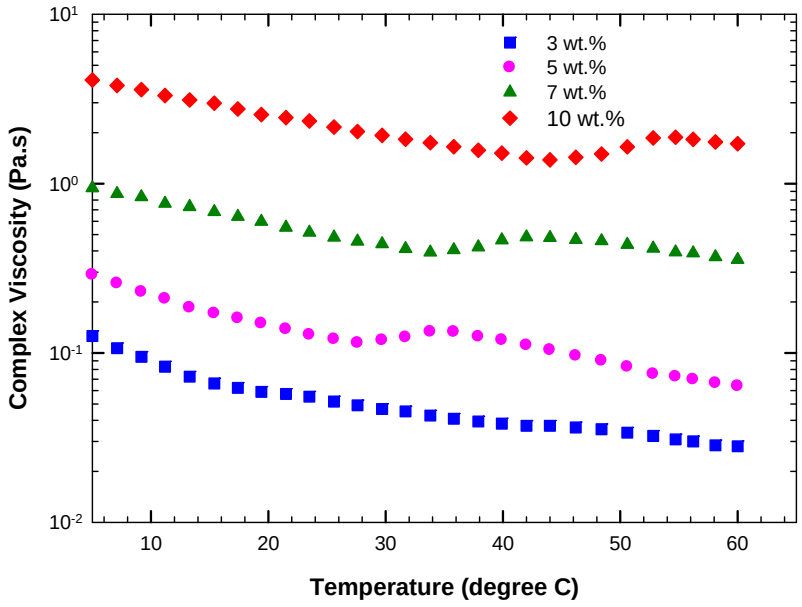

Figure 7-6: Effect of temperature on the complex viscosity of CNC suspensions at various concentrations and at a constant angular frequency of 1 rad/s.

7.2. Effect of temperature on the microstructure of CNC suspensions

To further study the viscosity increase observed for biphasic samples at a critical temperature (Figures 7-5 and 7-6), polarized optical microscopy was used to capture any change in the microstructure of sample while being sheared at different temperatures. POM micrographs of 5 wt. % sample, at a constant shear rate of 0.1 s^{-1} and for different temperatures, are presented in Figure 7-7, where variations in microstructure can be observed particularly at 40 °C.

As can be seen in Figure 7-7, the size of chiral nematic domains decreases by increasing temperature, especially from 30 °C to 40 °C. In other words, at higher temperature, the fraction of isotropic phase increases leading to smaller size chiral nematic ordered phase with more packed structure with lower pitch size (Pan et al. 2010). This sudden increase in the number of isotropic regions at a specific temperature causes an increase in viscosity. Change in viscosity due to change in the relative fractions of isotropic and liquid crystalline regions at different temperatures has previously been reported (Papkov et al. 1974). The POM micrographs in Figure 7-7 thus confirm that the observed

minimum in viscosity versus temperature at a given shear rate or frequency is not an experimental artifact.

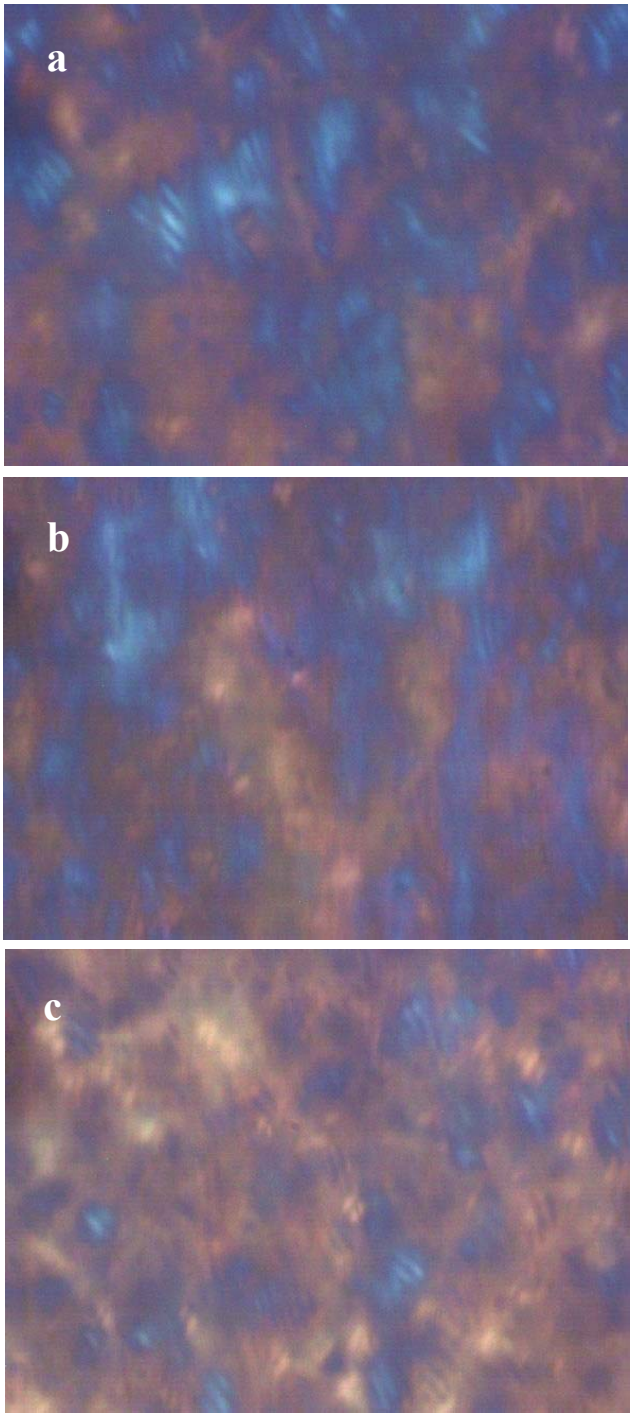

Figure 7-7: Polarized optical micrographs at (a) 20 °C, (b) 30 °C, and (c) 40 °C of 5 wt.% CNC suspension under constant shear rate of 0.1 s^{-1}.

7.3. Summary

Based on the results and discussion in this chapter, it can be concluded that for isotropic CNC suspensions (low concentrations) the viscosity decreases with increasing temperature. The viscosity versus temperature for biphasic CNC suspensions (above the critical concentration for isotropic to chiral nematic transition), at low shear rates, shows a sudden upturn at a critical temperature (between 30 and 40 ºC). This upturn in the low shear rate viscosity has been shown to be due to formation of more packed chiral nematic ordered domains at the critical temperature. The formation of smaller size chiral nematic ordered domains and change in the fraction of isotropic phase at higher temperatures has been visualized by polarized light microscopy.

CHAPTER 8: EFFECTS OF DEGREE OF SULFATION ON THE MICROSTRUCTURE AND RHEOLOGY OF CNC AQUEOUS SUSPENSIONS[5]

As discussed before, CNC aqueous suspensions prepared by sulfuric acid hydrolysis are electrostatically stabilized due to anionic sulfur half ester groups on the surface of nanocrystals. By increasing the CNC concentration, the suspension experiences two different transitions, namely, isotropic to chiral nematic liquid crystal above a first critical concentration (Marchessault et al. 1961, Revol et al. 1992, Dong et al. 1996) and chiral nematic liquid crystal to gel above a second critical concentration (Liu et al. 2011, Urena-Benavides et al. 2011). These microstructural transitions, which control the macroscopic flow behaviour of the material, strongly depend on the physical dimension and surface charge of CNC particles and also on the ionic strength of the system (Onsager 1949, Odjik 1986, Dong et al. 1998, Hamad and Hu 2010). In this chapter, the effects of degree of sulfation of CNC particles on these transitions are studied using rheometry and polarized optical microscopy. To do so, two different sets of CNC aqueous suspensions (CNC-A and CNC-B), hydrolyzed to produce different degrees of sulfation, are prepared and their microstructure and rheology are studied over a broad range of concentrations (1 to 15 wt. %). The hydrolysis condition used to prepare these sets of CNC suspensions is summarized in Table 8-1.

Table 8-1: Hydrolysis conditions for CNC suspensions with different degrees of sulfation (provided by FPInnovations)

Property / Sample	Pulp Source	Pulp Consistency (%)	Acid/Pulp (ml/g)	Reaction Temperature (ºC)	Reaction Time (min)	Final Sample wt.%	Yield (%)
CNC-A	BSKP	96.6	8.75	45	25	1.98	21
CNC-B	BSKP	96.4	6.00	45	25	3.80	32

[5] A version of this chapter is published: Shafiei-Sabet, S., Hamad, W. Y., and Hatzikiriakos, S. G. Rheol Acta, 52, 2013.

8.1. Characterization of CNC-A and CNC-B suspensions

During H_2SO_4 hydrolysis, anionic sulfuric ester groups ($SO3^-$) are introduced on the surface of cellulose nanocrystals. Physico-chemical properties of two sets of CNC, prepared to study the effect of degree of sulfation, characterized by elemental analysis and zetasizer measurements are reported in Table 8-2.

Table 8-2: Physico-chemical characteristics of CNC-A and CNC-B suspensions (provided by FPInnovations).

Property / Sample	Particle Size (nm) (based on equivalent hydrodynamic volume measured by Zetasizer)	Electrophoretic mobility (μm cm/(V.s))	Sulfur Content (wt.%)	OSO_3H /100 anhydroglucose units
CNC-A	48.4	-1.377	0.85	4.39
CNC-B	46.0	-3.834	0.69	3.55

Elemental analysis of the two sets of CNC suspensions under study yielded 0.85 and 0.69 wt. % S, which leads to 4.39 and 3.55 OSO_3H/100 anhydroglucose units for CNC-A and CNC-B, respectively (based on calculations and assumptions in Hamad and Hu 2010). Although CNC-A has higher degree of sulfation, the measured electrophoretic mobility is lower than that of CNC-B. This discrepancy can be attributed to lower PH of the CNC-A sample which affected the zetasizer results. The acid/pulp ratio used to produce CNC-A sample was higher than that of CNC-B (see Table 8-1) which resulted in lower PH of the CNC-A sample and consequently smaller electrophoretic mobility.

Figure 8-1 shows transmission electron microscopy (TEM) of these two samples. As can be seen in Figure 8-1, the size and shape of the nanocrystals are practically the same for CNC suspensions with different degrees of sulfation, thereby allowing to independently examine the effects of surface charge on suspension rheology. The isolated nanocrystals were 7±3 nm wide and 100±8 nm long, giving an average aspect ratio (L/D) in the range 10 to 20.

Both CNC-A and CNC-B suspensions formed chiral nematic liquid crystal structures above a critical concentration of 3 wt. % and 4 wt. %, respectively. Representative

polarized optical micrographs of 7 wt. % CNC-A and CNC-B, with different degrees of sulfation, are shown in Figure 8-2 in which the fingerprint textures, characteristic of chiral nematic liquid crystals, clearly appear.

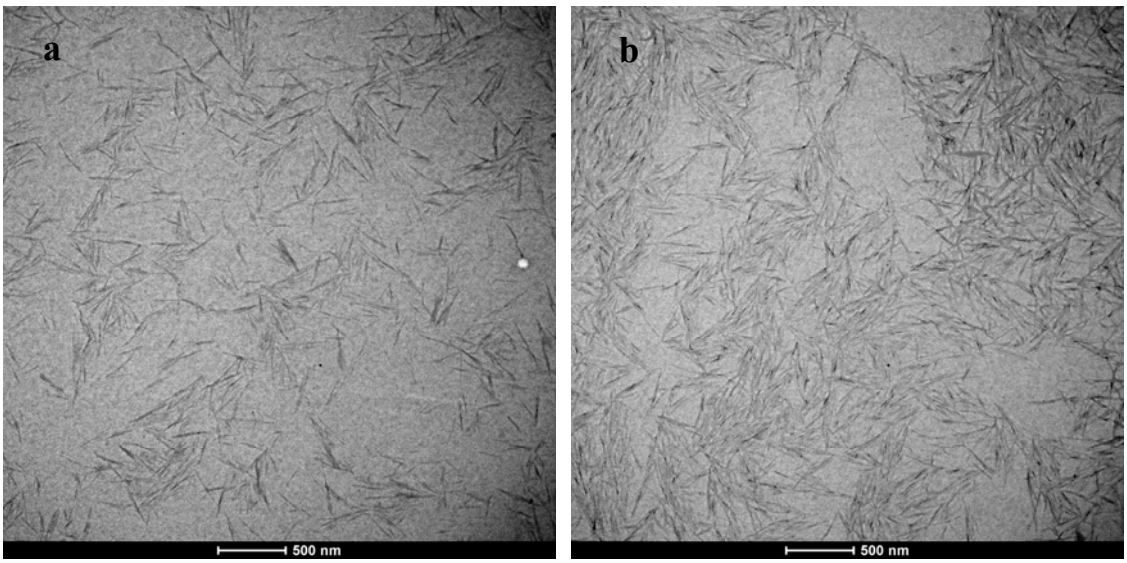

Figure 8-1: TEM micrographs of samples (a) CNC-A, and (b) CNC-B.

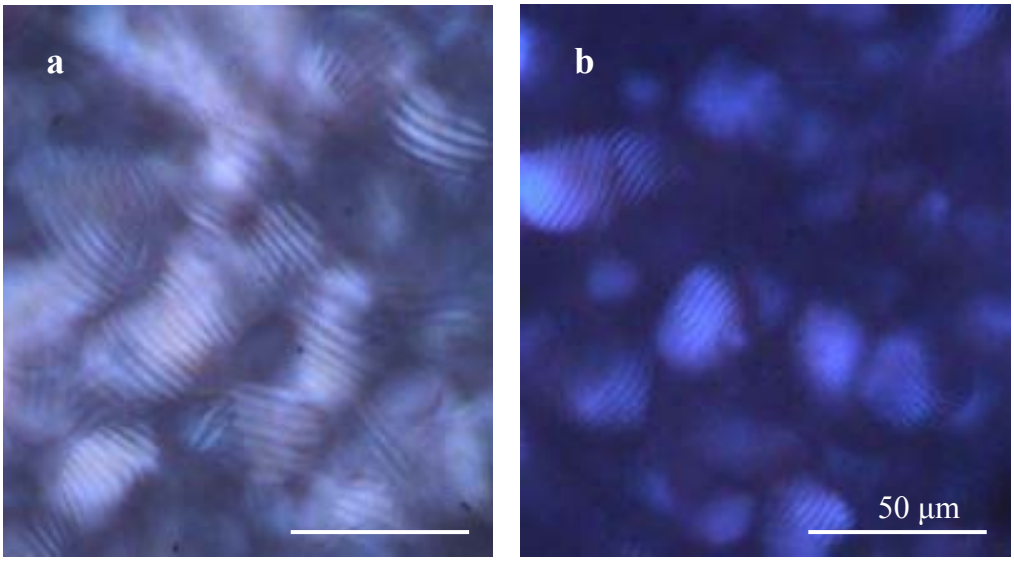

Figure 8-2: Polarized optical micrographs of 7 wt. % (a) CNC-A and (b) CNC-B suspensions at 25℃. Scale bars = 50 µm.

8.2. Shear rheology of CNC-A and CNC-B suspensions

CNC aqueous suspensions at different concentrations were prepared from both CNC-A and CNC-B. To prepare well dispersed CNC suspensions, the samples were sonicated. A systematic study of the effects of sonication on viscosity of CNC suspensions have been presented in chapter 6 of this thesis. Based on the results and discussion in chapter 6, it has been shown that by increasing the amount of applied ultrasound energy (J/g of CNC), the viscosity decreases. This decrease in viscosity is significant up to 1000 J/g of CNC, due to breakage of aggregates in the system. By further increasing the applied sonication energy, the viscosity profile slightly changes with some changes occurring in the liquid crystalline structure. Similar experiments have also been performed in this part of study for CNC-A and CNC-B suspensions, and the results are perfectly consistent with those in chapter 6. All the suspensions prepared for rheological testing in this chapter are sonicated for 1000 J/g of CNC, since it was previously concluded as a level of sonication sufficient to break most of the aggregates.

Figure 8-3 shows the steady-state viscosity curves for 5 wt.% CNC-A (Figure 8-3-a) and CNC-B (Figure 8-3-b) suspensions before and after 1000 J/g of CNC sonication. According to Figure 8-3, the decrease in the viscosity due to sonication is more pronounced in the case of CNC-B possessing a lower degree of sulfation. Lower surface charges cause a decrease in the electrostatic repulsion of nanocrystals, which leads to a higher probability of aggregation. Applied ultrasound energy breaks all these aggregates and the viscosity then drops significantly.

The results of steady-state shear tests on the two different sets of CNC suspensions (CNC-A and CNC-B) at various concentrations ranging from 1 to 15 wt. % are shown in Figures 8-4 and 8-5, respectively. According to the viscosity profiles in these figures, by increasing the concentration, two transitions in the rheological behaviour were observed: (i) a transition from isotropic to liquid crystal, and (ii) a transition from liquid crystal to gel. For CNC-A suspensions (Figure 8-4-a and b), the 1 wt. % CNC suspension behaves like an isotropic sample showing a Newtonian plateau at low shear rates, followed by shear-thinning at intermediate shear rates due to alignment of the nano-rods in the shear direction, and another plateau at high shear rates where all the nano-rods have been

aligned, and therefore no further change in the viscosity occurs (Bercea and Navard 2000). By increasing the concentration above 3 wt .%, liquid crystalline phases are formed in the suspension and the viscosity profile changes to the three-region profile, typical of liquid crystals (Onogi and Asada 1980).

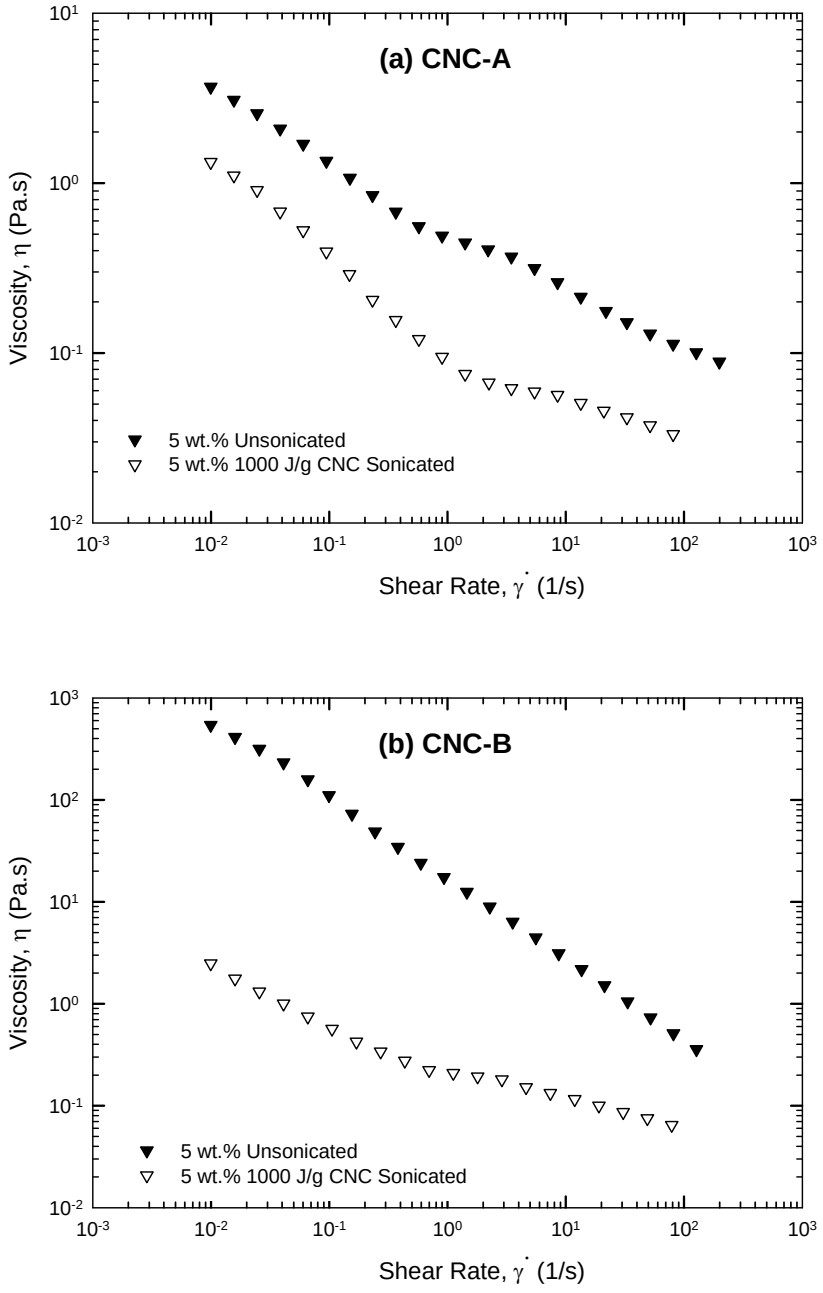

Figure 8-3: Effect of ultrasound energy on the viscosity material function of two different CNC suspensions, (a) CNC-A and (b) CNC-B.

Figure 8-4-a shows that this transition from isotropic to anisotropic chiral nematic liquid crystal for CNC-A occurs at about 3 wt. %, above which the viscosity profile consists of three different regions. Namely, (i) a shear thinning region can be seen at low shear rates (due to alignment of chiral nematic liquid crystal domains), (ii) a plateau at intermediate shear rates, where the domains have been all oriented along the shear direction, and (iii) a second shear thinning region at high shear rates, where liquid crystal domains break and individual nanocrystals orient along the shear flow direction. This miscrostructural change under shear has been confirmed by neutron scattering in a study by Orts et al. (1998) and polarized optical microscopy in Chapters 5 and 6 of this thesis.

By further increasing the CNC concentration (Figure 8-4-b), the viscosity profile goes through another change from a three-region profile to one where a single shear thinning behaviour is observed over the whole range of investigated shear rates. This change can be attributed to another transition from liquid crystal to gel-like structure, where gel formation inhibits the formation of chiral nematic ordered phases. According to Figure 8-4-b, this transition occurs at about 12 wt. % for CNC-A, the suspension possessing high surface charge. More evidence to the gel formation will be presented in section 8.4 of this chapter (linear viscoelastic measurements).

For CNC-B, the suspension with a lower degree of sulfation, rheological measurements (Figure 8-5-a) reveal that the transition from isotropic to anisotropic and the formation of chiral nematic liquid crystals occur at about 4 wt.%, above which the three-region viscosity curves often observed in liquid crystalline CNC suspensions become evident. By further increasing the CNC concentration (Figure 8-5-b), the suspension shows a tendency to form a gel and goes through a second transition, liquid crystal to gel, at about 10 wt. % (relatively at a lower concentration compared with CNC-A). This transition is more clearly shown in section 8.4 of this chapter where the linear viscoelastic moduli of various suspensions are presented.

The tendency of CNC-B suspensions to form gel apparently inhibits the formation of chiral nematic liquid crystal phases at concentrations where they are readily observed for the CNC-A nanocrystals. These results are consistent with studies by Araki et al. (1998

and 1999), who also reported changes in viscosity behaviour of cellulose nanocrystals prepared by different methods. Although the factors governing the relative tendencies of CNC particles to gel rather than form ordered phases are not fully understood, knowing that the dimensions and shape of CNC particles in these two sets of CNC samples are equal (see Figure 8-1). However, it can be concluded that a lower degree of sulfation, which leads to lower electrostatic repulsion, is likely to be the main parameter contributing to gel formation (gelation process).

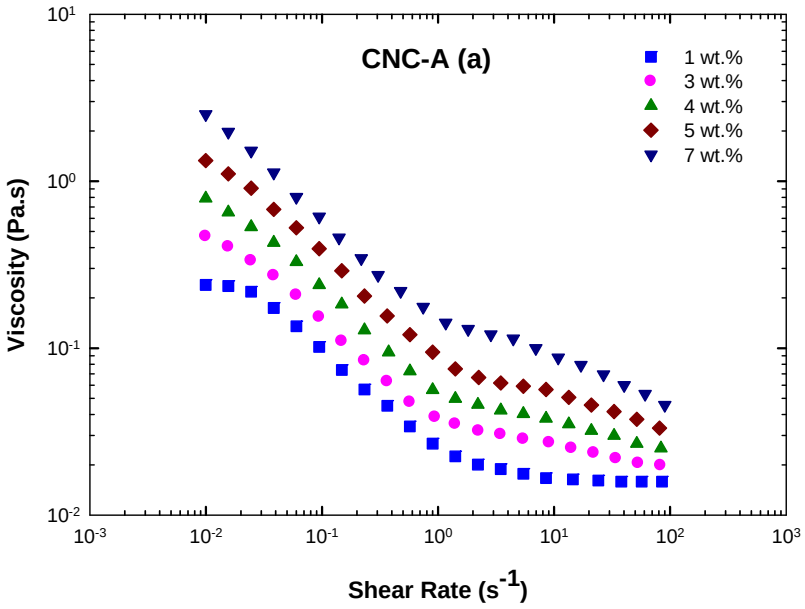

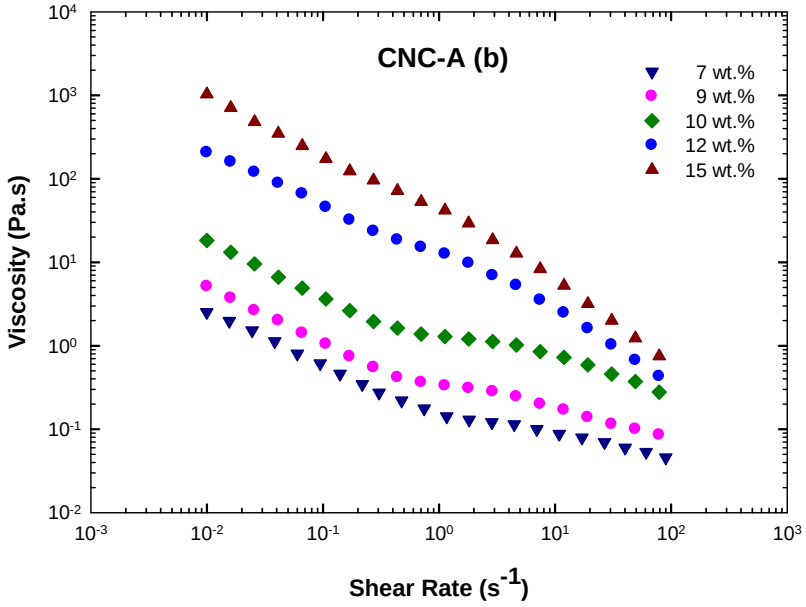

Figure 8-4: The viscosity material function of CNC-A suspensions, sonicated for 1000 J/g of CNC, at concentrations of 1-7 wt.% (a), and 7-15 wt.% (b).

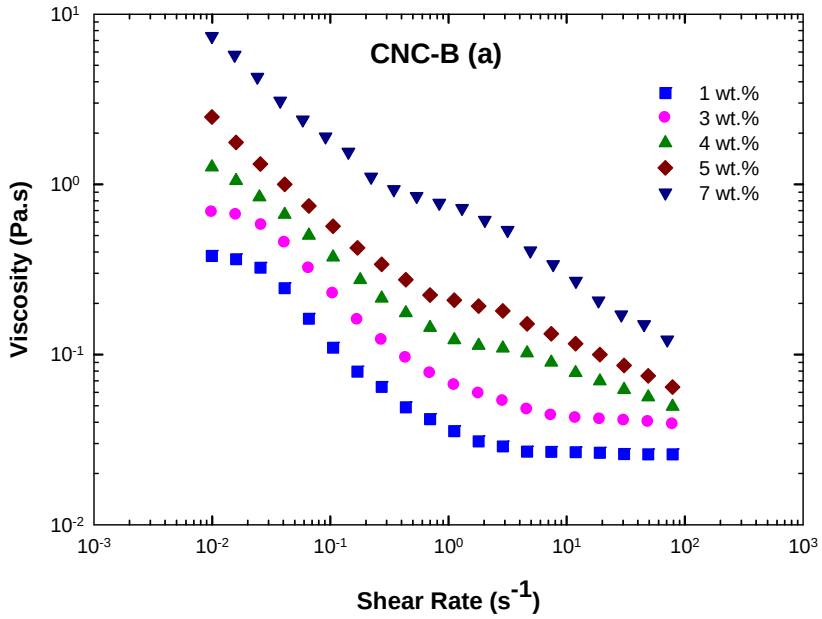

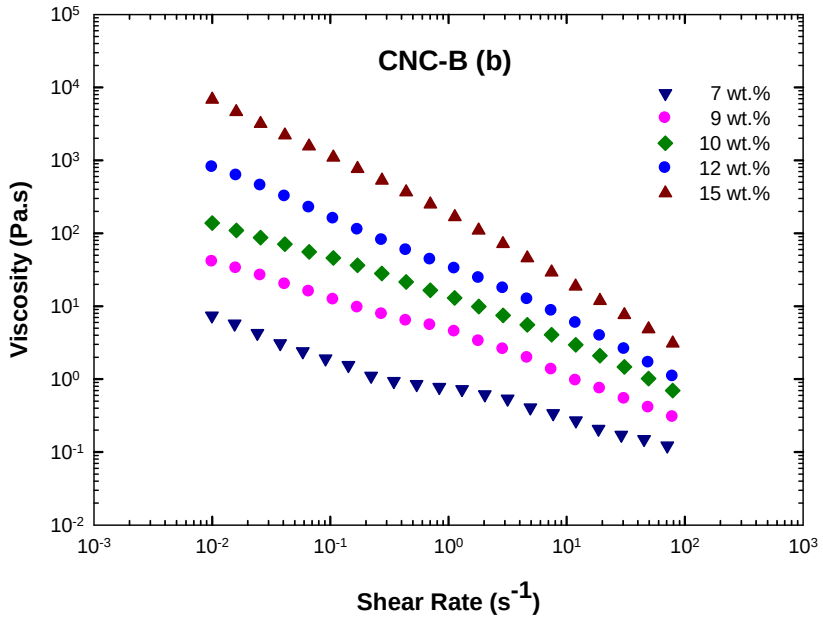

Figure 8-5: The viscosity material function of CNC-B suspensions, 1000 J/g of CNC, at concentrations of 1-7 wt.% (a), and 7-15 wt.% (b).

To follow changes in the structure of these suspensions under shear, polarized optical microscopy has also been used online, coupled with the rheometer, to capture in-situ POM micrographs at various shear rates. Typical micrographs of 9 wt. % CNC-A suspension (a liquid crystalline sample), and a 12 wt. % CNC-A suspension (a gel) are shown in Figures 8-6 and 8-7, respectively. For 9 wt.% CNC-A sample (Figure 8-6), the sample shows fingerprint texture characteristic of chiral nematic ordered domains at 0.01 s^{-1} (micrograph a in Figure 8-6), and by increasing shear rates the ordered domains deform and align in shear direction (micrographs b-e in Figure 8-6) which eventually break down (micrograph f in Figure 8-6 appears black). However, for the 12 wt. % CNC-A sample (Figure 8-7), the sample is a birefringent gel at rest (micrograph a in Figure 8-7), and under shear the gel structure breaks but remains birefringent up to shear rate of 1 s^{-1}.

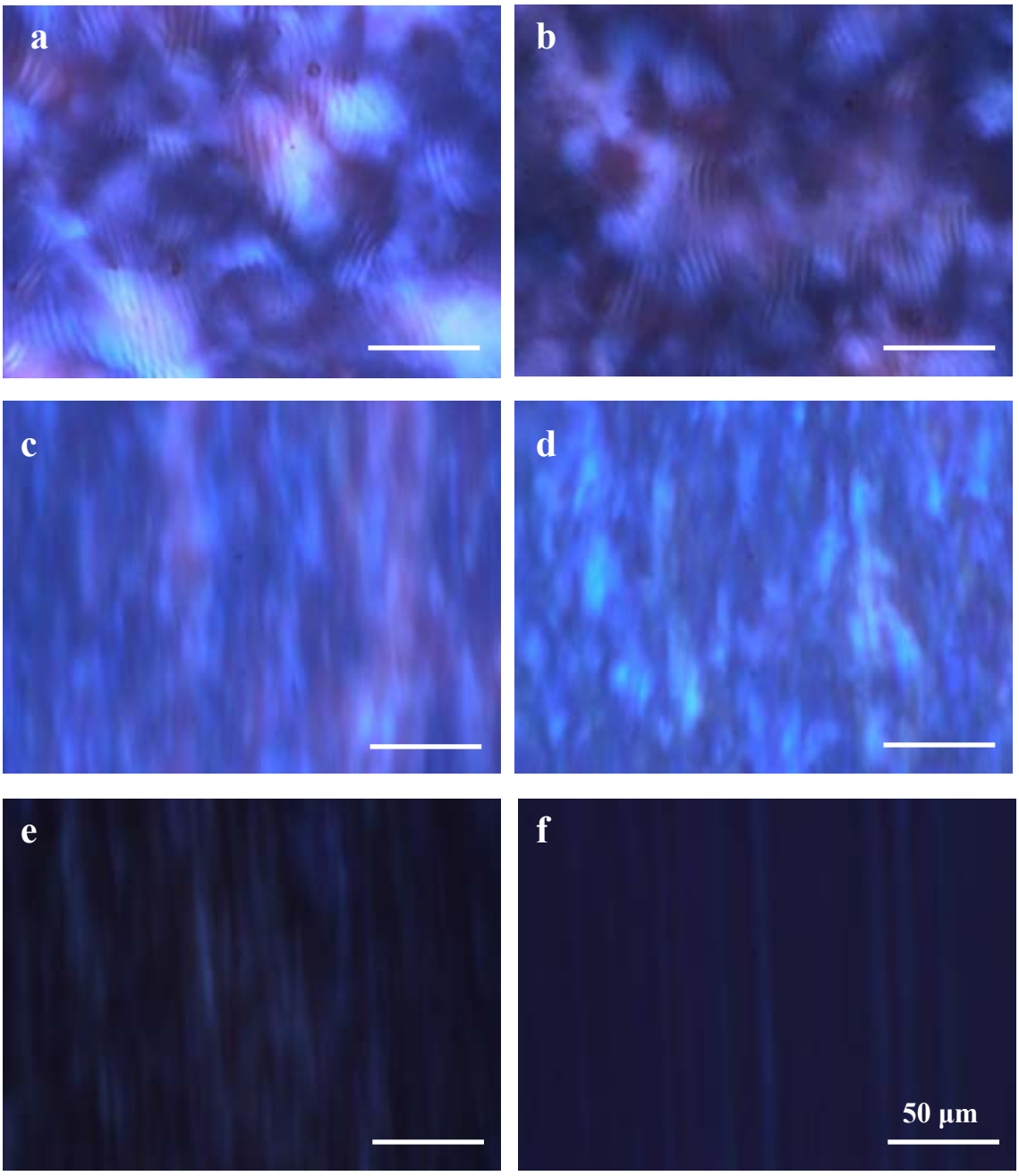

Figure 8-6: Polarized optical micrographs of 9 wt. % CNC-A suspensions at rest (a) and during steady shear tests at shear rates of (b) 0.01 s^{-1}, (c) 0.1 s^{-1}, (d) 0.5 s^{-1}, (e) 1 s^{-1}, (f) 10 s^{-1}.

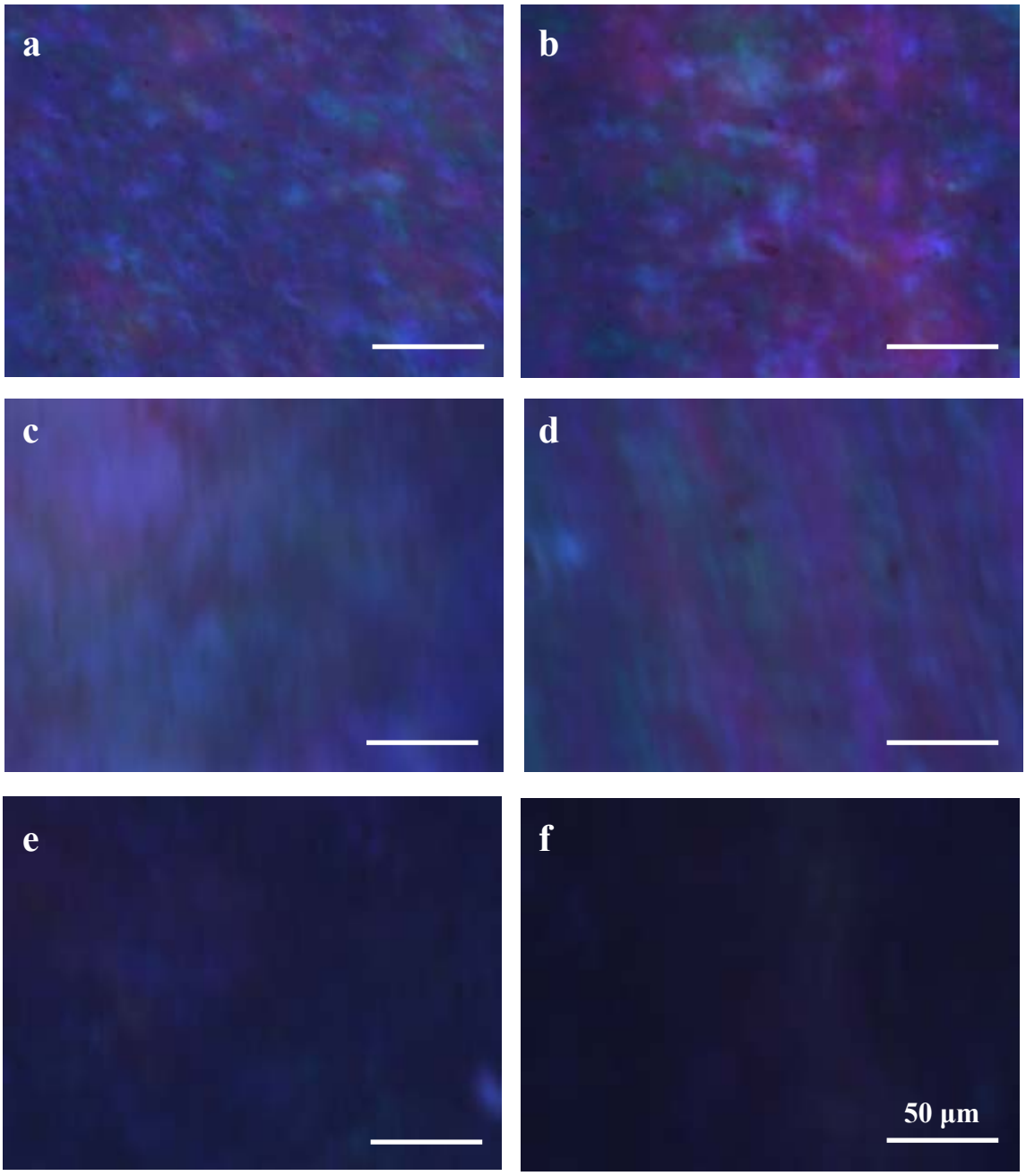

Figure 8-7: Polarized optical micrographs of 12 wt.% CNC-A suspensions at rest (a) and during steady shear tests at shear rates of (b)0.01 s^{-1}, (c) 0.1 s^{-1}, (d) 0.5 s^{-1}, (e) 1 s^{-1}, (f) 10 s^{-1}.

8.3. Morphology development by increasing concentration in CNC suspensions

As mentioned, CNC suspensions experience two different transitions by increasing the CNC concentration. To capture micrographs of samples at different concentrations in order to follow phase transitions, polarized optical microscopy has been used online with a rotational rheometer. Representative micrographs of CNC-A and CNC-B suspensions at different concentrations and at the shear rate of 0.01 s^{-1} are shown in Figures 8-8 and 8-9, respectively. For CNC-A samples (Figure 8-8), at 3 wt. % the micrograph shows the existence of small domains of liquid crystalline structure (fingerprint texture) in a biphasic region. By increasing the concentration up to 7 wt. %, the fraction of liquid crystal domains in the biphasic system increases. At 9 wt. %, the liquid crystalline structure appears in the entire micrograph and the fingerprint texture, which is characteristic of cholesteric liquid crystals, can be seen all across the sample. Further increase in CNC concentration results in birefringent gels and no fingerprint can be observed in the POM micrographs of suspensions with concentrations above 12 wt. %.

For CNC-B samples (Figure 8-9), at 3 wt. % the micrograph appears black indicating no liquid crystal ordered phases at this concentration. The fingerprint patterns begin to appear at 5 wt. % , and disappear at 10 wt. %, where the micrograph shows a birefringent gel structure (a random structure with bright colours). Rheological characterization of these samples also confirms the occurrence of gel formation in CNC-B suspensions. In the case of CNC-B, a lower degree of sulfation results in decreased intermolecular repulsive interactions which further results in gel phase formation at a lower concentration. On the other hand, the higher surface charge in CNC-A favours the formation of anisotropic liquid crystalline phases. Due to repulsive particle interactions, a lower concentration of CNC particles is enough to frustrate packing in random orientation and transition from isotropic to anisotropic occurs.

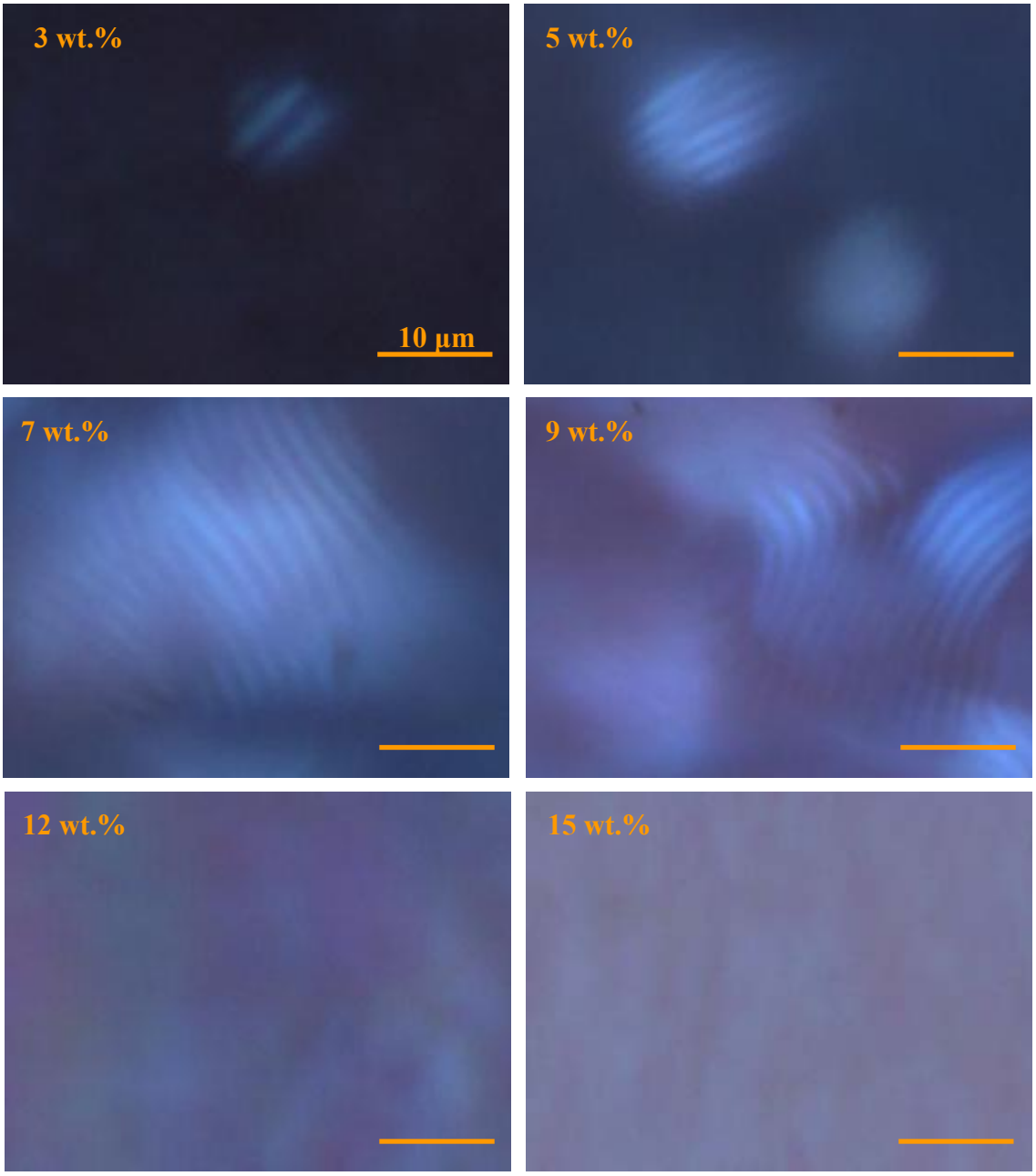

Figure 8-8: Polarized optical micrographs of CNC-A suspensions at different concentrations, taken at shear rate of 0.01 s^{-1}. The scale bar is 10 µm.

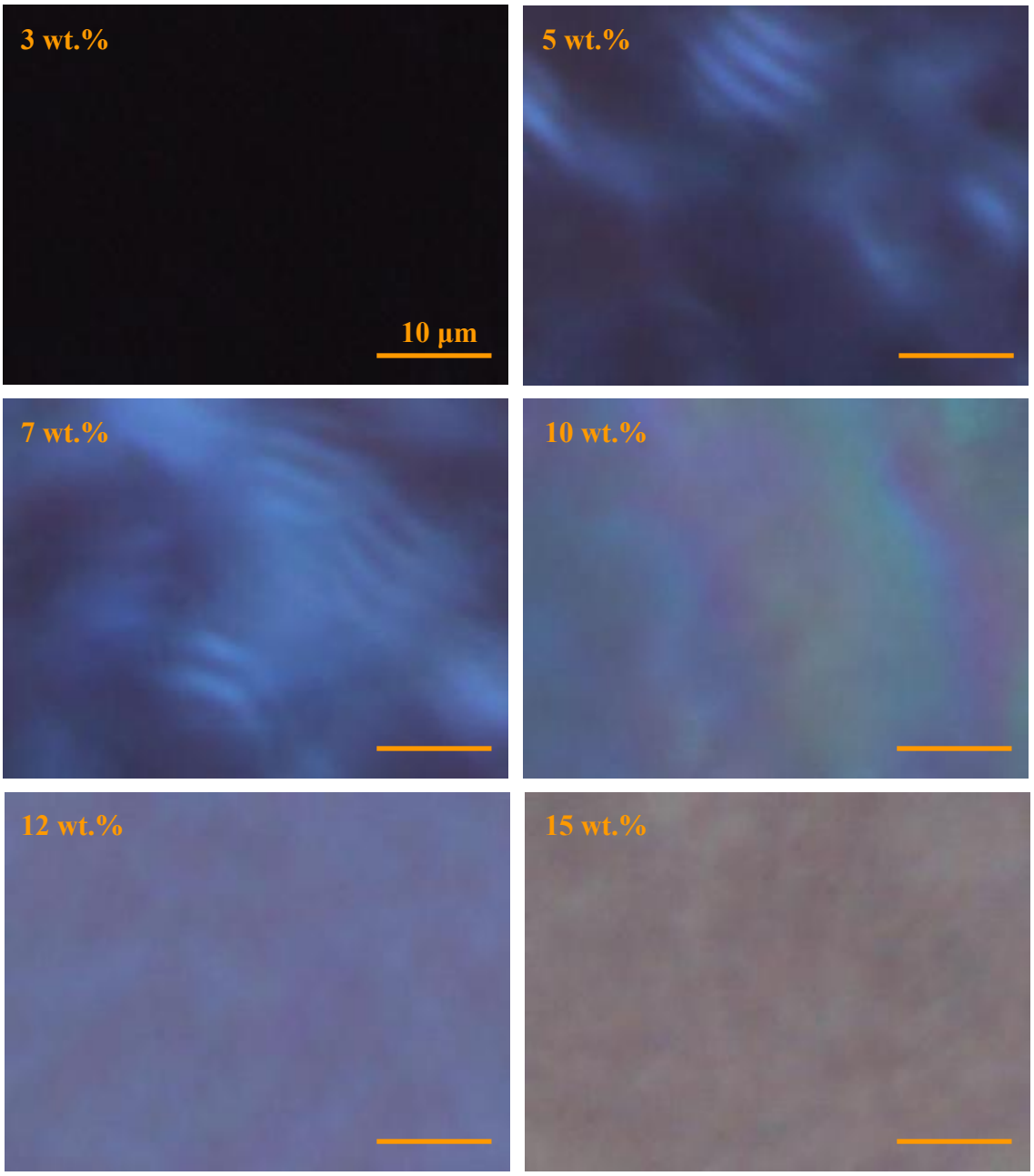

Figure 8-9: Polarized optical micrographs of CNC-B suspensions at different concentrations, taken at shear rate of 0.01 s^{-1}. The scale bar is 10 µm.

8.4. Linear viscoelastic measurements of CNC-A and CNC-B suspensions

To carefully examine the observed gel transition in CNC suspensions at high concentration, isothermal frequency sweep tests were performed to measure the linear

viscoelastic material function of these suspensions. The storage modulus, G' and loss modulus, G" of CNC-A and CNC-B suspensions at different concentrations are shown in Figures 8-10 and 8-11, respectively. Only a few concentrations are shown for the sake of clarity. For CNC-A suspensions, samples with concentrations of 10 wt. % and lower behaved as predominantly viscous fluids (loss modulus, G", being higher than storage modulus, G', over the whole investigated frequency range). For the 12 wt. % sample, a gel-like behaviour was observed, where G' and G" overlap over an extended range of frequency. At 15 wt. % concentration, the behaviour resembles that of a viscoelastic solid, where the G' is independent of frequency and higher than G" over the entire investigated frequency range, indicating formation of a stiff gel.

Based on the rheological data presented in Figure 8-10, for CNC-A suspensions having a higher degree of sulfation, and at the temperature used for rheological measurements (25 ºC), the transition from liquid crystalline to gel occurs at about 12 wt. %. These results are supported by the POM micrographs presented in Figure 8-8 which have clearly shown the disappearance of fingerprint texture upon transition from liquid crystal into gel phase.

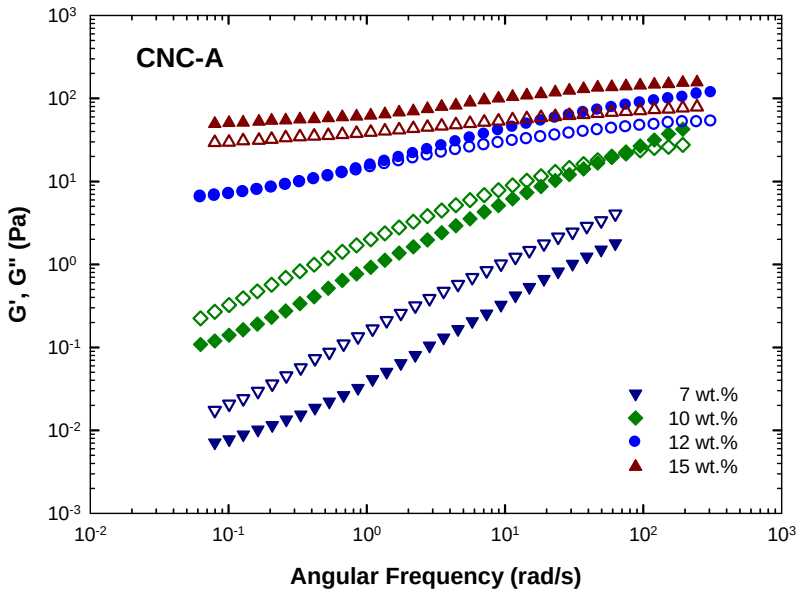

Figure 8-10: Storage modulus, G' (solid symbols), and loss modulus, G" (open symbols), versus angular frequency, ω, for CNC-A suspensions sonicated for 1000 J/g of CNC and at different concentrations.

For CNC-B suspensions (Figure 8-11), at 7 wt.% the sample is liquid-like and by increasing the concentration, a gel-like behaviour is observed at 10 wt.% above which the sample shows solid-like viscoelastic behaviour. Gel formation at this concentration is consistent with the optical microscopy results presented in Figure 8-9. Comparing the results in Figures 8-10 and 8-11, it can be seen that gel formation occurs at a lower concentration for CNC-B, the one possessing a lower degree of sulfation, which was expected according to the lower surface charge of the samples compared to those of CNC-A.

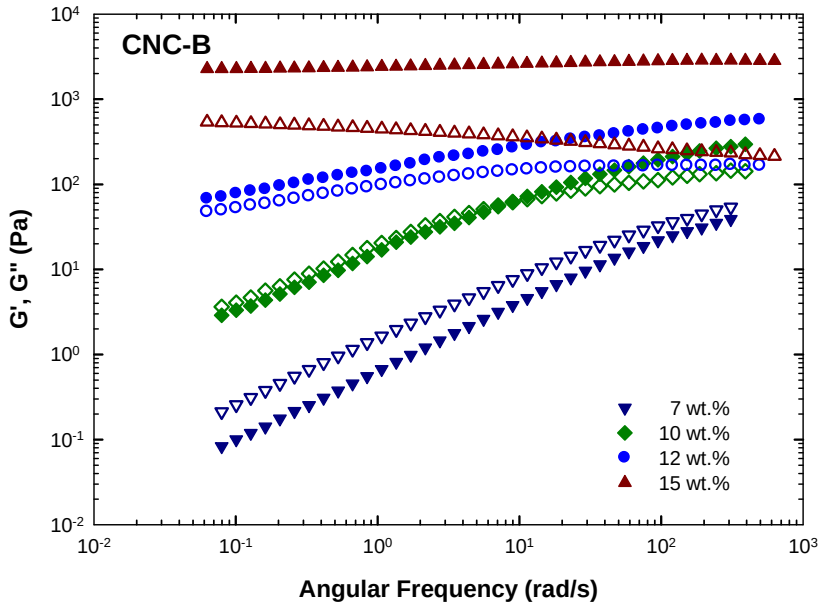

Figure 8-11: Storage modulus, G' (solid symbols), and loss modulus, G" (open symbols), versus angular frequency, ω, for CNC-B suspensions sonicated for 1000 J/g of CNC and at different concentrations.

8.5. Applicability of Cox-Merz Rule for CNC suspensions of different concentrations

As discussed in section 6.4 of Chapter 6, lyotropic liquid crystals and gels do not obey the Cox−Merz rule. Failure of the Cox-Merz rule indicates structural formation that can be preserved under linear viscoelastic measurements (complex viscosity) but breaks down under shear (absolute viscosity). Thus, as the structural formation in the sample

becomes more significant (in case of gel formation, for example), a stronger deviation from this rule will be observed. In order to study the applicability of the Cox−Merz rule, the complex and shear viscosities of CNC-A and CNC-B suspensions at different concentrations (sonicated at 1000 J/g of CNC) were compared and plotted in Figures 8-12 and 8-13, respectively. For CNC-A (Figure 8-12), the 1 wt. % isotropic sample obeys the Cox-Merz rule. By increasing the CNC concentration and due to the formation of chiral nematic ordered domains, the behaviour deviates from the Cox−Merz rule. The deviation becomes more significant with further increase in the concentration.

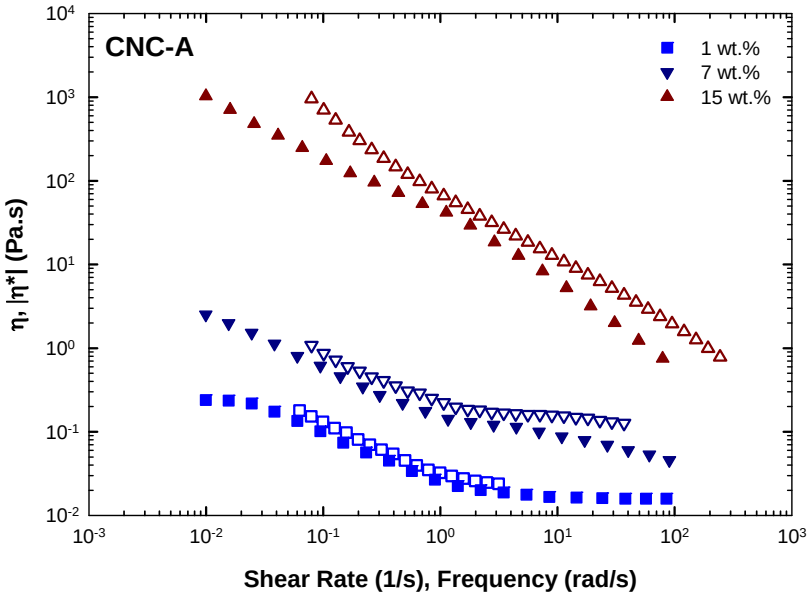

Figure 8-12: Cox-Merz plot for CNC-A suspensions at different concentrations (sonicated at 1000 J/g of CNC). All the concentrations of 1-15 wt. % have been tested, but results only for 1, 7, and 15 wt. % are presented in this figure for the sake of clarity. Solid symbols are shear viscosities and open symbols are complex viscosities.

In the case of CNC-B samples (Figure 8-13), the Cox-Merz rule applies up to 3 wt. % (isotropic samples), thereby confirming that there is minimal structural formation at this level of concentration, which is in agreement with the results from polarized light microscopy (Figure 8-9). At concentrations above 4 wt. %, the rule deviates for all the samples, especially at higher shear rates (or frequencies). A further increase in the

concentration, and going through gelation, leads to significant deviation from the Cox-Merz rule throughout the entire shear rate (or frequency) range. Shear flow breaks the gel and affects the structure, and therefore, the dynamic low strain data do not follow the steady state shear data.

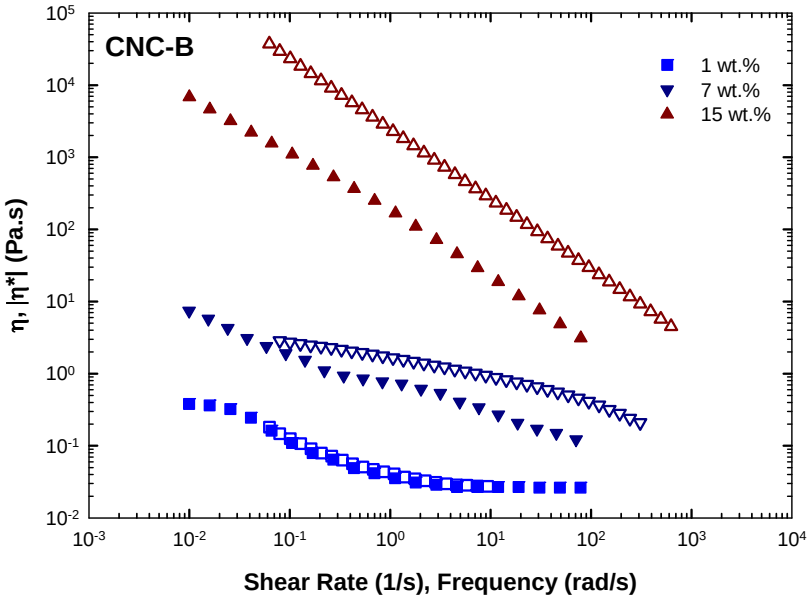

Figure 8-13: Cox-Merz plot for CNC-B suspensions at different concentrations (sonicated at 1000 J/g of CNC). All the concentrations of 1-15 wt. % have been tested, but results only for 1, 7, and 15 wt. % are presented in this figure for the sake of clarity. Solid symbols are shear viscosities and open symbols are complex viscosities.

8.6. Summary

In this chapter, the microstructure and rheological behaviour of two different sets of cellulose nanocrystal suspensions, possessing different degrees of sulfation, were studied. By increasing the CNC concentration, two different microstructural transitions, namely isotropic to chiral nematic and chiral nematic to gel occurs at first and second critical concentrations. It has been shown that, the degree of sulfation of CNC particles significantly affects these critical concentrations. Higher degree of sulfation favours the formation of anisotropic chiral nematic ordered phases in CNC suspensions, where the fingerprint texture, characteristic of cholesteric liquid crystals, can be observed under

polarized optical microscopy. However, the samples having lower degree of sulfation showed a significant tendency to form gel at relatively lower concentrations where the fingerprint texture vanishes.

CHAPTER 9: EFFECTS OF IONIC STRENGTH ON THE MICROSTRUCTURE AND RHEOLOGY OF CNC AQUEOUS SUSPENSIONS[6]

As discussed before, by increasing the concentration of cellulose nanocrystals, CNC suspensions form chiral nematic anisotropic phases above a critical concentration and gels above a second critical concentration. The dimensions and surface charge (degree of sulfation) of nanocrystals, and the ionic strength of the system are the most important factors governing the microstructural transitions from isotropic to chiral nematic and from chiral nematic anisotropic to gel formation (Dong et al. 1996, Dong and Gray 1997, Beck-Candanedo et al. 2005). The effect of ionic strength on the microstructure and rheology of CNC aqueous suspensions is independently studied in this chapter. In order to study the effect of ionic strength on the rheology of CNC suspensions at various microstructural states (isotropic, chiral nematic anisotropic, and gel), 15 wt.% CNC suspensions in DI water and NaCl solution of different molarities (1-15 mM) were prepared and sonicated (1000 J/g of CNC). These suspensions were further diluted with DI water and NaCl solutions to obtain the desired cellulose concentrations (1-15 wt %) and NaCl concentrations (0-15 mM).

9.1. Effects of ionic strength on physico-chemical properties of CNC suspensions

Figure 9-1 shows the TEM photomicrograph of the CNC used for the study of the effect of ionic strength presented in this chapter. The surface properties of CNC, obtained by elemental analysis, the ζ-potential measurements, and transmission electron microscopy (TEM), are summarized in Table 9-1. The elemental analysis of the CNC particles has shown that they contain 0.66 wt % of sulfur, which results in 3.39 SO_3^-/100 anhydroglucose units. As discussed in Chapter 7, the degree of sulfation on the surface of cellulose nanocrystals determines the surface charge density of cellulose nanocrystals, which in turn affects the stabilization of the suspension.

[6] A version of this chapter is under preparation for publication.

The presence of significant negative surface charges on CNC particles was confirmed with the measured value of ζ-potential of these nanocrystals (−52 mV), indicating a stable suspension.

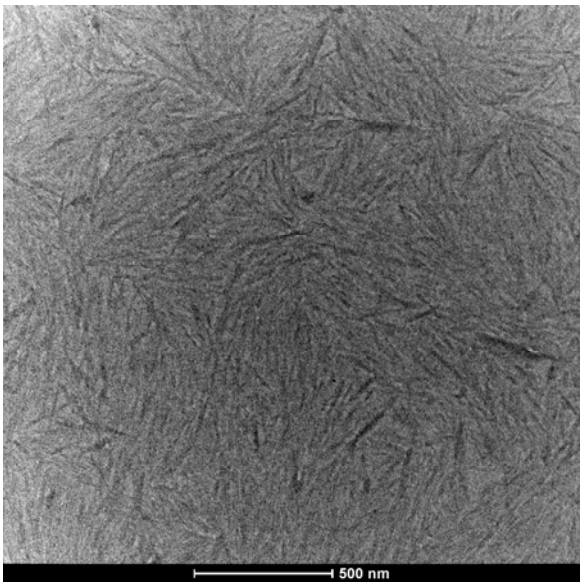

Figure 9-1: TEM photomicrograph of CNC suspensions.

Table 9-1: Dimensions and surface characteristics of CNC suspensions prepared by FPInnovations and studied in this chapter.

	Equivalent Hydrodynamic Particle Size (nm) (from Zetasizer)	ζ-potential (mV)	Sulfur Content (%)	OSO_3H/ 100 anhydroglucose units	Nanocrystal Dimensions (nm) (from TEM)
CNC	76±2 nm	-52±4	0.66	3.39	100× 7

The aqueous suspension of these nanocrystals formed chiral nematic liquid crystal structures above the critical concentration of 4 wt. %. Representative polarized optical micrographs of 7 wt. % CNC aqueous suspension is shown in Figure 9-2 in which the fingerprint patterns, characteristic of chiral nematic liquid crystals, clearly appeared.

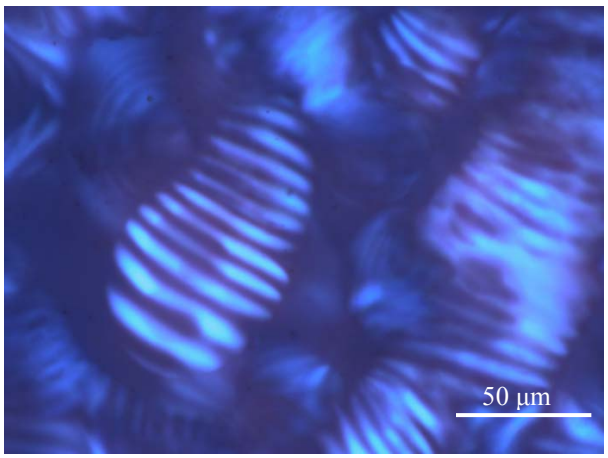

Figure 9-2: Representative POM micrograph of a 7 wt.% CNC aqueous suspension at rest. The scale bar is 50 µm.

CNC suspensions at constant concentration of CNC and different concentrations of NaCl have been prepared which allows to study the effect of NaCl addition, independently. The zeta potentials of these samples have been measured to explore the colloidal stability of CNC suspensions with different electrolyte concentrations. The CNC particles have zeta potential of −52 mV without any addition of electrolyte; high zeta potential values have also been reported by Boluk et al. (2011). The zeta potential values measured for CNC suspensions as a function of the nominal NaCl concentrations of 0 to 10 mM are plotted in Figure 9-3. The points in the plot are the mean values of 10 measurements and the error bars represent the standard deviation from the mean. The presence of NaCl lowers the absolute value of zeta potential of CNC particles which is due to the adsorption of Na^+ counter-ions on the negatively charged CNC surfaces thereby compressing the double layer surrounding the nanocrystals.

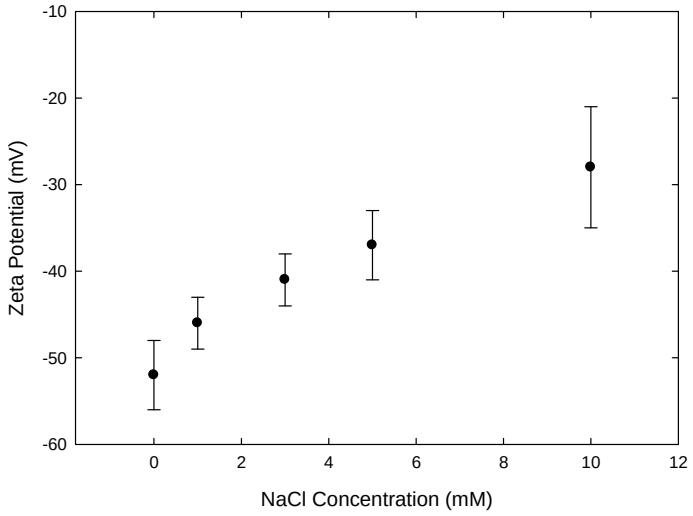

Figure 9-3: The zeta potential of 0.5 wt.% CNC aqueous suspensions versus NaCl concentration.

The results of zetasizer measurements, tabulated in Table 9-2, shows that by adding NaCl to CNC aqueous suspensions, the equivalent hydrodynamic size of the sample decreases from 0 to 5 mM NaCl addition above which the hydrodynamic size increases significantly. The decrease in size is thought to be due to screening the electrical double layer by added Na^+ counter-ions, thus the particle with thinner double layer result in smaller size measured by the zetasizer technique. By further increasing the concentration of inorganic salt, the suspension becomes unstable and aggregation occurs. The observed increase in the hydrodynamic size of the nanocrystals at high NaCl concentration is attributed to the existence of these aggregates in the suspensions. The result of zetasizer measurements for even higher concentration of salt (15 mM NaCl) was not reproducible at all, due to extensive aggregation, and thus are not included in Table 9-2.

Table 9-2: Physico-chemical characteristics of CNC suspensions studied in this chapter.

Property / Sample	Equivalent Hydrodynamic Particle Size (nm) (measured by Zetasizer)	ζ-potential (mV)	Conductivity (mS/cm)
0 mM Nacl	76 ± 0.6	- 52 ± 4	0.21
1 mM NaCl	65 ± 0.3	- 46 ± 3	0.25
3 mM NaCl	60 ± 1.2	- 41 ± 3	0.32
5 mM NaCl	62 ± 2	- 37 ± 4	0.85
10 mM NaCl	78 ± 3.5	- 28 ± 7	1.41

9.2. Effects of ionic strength on the shear rheology of CNC suspensions

The steady-state shear viscosity curves of CNC suspensions in DI water over a broad range of CNC concentrations (1-15 wt.%) are shown in Figure 9-4. According to the viscosity profiles in Figure 9-4, by increasing the concentration, two transitions in rheological behaviour are observed: a transition from isotropic to liquid crystal, and a transition from liquid crystal to gel. Samples of 1 and 3 wt.% CNC suspension behave like an isotropic sample showing a Newtonian plateau at low shear rates, followed by shear thinning at intermediate shear rates due to alignment of the nanocrystals along the shear direction, and another plateau at high shear rates where all the particles have been aligned, thus no further change in the viscosity occurs (Bercea and Navard 2000). By increasing the concentration above 3 wt.%, liquid crystalline phases are formed in the suspension and the viscosity profile changes to the three-region profile, typical of liquid crystal polymer solutions (Onogi and Asada 1980). This transition from isotropic to anisotropic chiral nematic liquid crystal occurs between 3 and 4 wt. %, above which the viscosity profile consists of three different regions. Namely, a shear thinning region (region I) at low shear rates due to alignment of chiral nematic liquid crystal domains, a plateau (region II) at intermediate shear rates, where the domains have been all oriented along the shear direction, and a second shear thinning (region III) at high shear rates,

where the shear stress is high enough to destroy the liquid crystal domains and free the nanocrystals so that individual nanocrystals orient themselves along the shear flow direction (these microstructural changes have been confirmed by polarized optical microscopy results, which were presented and discussed in Chapters 5-8 of this thesis).

Further increase in the CNC concentration changes the viscosity profile from a three-region profile to the one showing a single shear thinning over the whole range of investigated shear rates indicative of gel formation. This second structural transition occurs at 12 wt.% for aqueous CNC suspension studied in this chapter.

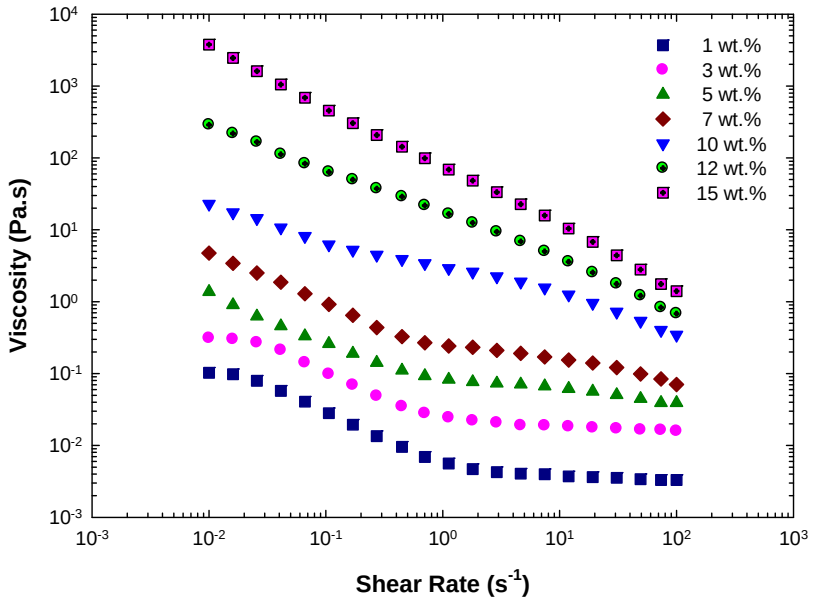

Figure 9-4: The viscosity material function of CNC suspensions in DI water, sonicated for 1000 J/g of CNC, at different concentrations.

To study the effects of adding NaCl on suspension rheology, independent of concentration, the steady-state shear viscosity of samples at constant concentrations and different NaCl molarities were measured. Figure 9-5 shows the steady state viscosity versus shear rate for 3 wt.% CNC suspension (isotropic sample) in the presence of NaCl salt (0 to 10 mM). According to Figure 9-5, the viscosity of the isotropic sample decreases as the ionic strength increases. This decrease in the viscosity was expected

since the presence of NaCl compresses the thickness of electrical double layer of particles which reduces the electro-viscous effects in the suspension of these charged nanocrystals. The effect of electro-viscous interactions on the viscosity of CNC suspensions at semi-dilute concentration regime has also been reported by Boluk et al 2011.

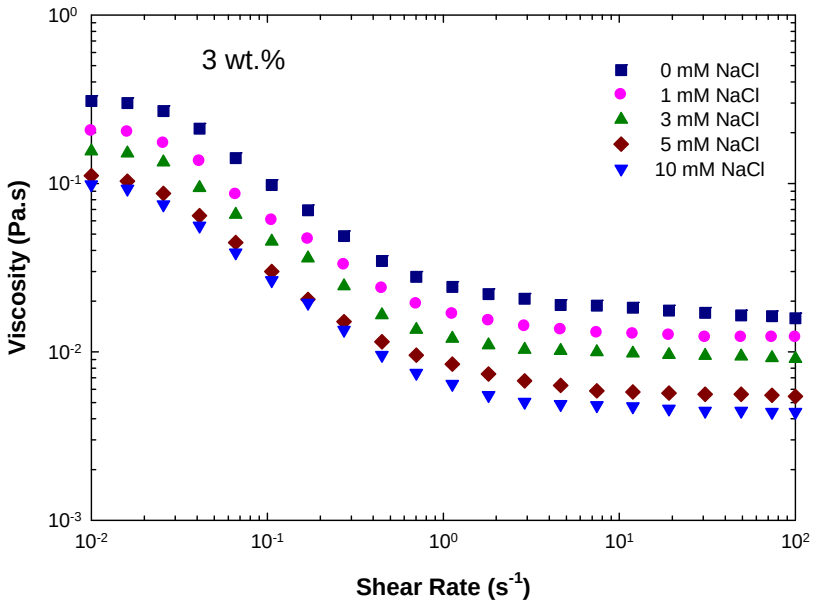

Figure 9-5: Shear rate dependence of viscosity of 3 wt.% CNC suspensions at different electrolyte concentrations. The viscosity data at 15 mM NaCl concentration were not included in this figure due to indication of coagulation.

There are three possible electro-viscous effects which can contribute in the viscosity measurements of charged rigid Brownian particles (Conway and Dobry-Duclaux 1960). (1) Primary electro-viscous effect due to the deformation of the double layer around particles under the shear flow, (2) secondary electro-viscous effect due to overlapping of double layers when two particles are sheared under external fluid motion, and (3) a tertiary effect due to dimensional changes of charged swelled particles with electrolyte concentration. Since CNC is highly crystalline, particle swelling and its collapse in the presence of salt are not an issue and the tertiary effect does not apply in the case of CNC suspensions (Boluk et al 2011). The primary and secondary electro-viscous contributions to suspension viscosity is reduced as the ionic strength increases; NaCl compresses the

double layer and thus the distortion of a thinner double layer by shear is small and at the same time less overlapping. Interactions between compressed double layers will be less, resulting in lower viscosity at higher ionic strength.

In order to study the effects of adding NaCl on the rheological behaviour of biphasic samples, the steady-state shear viscosity versus shear rate for 7 and 10 wt.% CNC suspensions (biphasic samples containing anisotropic chiral nematic ordered domains) at various NaCl concentrations (0 to 15 mM) are measured and shown in Figures 9-6 and 9-7, respectively. According to Figures 9-6 and 9-7, samples without NaCl show a three-region viscosity profile. By the addition of NaCl up to 5 mM, the viscosity decreases at high shear rates, although it increases at the low shear rate region (region I). At high shear rates, where the chiral nematic ordered domains are broken and individual particles are aligned in the shear direction (according to the results presented in previous chapters), interactions of individual nanocrystals cause a decrease in the suspension viscosity by increasing ionic strength, as expected. On the other hand, at low shear rates (region I), there are anisotropic ordered domains which are contributing to the viscosity of the system. Increase in the viscosity of region I can be attributed to the structural changes in the chiral nematic domains. By increasing the amount of added NaCl, the electrical double layer around the cellulose nanocrystals becomes thinner, and thus, the effective diameter and apparent volume of the charged rods decrease, leading to a stronger chiral interaction (Dong et al. 1996). By increasing the chiral interaction, nanocrystals form smaller size liquid crystal domains with more packed structures (smaller pitch size), which results in higher viscosity at low shear rates. The stronger the interaction, the smaller is the pitch. Hirai et al. (2009) also reported a decrease in the anisotropic domain size with an increase in the NaCl concentration from 0 to 2.75 mM for bacterial cellulose-derived nanocrystals.

By further addition of NaCl (10 and 15 mM), the viscosity increases significantly over the whole shear rate investigated and shows a single shear thinning behaviour. This is thought to be due to gel formation and aggregation of particles as a result of decrease in repulsive forces where the suspension is no longer stable.

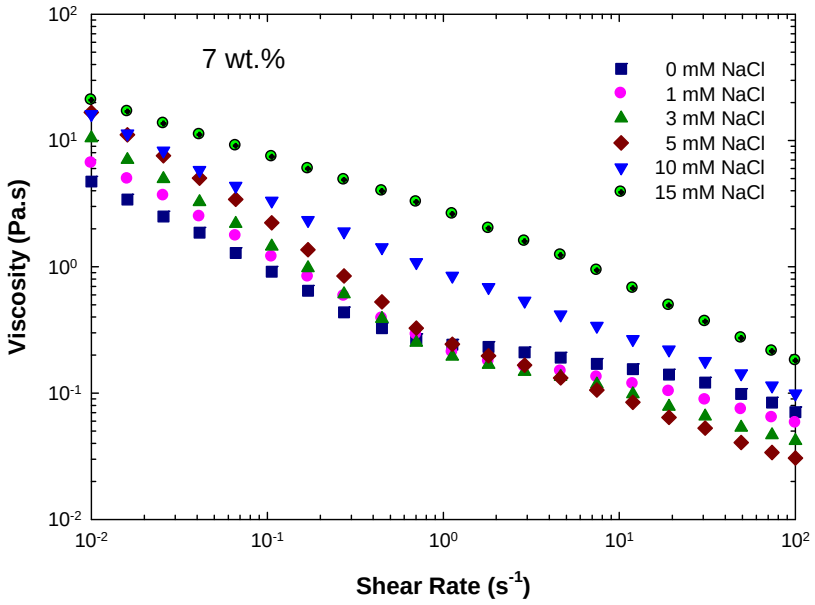

Figure 9-6: Shear rate dependence of viscosity of 7 wt.% CNC suspensions at different electrolyte concentrations.

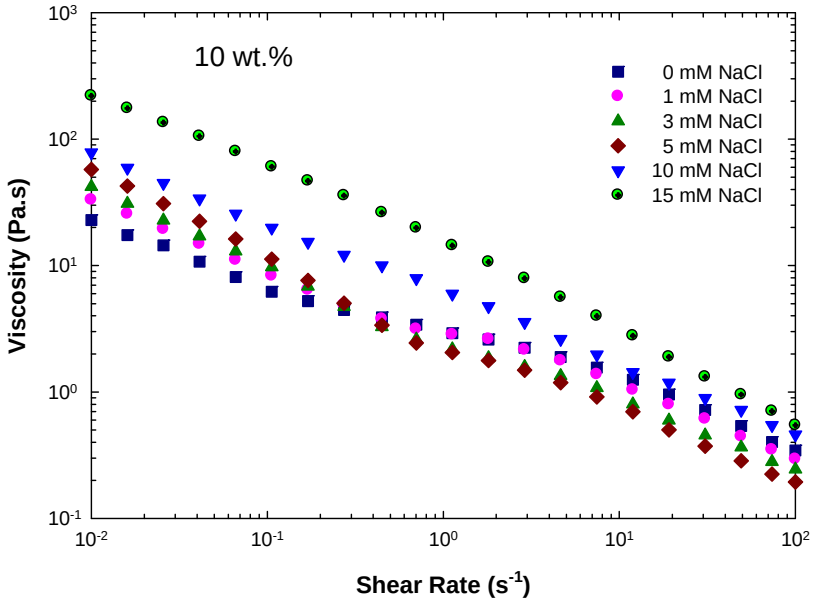

Figure 9-7: Shear rate dependence of viscosity of 10 wt.% CNC suspensions at different electrolyte concentrations.

To study the effects of adding NaCl on the rheological behaviour of gel samples, the steady-state viscosity versus shear rate for 12 and 15 wt.% CNC suspensions (the ones that showed rheological gel behaviour in Figure 9-4) at various NaCl concentrations (0 to 15 mM) are measured and shown in Figures 9-8 and 9-9, respectively. As can be seen in Figures 9-8 and 9-9, by addition of NaCl up to 5 mM, the gel viscosity decreases. Adding salt reduces the effective volume fraction and liquefies the sample. It also disturbs the hydrogen bonding and ionic interactions in this system of charged rods, resulting in formation of a weaker gel structure with lower viscosity. At higher salt concentration (10 and 15 mM), the repulsion forces are screened, aggregation occurs, resulting in the observed gelation and viscosity increase.

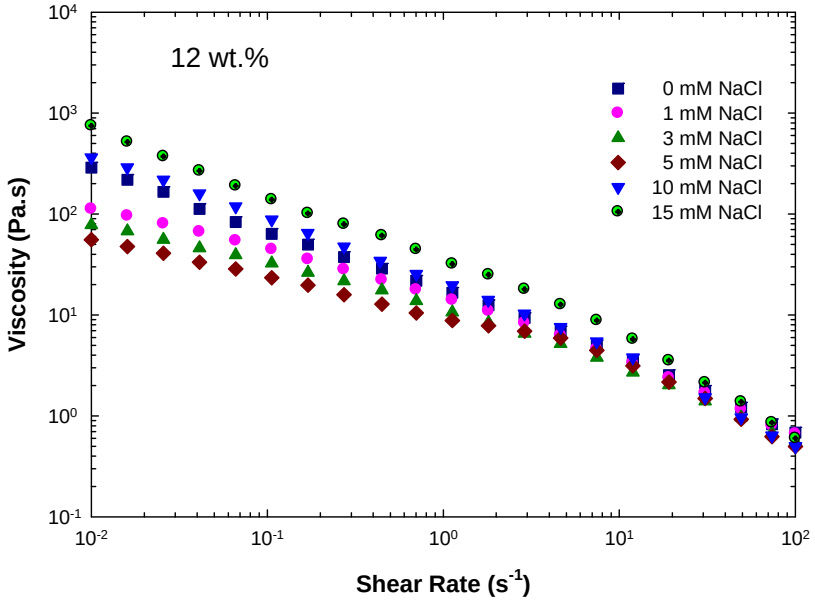

Figure 9-8: Shear rate dependence of viscosity of 12 wt.% CNC suspensions at different electrolyte concentrations.

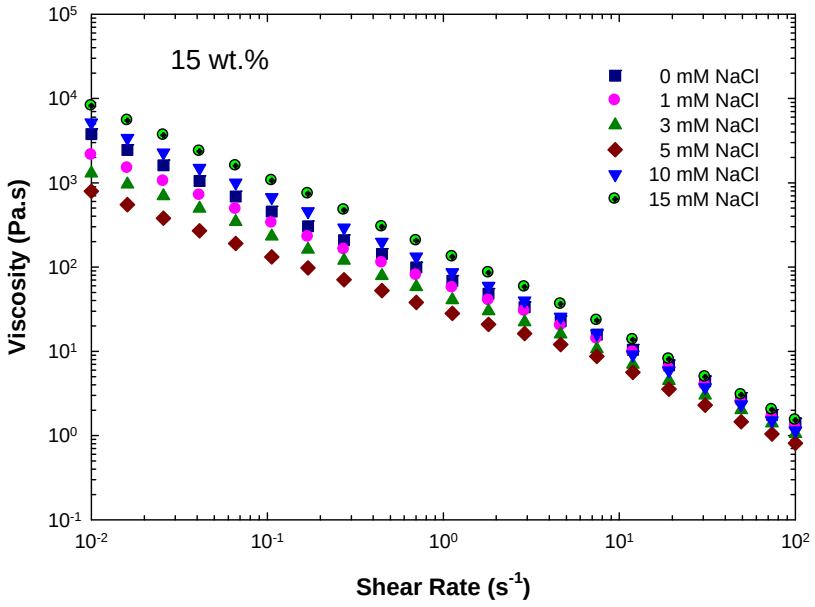

Figure 9-9: Shear rate dependence of viscosity of 15 wt.% CNC suspensions at different electrolyte concentrations.

9.3. Effects of ionic strength on the microstructure of CNC suspensions

To follow the microstructural changes by adding NaCl to CNC suspensions, polarized optical microscopy has been used in combination with a rotational rheometer to capture POM micrographs of samples. As discussed earlier, for biphasic samples, the viscosity of region I increases by addition of NaCl from 0 to 5 mM. This was thought to be due to microstructural changes in anisotropic chiral nematic phases. To further study this surprising observation, the POM micrographs of 7 wt.%, and 9 wt.% CNC aqueous suspensions at various NaCl concentrations are shown in Figures 9-10 and 9-11, respectively. These two concentrations were chosen since they are well above the critical concentration for chiral nematic liquid crystal phase formation. According to Figures 9-10 and 9-11, it can be seen that, the suspension without NaCl appears to have chiral nematic domains with size of about 100 microns. By adding NaCl to the suspension, the size of the chiral nematic domains decreases significantly and finally vanishes for NaCl concentration above 10 mM. Addition of inorganic salt compresses the electrical double layer and thus the intensity of chiral interaction between rod-like nanocrystals increases resulting to less effective diameter and apparent volume fraction of nanocrystals. The

stronger the chiral interaction, the more packed the chiral nematic phases become. A decrease in the fraction of the chiral nematic phase and the pitch size by adding NaCl were also reported by Dong et al. (1996) for cotton cellulose nanocrystals and Hirai et al. (2009) for bacterial cellulose nanocrystals.

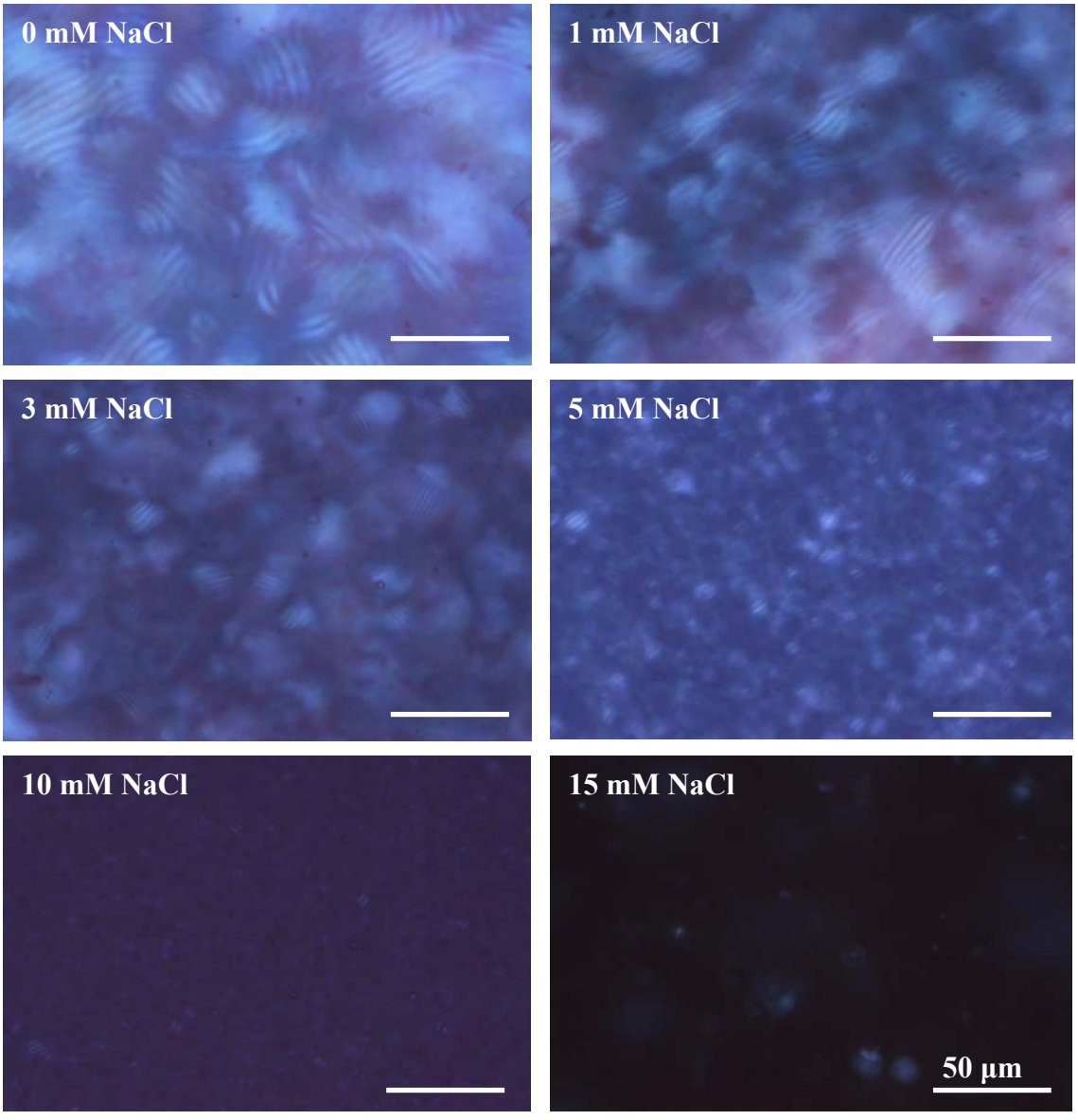

Figure 9-10: Polarized optical micrographs of 7 wt.% CNC suspensions at different NaCl concentrations, taken at shear rate of 0.01 s^{-1}. The scale bar is 50 µm.

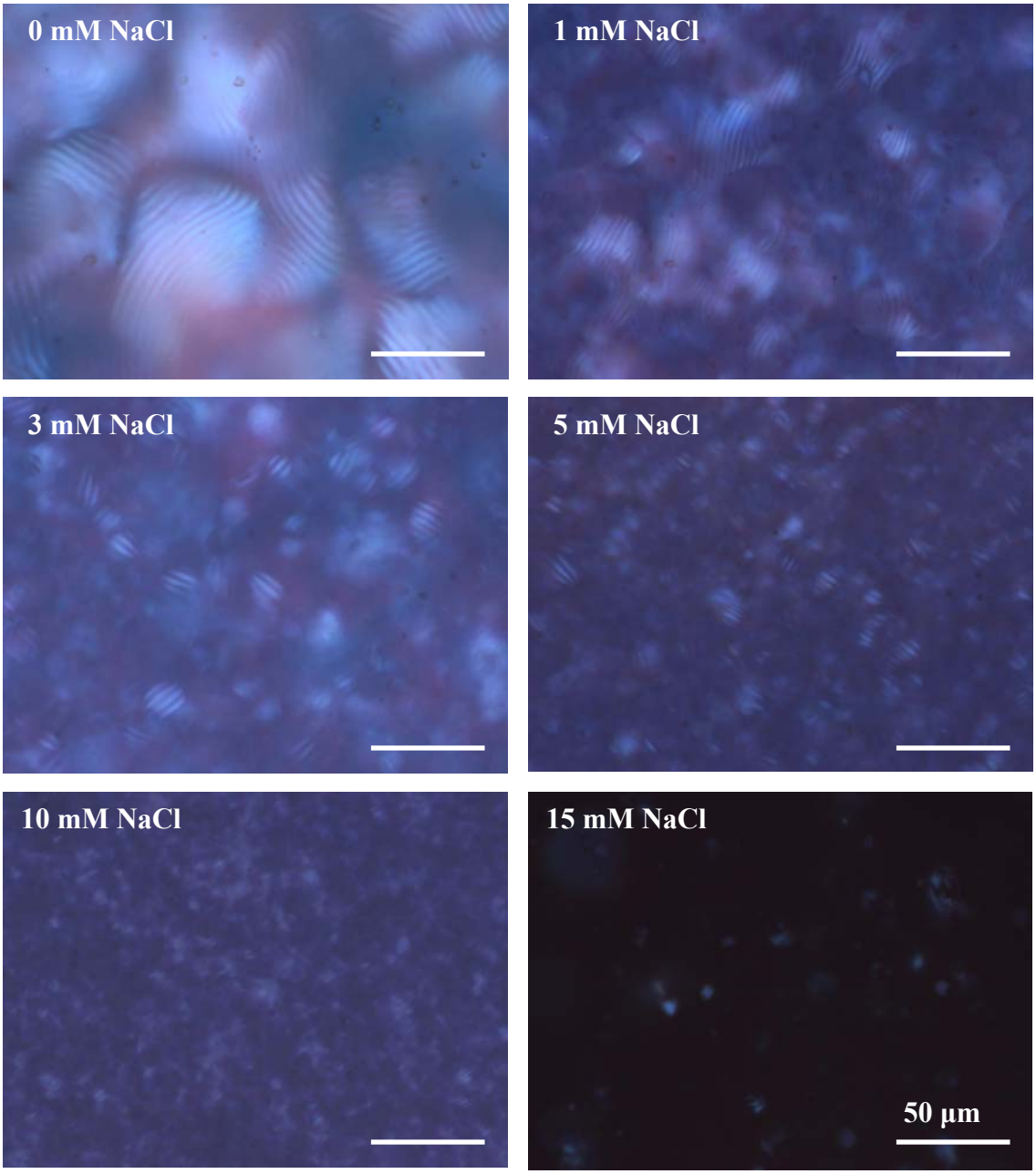

Figure 9-11: Polarized optical micrographs of 9 wt.% CNC suspensions at different NaCl concentrations, taken at shear rate of 0.01 s-1. The scale bar is 50 µm.

9.4. Linear viscoelastic measurements of CNC suspensions

To further examine the gel formation in CNC suspensions at high concentrations, and study the effect of NaCl addition on this transition, isothermal frequency sweep tests were performed to measure the linear viscoelastic material function of CNC suspensions

at various NaCl concentrations. The storage modulus, G', and loss modulus, G", of CNC suspensions at different concentrations without addition of NaCl are shown in Figure 9-12. As can be seen in Figure 9-12 , the 7 and 10 wt.% samples (having anisotropic chiral nematic structure) show a fluid-like behaviour (G">G' over the whole investigated frequency range for 7 wt.% and over an extended frequency range with a cross-over at about 200 rad/s for 10 wt.%). The 12 wt.% sample shows a gel-like behaviour (overlapping of G' and G" over an extended range of frequencies) and finally the 15 wt.% suspension shows a solid-like behaviour (G'>G" and almost independent of frequency, characteristic of a stiff gel). These results are consistent with those observed in shear viscosity curves in Figure 9-4. Similar plots including the complex viscosities at various constant ionic strength (0, 1, 3, 5, 10, and 15 mM NaCl) can be found in the appendix (Figures A2 to A7 in the appendix).

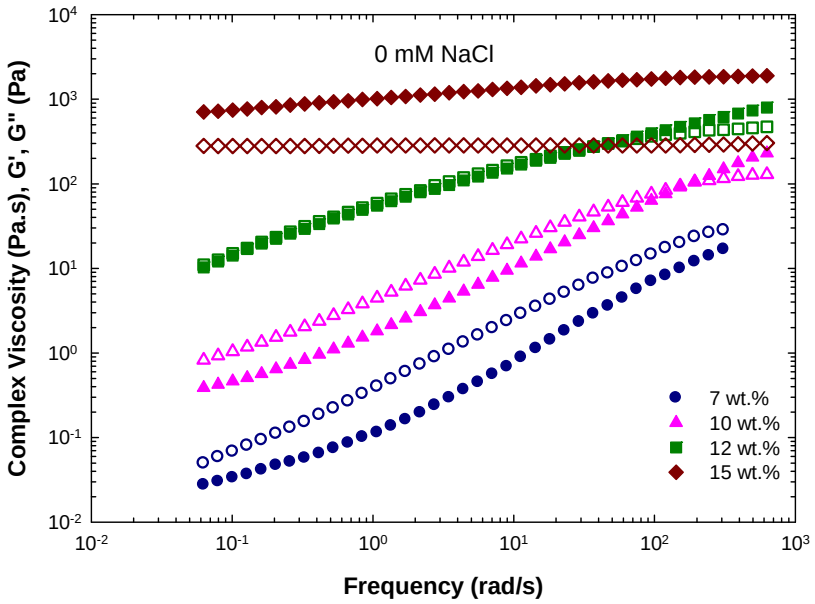

Figure 9-12: Storage modulus, G' (filled symbols), and loss modulus, G" (open symbols), versus angular frequency, ω, at different CNC concentrations without NaCl.

To study the effects of adding NaCl on the viscoelastic properties of these CNC suspensions, the storage modulus, G', and loss modulus, G" of the samples at various constant concentration and different ionic strength were measured and plotted in Figures

9-13, 9-14, 9-15 and 9-16 for 7, 10, 12, and 15 wt.% CNC suspensions, respectively. The viscoelastic material functions were measured at 6 different NaCl concentrations, however, only the data of 0, 3, 5, and 15 mM NaCl are presented in these figures for the sake of clarity. Similar plots containing the results for other NaCl concentrations and the complex viscosities can be found in the appendix (Figures A8 to A11 in the appendix).

According to Figure 9-13, for 7 wt.% suspensions the modulus increases by adding NaCl up to 5 mM which can be attributed to the existence of smaller domains with more packed structure, although all these suspensions show viscoelastic liquid-like behaviour (G'<G"). In the case of 7 wt.% suspension with 15 mM NaCl the behaviour changes to a gel-like and the modulus shows a very significant increase. This is thought to be due to the occurrence of extensive aggregation in the system which causes the gelation at this relatively low concentration. The same changes occur in the case of 10 wt.% sample (see Figure 9-14) confirming that the mechanism by which addition of NaCl affects the structure is the same for biphasic samples containing chiral nematic ordered domains.

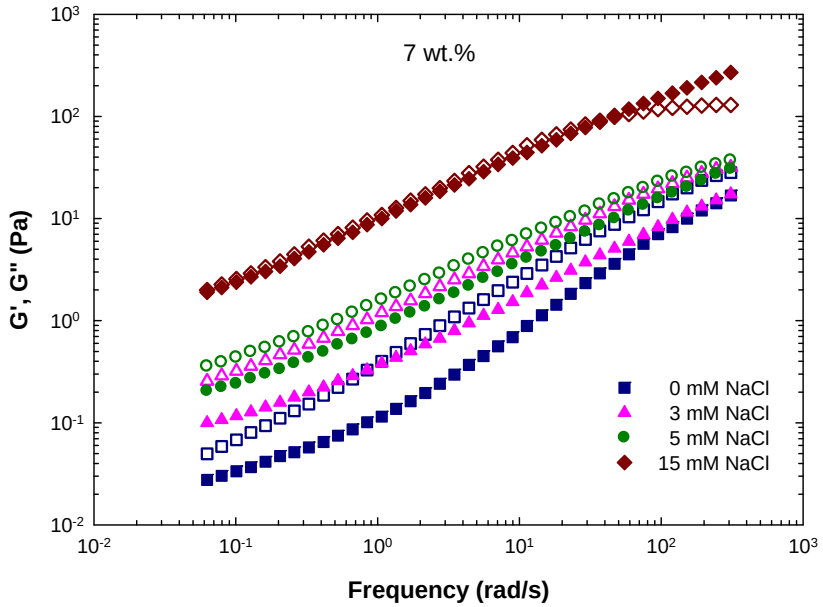

Figure 9-13: Storage modulus, G' (filled symbols), and loss modulus, G" (open symbols), versus angular frequency, ω, for 7 wt.% CNC suspension at different NaCl concentrations.

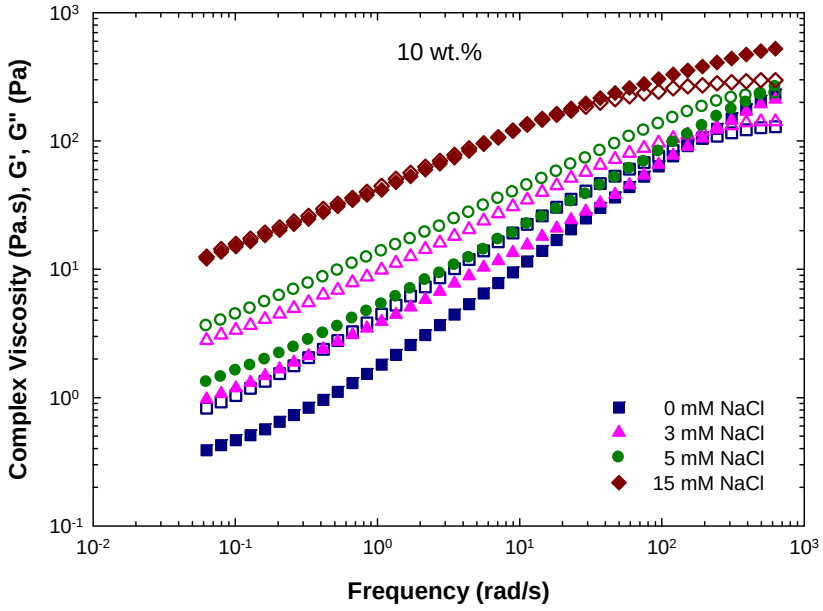

Figure 9-14: Storage modulus, G' (filled symbols), and loss modulus, G" (open symbols), versus angular frequency, ω, for 10 wt.% CNC suspension at different NaCl concentrations.

For 12 wt.% CNC suspensions (Figure 9-15), the sample shows a gel-like behaviour (overlapping G' and G" for an extended frequency range) without NaCl, and by addition of NaCl up to 5 mM the modulus decreases and the behaviour changes to the one typical of viscoelastic liquid (G'<G"). These results are consistent with those observed in steady-state shear viscosity at low shear rates (refer to Figure 9-8). At higher concentration of NaCl, the modulus increases significantly showing a stiff gel behaviour (G' being larger than G" and shows a weak dependency on frequency); as discussed before, the sample is not stable at this high electrolyte concentration and extensive aggregation occurs in the system.

In the case of 15 wt.% (Figure 9-16), the sample, without NaCl, behaves like a viscoelastic solid with G' being higher than G" over the whole investigated frequency range and being almost independent of frequency. By addition of NaCl, the modulus drops up to NaCl concentration of 5 mM, although it remains independent of frequency

(solid-like). Increase in the modulus due to the presence of aggregates at very high NaCl concentration is observed for this sample as well.

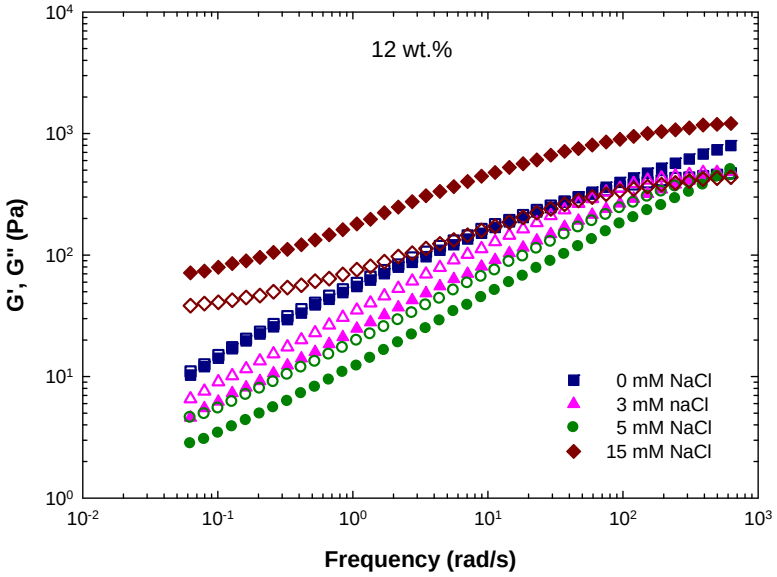

Figure 9-15: Storage modulus, G' (filled symbols), and loss modulus, G" (open symbols), versus angular frequency, ω, for 12 wt.% CNC suspension at different NaCl concentrations.

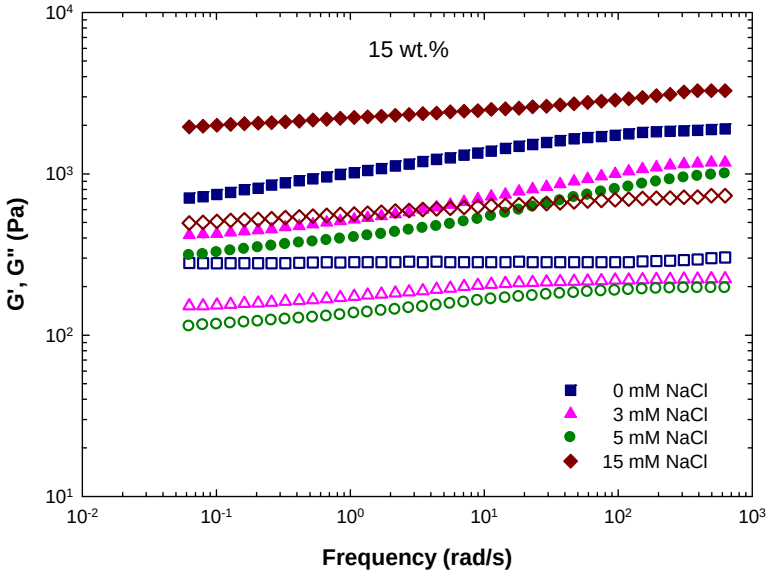

Figure 9-16: Storage modulus, G' (filled symbols), and loss modulus, G" (open symbols), versus angular frequency, ω, for 15 wt.% CNC suspension at different NaCl concentrations.

9.5. Summary

The effects of ionic strength on the microstructure and rheological behaviour of CNC suspensions at three different concentration regimes, namely, isotropic, anisotropic chiral nematic and gels have been studied in this chapter. It has been shown that for isotropic CNC suspensions, increasing the ionic strength of the system up to 5mM NaCl concentration weakens the electro-viscous effects and thus reduces the viscosity of these suspensions. For biphasic samples (above critical concentration for isotropic to chiral nematic transition), increasing ionic strength up to 5 mM NaCl concentration decreases the size of chiral nematic domains resulting in an increase in the viscosity of the samples at low shear rates. On the other hand, at high shear rates, where all the ordered domains are broken, the viscosity decreases by NaCl addition. For gels, the viscosity decreases by addition of NaCl due to debilitation of hydrogen bonding interaction between the particles, and thus, formation of weaker gel structure. However, further addition of NaCl (10 and 15 mM NaCl concentration) de-stabilizes the CNC suspension, resulting in extensive aggregation in the system and thus increases the viscosity of all samples.

CHAPTER 10: CONCLUSIONS AND CONTRIBUTION TO KNOWLEDGE

10.1. Conclusions

The physico-chemical and rheo-optical characterizations performed in this study have led to the following conclusions:

- CNC particles, prepared for this study, contain anionic sulfur ester groups (SO_3^-) on their surface. The ζ-potential of these CNC suspensions is negative, with an absolute value higher than 30 mV and thus, their aqueous suspensions are stable. These nanocrystals are rod-like with length of 100±8 nm and diameter of 7±3 nm, obtained by TEM.

- CNC aqueous suspensions form a chiral nematic liquid crystal phase above a critical concentration (3-4 wt.%), revealing "fingerprint" patterns indicative of the chiral nematic phase under a polarized light microscope. The transition from isotropic to chiral nematic anisotropic phase can be obtained by measuring the suspension rheology and characterizing the shape of their viscosity profile (three-region viscosity profile). Rheo-optical measurements have shown that when the biphasic suspension is subjected to increasing shear rate, the chiral nematic domains deform and align in the shear direction and finally break at high shear rates (> 10 s^{-1}), where the fingerprint patterns disappear.

- CNC suspensions at even higher concentrations form gel. Gel formation was also evaluated by studying the rheological behaviour of the sample (a single shear thinning is observed over the whole investigated shear rate range for gels). Gel formation at high concentrations has also been confirmed by isothermal frequency sweep tests. It was found that the critical concentration for gel formation depends on the surface charge and ionic strength of the system.

- Application of ultrasound energy (sonication) is necessary to fully disperse CNC particles and break the aggregates in high-concentration suspensions. This results into a significant decrease in the viscosity of the samples after sonication. Further

sonication results in the microstructure of chiral nematic ordered domains to change so that larger chiral nematic domains with larger pitch size are formed. This sonication-induced microstructural change has been confirmed by polarized microscopy experiments. These changes in microstructure consequently change the rheological behaviour of CNC suspensions. Application of 1000 Joules of ultrasound energy per gram of CNC in the sample has been found to be an optimum level of sonication for further rheological evaluation, since this level of energy input was shown to be sufficient for breaking the aggregates in the system. Beyond this level of energy, the viscosity profile of samples does not change its shape, especially in intermediate and high-shear rate regions.

- The rheological measurements of CNC suspensions at different temperatures have shown that for biphasic samples, the size of chiral nematic domains decreases with increasing temperature, especially from 30 °C to 40 °C, thereby increasing the fraction of the isotropic phase. This change in the microstructure of the suspension was confirmed with an increase in the viscosity at the corresponding temperature.

- The degree of sulfation of CNC particles affects the critical concentrations at which the microstructural transitions occur. A higher degree of sulfation favours the formation of the chiral nematic liquid crystal phase and hinders the gel formation.

- For isotropic CNC suspensions (low CNC concentrations), increasing the ionic strength of the system by the addition of NaCl (up to 5 mM NaCl concentration) reduces the viscosity, due to weakening of the electro-viscous effects on the viscosity of these suspensions. For biphasic samples (above the critical concentration for isotropic to chiral nematic transition), addition of NaCl (up to 5 mM NaCl concentration) decreases the size of chiral nematic domains, resulting in an increase in viscosity of the samples at low shear rates. On the other hand, at high shear rates, where all the domains are broken, the viscosity decreases by NaCl addition. For gels (high concentration of CNC), the viscosity of the gels

decreases through the addition of NaCl (up to 5 mM NaCl concentration), due to decrease in effective volume fraction of the rods and thus, formation of a weaker gel structure. However, further addition of NaCl (10 and 15 mM NaCl concentration) de-stabilizes the CNC suspension, resulting in extensive aggregation in the system and thus increases the viscosity of all samples.

10.2. Contributions to knowledge

The main aim of this study was to characterize the microstructure and rheological behaviour of CNC aqueous suspensions and to correlate their microstructure with rheology. This study was focused on the effects of different parameters (concentration, temperature, sonication, degree of sulfation, and ionic strength of the system) on the microstructure, and thus, rheology of these suspensions. This new understanding should have significant impact on better control of CNC production, as well as exploration of new industrial applications.

The results mostly presented in Chapter 5 showed that CNC suspensions goes through two different microstructural transitions by increasing the CNC concentration, namely from isotropic to anisotropic chiral nematic structure above a first critical concentration and from anisotropic chiral nematic to gel structure above a second critical concentration.

Chapter 6 showed that the ultrasound treatment significantly reduces the viscosity of the sample up to 1000 J/g of CNC after which the change in viscosity levels off. By further application of ultrasound treatment, higher degree of sonication, the size of chiral nematic domains in the system and the chiral nematic pitch size increases. This sonication-induced microstructural changes, visualized by polarized optical microscopy, have been correlated with the change observed in the shear rheological behaviour of the samples. This systematic study of the effects of sonication was done for the first time in the literature and thus the present data could provide a baseline for future studies in this field. On the other hand, it has been shown in Chapter 9 that addition of NaCl up to 5 mM decreases the size of chiral nematic domains as well as the pitch size. These results suggest the possibility of manipulating the pitch size in chiral nematic domains of CNC

suspensions by sonication and/or NaCl addition. These data could be useful to extend the application of CNC materials related to their optical properties.

The changes in microstructure of CNC aqueous suspensions by temperature was also studied and correlated with rheological behaviour of samples, presented in Chapter 7 of this thesis.

The effects of degree of sulfation on the critical concentrations for the occurrence of microstructural transitions in CNC suspensions and its subsequent effects on rheology of these materials have been studied and presented in Chapter 8. The corresponding data showed that lowering the degree of sulfation results into delay in chiral nematic phase formation and increases the tendency of the CNC suspensions to gel rather than form chiral nematic structure.

CHAPTER 11: RECOMMENDATIONS FOR FUTURE WORK

- The chiral nematic ordered domains in biphasic CNC suspensions have been shown to be very sensitive to the applied flow field. The microstructure changes and rheological behaviour under shear flow have been studied in this work. Studying the microstructural changes under elongational flow would also be also of great importance and will enhance the overall understanding of the rheological behaviour of CNC suspensions.

- This study focused on the CNC suspensions in DI water. Dispersing CNC in other solvents and studying the microstructural transitions and comparing them with the results presented here would be useful. Performing such studies to evaluate the effects of different solvents is recommended.

- The effects of temperature, presented in Chapter 7, have the potential to be investigated in more detail. A comprehensive study of the microstructure of CNC suspensions over an extended range of temperatures is recommended.

- This study covered the effects of degree the of sulfation and ionic strength on gel formation in CNC aqueous suspensions. However, there might be other factors governing gel formation in CNC suspensions, other than chiral nematic liquid crystal formation. More detailed study of the gelation process is recommended.

- Since CNC particles are charged rods, studying the rheology of CNC suspensions under application of an electrical field (electro-rheology) will also be of great interest.

REFERENCES

Adamson, A. W. (1990). Physical chemistry of surfaces. *5th ed., Wiley, New York*, 526.

Araki, J., Wada, M., Kuga, S., and Okano, T. (1998). Flow properties of microcrystalline cellulose suspension prepared by acid treatment of native cellulose. *Colloids and Surfaces*, A: Physicochemical and Engineering Aspects, 142 (1), 75-82.

Araki, J., Wada, M., Kuga, S., and Okano T. (1999). Influence of surface charge on viscosity behavior of cellulose microcrystal suspension. *J Wood Sci*, 45, 258-261.

Araki, J., Wada, M., Kuga, S., and Okano T. (2000). Birefringent glassy phase of a cellulose microcrystal suspension. *Langmuir*, 16 (6), 2413-2415.

Araki, J., and Kuga, S. (2001). Effect of trace electrolyte on liquid crystal type of

cellulose microcrystals. *Langmuir*, 17, 4493–4496.

Azizi Samir, M., Alloin F., Sanchez J., El Kissi N., and Dufresne A. (2004). Preparation of cellulose whiskers reinforced nanocomposites from an organic medium suspension. *Macromolecules*, 37(4), 1386-1393.

Beck, S., Bouchard, J., and Berry, R. (2010). Controlling the reflection wavelength of iridescent solid films of nanocrystalline cellulose. *Biomacromolecules*, 12, 167-172.

Beck-Candanedo, S., Roman, M., and Gray, D. G. (2005). Effect of reaction conditions on the properties and behavior of wood cellulose nanocrystal suspensions. *Biomacromolecules*, 6, 1048−1054.

Bercea, M., and Navard P. (2000). Shear dynamics of aqueous suspensions of cellulose whiskers. *Macromolecules*, 33, 6011-6016.

Boluk, Y., Lahiji, R., Zhaod, L., and McDermott, M. T. (2011). Suspension viscosities and shape parameter of cellulose nanocrystals (CNC). *Colloids and Surfaces* A. Physicochem Eng. Aspects, 377, 297-303.

Conway, B. E., and Dobry-Duclaux, A. (1960). Viscosity of suspensions of electrically charged particles and solutions of polymeric electrolytes. in: F.R. Eirich (Ed.), *Rheology*, *Academic Press*, New York, 1960.

Davis, V. A., Ericson, L. M., Parra-Vasquez, A., Fan, H., Wang, Y., Prieto, V., Longoria, J. A., Ramesh, S., Saini, R. K., Kittrell, C., Billups, W. E., Adams, W. W., Hauge, R. H., Smalley, R. E., and Pasquali, M. (2004). Phase behavior and rheology of SWNTs in superacids. *Macromolecules*, 37, 154-160.

De Souza Lima, M. M. D., and Borsali, R. (2004). Rodlike cellulose microcrystals: structure, properties, and applications. *Macromol. Rapid Commun*. , 25 (7), 771-787.

DeVries, H. I. (1951). Rotatory power and other optical properties of certain liquid crystals. *Acta Crystallogr*., 4, 219-226.

Dong, X. M., Kimura, T., Revol, J. F., and Gray, D. G. (1996). Effects of ionic strength on the isotropic-chiral nematic phase transition of suspensions of cellulose crystallites. *Langmuir*, 12 (8), 2076–2082.

Dong, X. M., Revol, J. F., and Gray, D. G. (1998). Effect of microcrystallite preparation conditions on the formation of colloid crystals of cellulose. *Cellulose*, 5, 19-32.

Dong, X. M., and Gray, D. G. (1997). Effect of counterions on ordered phase formation in suspensions of charged rodlike cellulose crystallites. *Langmuir*, 13, 2404-2409.

Dubief, D., Samain, E., and Dufresne, A. (1999). Polysaccharide microcrystals reinforced amorphous poly (β-hydroxyoctanoate) nanocomposite materials. *Macromolecules*, 32, 5765-5771.

Favier, V., Chanzy, H., and Cavaille, J. Y. (1995). Polymer nanocomposites reinforced by cellulose whiskers. *Macromolecules*, 28, 6365-6367.

Fleming, K., Gray, D. G., Prasannan, S., and Matthews, S. (2000). Cellulose crystallites: A new and robust liquid crystalline medium for the measurement of residual dipolar couplings. *J. Am. Chem. Soc*., 122(21), 5224-5225.

Fleming, K., Gray, D. G., and Matthews, S. (2001). Cellulose crystallites. *Chemistry –A European Journal*, 7(9), 1831-1835.

Grunert, M., and Winter, W. T. (2002). Nanocomposites of cellulose acetate butyrate reinforced with cellulose nanocrystals. *Journal of Polymers and the Environment*, 10(1/2), 27-30.

Hamad, W. (2006). On the development and applications of cellulosic nanofibrillar and nanocrystalline materials. *The Canadian Journal of Chemical Engineering*, 84, 513- 519.

Hamad, W. Y., and Hu, T. Q. (2010). Structure-process-yield interrelation in nanocrystalline cellulose xxtraction. *The Canadian Journal of Chemical Engineering*, 88 (3), 392−402.

Heux, L., Chauve, G., and Bonini, C. (2000). Nonflocculating and chiral-nematic self ordering of cellulose microcrystals suspensions in nonpolar solvents. *Langmuir*, 16(21), 8210-8212.

Hirai, A, Inui, D., Horii, F., and Tsuji, M. (2009). Phase separation behavior in aqueous suspensions of bacterial cellulose nanocrystals prepared by sulfuric acid treatment. *Langmuir*, 25, 497-502.

Hult, E., Larsson, P. T., and Iversen, T. (2001). Cellulose fibril aggregation- an inherent property of kraft pulps. *Polymer*, 42(8), 3309-3314.

Jakob, H. F., Fengel, D., Tschegg, S. E., and Fratzl, P. (1995). The elementary cellulose fibril in picea abies: Comparison of transmission electron microscopy, small-angle Xray scattering, and wide-angle X-ray scattering results. *Macromolecules*, 28(26), 8782-8787.

Kang, K., Lettinga, M. P., Dogic, Z. and Dhont, J. K. G. (2006). Vorticity banding in rodlike virus suspensions. *Phys Rev E* 74, 026307-1-12.

Kontturi, E., Tammelin, T., and Österberg, M. (2006). Cellulose-model films and the fundamental approach. *Chem. Soc. Rev.*, 35 (12), 1287-1304.

Larson, R. G. (1999). The structure and rheology of complex fluids; *Oxford University Press*: New York.

Lettinga, M. P., Dogic, Z., Wang, H. and Vermant, J (2005). Flow behavior of colloidal rodlike viruses in the nematic phase. *Langmuir*, 21, 8048-8057.

Liu, D., Zhong, T., Chang, P., Li, K., and Wu, Q. (2010). Starch composites reinforced by bamboo cellulosic crystals. *Bioresource Technology*, 101(7), 2529-2536.

Liu, H., Liu, D., Yao, F., and Wu, Q. (2010). Fabrication and properties of transparent polymethylmethacrylate/ cellulose nanocrystals composites. *Bioresource Technology*,

101(14), 5685-5692.

Liu, D., Chen, X., Yue, Y., Chen, M., and Wu, Q. (2011). Structure and rheology of nanocrystalline cellulose. *Carbohydr. Polym.*, 84, 316-322.

Ljungberg, N., Bonini, C., Bortolussi, F., Boisson, C., Heux, L., and Cavaille, J. Y. (2005). New nanocomposite materials reinforced with cellulose whiskers in atactic polypropylene: effect of surface and dispersion characteristics. *Biomacromolecules*, 6, 2732-2739.

Marchessault, R. H., Morehead, F. F., and Walter, N.M. (1959). Liquid crystal systems from fibrillar polysaccharides. *Nature*, 184, 632-633.

Marchessault, R. H., Morehead, F. F., and Koch, M. J. (1961). Some hydrodynamic properties of neutral suspensions of cellulose crystallites as related to size and shape. *J. Colloid Sci.* 16, 327-344.

Mewis, J. (1979). Thixotropy – a general review. *J. Non-Newtonian Fluid Mech*. 6, 1-20.

Mewis, J., and Spaull, A. J. B. (1976). Rheology of concentrated dispersions. *Adv. Colloid Interface Sci.* 6, 173-200.

Nishio, Y., Kai, T., Kimura, N., Oshima, K., and Suzuki, H. (1998). Controlling the selective light reflection of a cholesteric liquid crystal of (hydroxypropyl) cellulose by electrical stimulation. *Macromolecules*, 31, 2384-2386.

Noel, C., and Navard, P. (1991). Liquid crystal polymers. *Progress in Polymer Science*. 16 (1), 55-110.

Odjik, T. (1986). Theory of lyotropic polymer liquid crystals. *Macromolecules*, 19 (9), 2313-2329.

Onogi, S., and Asada, T. (1980). Rheology and rheo-optics of polymer liquid crystals *Rheology: Principles, Plenum Publishing Corporation*; in: "Rheology", Astarita, G., Marrucci, G., and Nicolais, L. *Eds., Plenum*, New York (1980), Vol. 3.

Onsager, L. (1949). The effects of shape on the interaction of colloidal particles. *Ann. N.Y. Acad. Sci.*, 51, 627-659.

O'Sullivan, A. C. (1997). Cellulose: the structure slowly unravels. *Cellulose*, 4 (3), 173-207.

Orts, W. J., Godbout, L., Marchessault, R. H., and Revol, J. F. (1998). Enhanced ordering of liquid crystalline suspensions of cellulose microfibrils: A small angle neutron scattering study. *Macromolecules*, 31 (17), 5717–5725

Orts, W. J., Shey, J., Imam, S. H., Glenn, G. M., Guttman, M. E., and Revol, J. F. (2005). Application of cellulose microfibrils in polymer nanocomposites. *Journal of Polymers and the Environment*, 13, 301-306.

Pääkkö, M., Ankerfors, M., Kosonen, H., Nykänen, A., Ahola, S., Österberg, M., Ruokolainen, J., Laine, J., Larsson, P.T., Ikkala, O., and Lindström, T. (2007) Enzymatic hydrolysis combined with mechanical shearing and high-pressure homogenization for nanoscale cellulose fibrils and strong gels. *Biomacromolecules*, 8, 1934-1941.

Pan, J., Hamad, W., and Straus, S. K. (2010). Parameters affecting the chiral nematic phase of nanocrystalline cellulose films. *Macromolecules*, 43 (8), 3851-3858.

Papkov, S. P., Kulichikhin, V. G., Kalmykova, V. D., and Malkin, A. Y. (1974). Rheological properties of anisotropic poly (para-benzamide) solutions. *J. Polym. Sci., Polym. Phys. Ed.*, 12, 1753-1770.

Ranby, B. G. (1951). The colloidal properties of cellulose micelles. *Discuss. Faraday Soc.*, No. 11, 158-164, discussion 208-213.

Revol, J. F., Bradford, H., Giasson, J., Marchessault, R. H. and Gray, D. G. (1992). Helicoidal self-ordering of cellulose microfibrils in aqueous suspension. *Int. J. Biol. Macromol.*, 14, 170-172.

Revol, J. F., Godbout, L., Dong, X. M., Gray, D. G., Chanzy, H., and Maret G. (1994). Chiral nematic suspensions of cellulose crystallites; phase separation and magnetic field orientation. *Liquid Crystals*, 16 (1), 127-134.

Revol, J. F., and Marchessault, R. H. (1994). In vitro chiral nematic ordering of chitin crystallites. *Int. J. Biol. Macromol*., 15, 329-335.

Revol, J. F., Godbout, L., and Gray, D. G. (1997). Solidified liquid crystals of cellulose with optically variable properties. U.S. Patent No. 5,629,055.

Revol, J. F., Godbout, L., and Gray, D. G. (1998). Solid self-assembled films of cellulose with chiral nematic order and optically variable properties. *J. Pulp Pap. Sci*., 24 (5), 146-149.

Ripoll, M., Holmqvist, P., Winkler, R. G., Gompper, G., Dhont, K. K. G. and Lettinga M. P. (2008) Attractive colloidal rods in shear flow. *Phys Rev Lett* 101, 168302-1-4.

Russel, W. B. (1978). Rheology of suspensions of charged rigid spheres. *Journal of Fluid Mechanics*, 85, 209-232.

Saito, T., Kimura, S., Nishiyama, Y., and Isogai A. (2007). Cellulose nanofibers prepared by TEMPO-mediated oxidation of native cellulose. *Biomacromolecules*, 8 (8), 2485-2491.

Schrag, J. L. (1997). Deviation of velocity gradient profiles from the "gap loading" and "surface loading" limits in dynamic simple shear experiments. *Transactions of the Society of Rheology*. page 399-413.

Shafiei-Sabet, S., Hamad, W. Y. and Hatzikiriakos, S. G. (2012). Rheology of nanocrystalline cellulose aqueous suspensions. *Langmuir*, 28, 17124-17133.

Shafiei-Sabet, S., Hamad, W. Y. and Hatzikiriakos, S. G. (2013). Influence of degree of sulfation on the rheology of cellulose nanocrystal suspensions. *Rheol Acta*, 52, 741– 751.

Simha, R. (1940). The influence of Brownian movement on the viscosity of solutions

J. Phys. Chem., 44, 25-34.

Sjöström, E. (1993). Wood chemistry: fundamentals and applications. *Academic Press Inc.*, San Diego, USA.

Smoluchowski, M. (1903). *Bull. Int. Acad. Sci.* Cracovie 184.

Straley, J. P. (1976). Theory of piezoelectricity in nematic liquid crystals, and of the cholesteric ordering. *Phys. Rev. A*, 14, 1835-1841.

Turbak, A. F., Snyder, F.,W. and Sandberg, K. R. (1983). Microfibrillated cellulose, a new cellulose product: Properties, uses, and commercial potential. *J. Appl. Polym. Sci.* : Appl. Polym. Symp., 37, 813.

Urena-Benavides, E. E., Ao, G., Davis, V. A., and Kitchens, C. L. (2011). Rheology and phase behavior of lyotropic cellulose nanocrystal suspensions. *Macromolecules*, 44, 8990−8998.

Wagberg, L., Winter, L., Odberg, L., and Lindstom, T. (1987). On the charge stoichiometry upon adsorption of a cationic polyelectrolyte on cellulosic materials. *Colloids Surface*, 27, 163-173.

Wierenga, A. M., and Philipse, A. P. (1997). Low-shear viscosities of (semi-)dilute, aqueous dispersions of charged boehmite rods: dynamic scaling of double layer effects. *Langmuir*, 13, 4574-4582.

Witter, R., Sternberg, U., Hesse, S., Kondo, T., Koch, F. T., and Ulrich, A. S. (2006). C-13 chemical shift constrained crystal structure refinement of cellulose I-alpha and its verification by NMR anisotropy experiments. *Macromolecules*, 39 (18), 6125-6132.

APPENDIX:

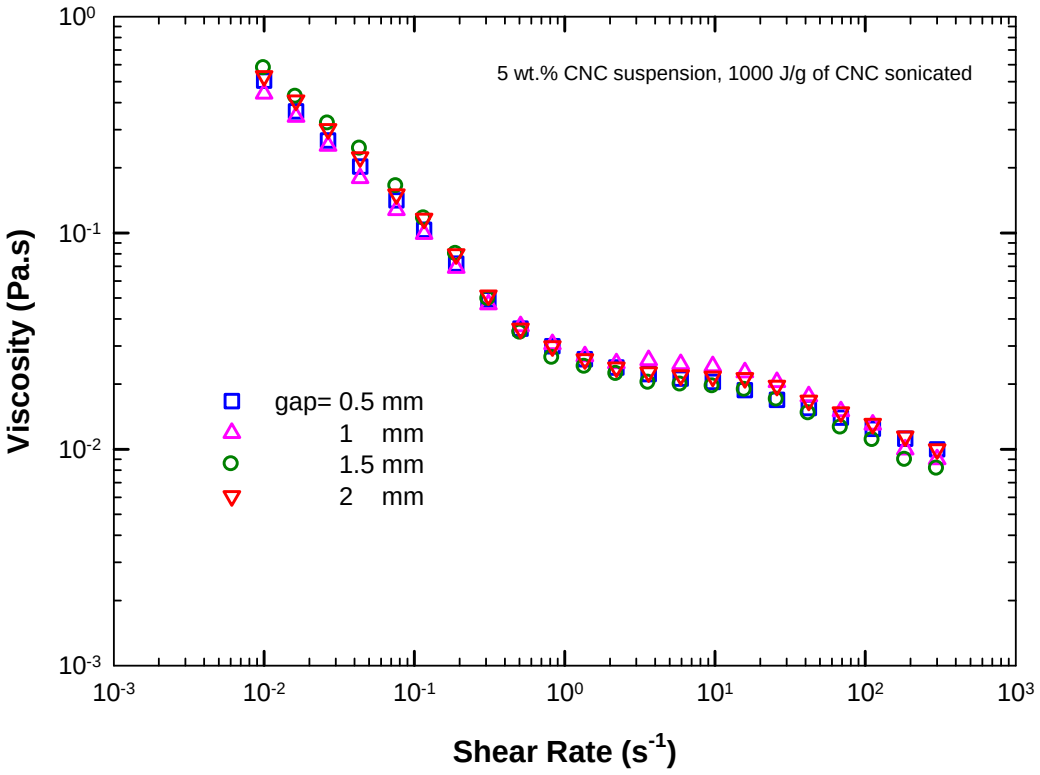

Figure A1: Steady state viscosity versus shear rate for a 5 wt.% CNC suspension, sonicated at 1000 J/g CNC measured by parallel plate geometry at different gap sizes.

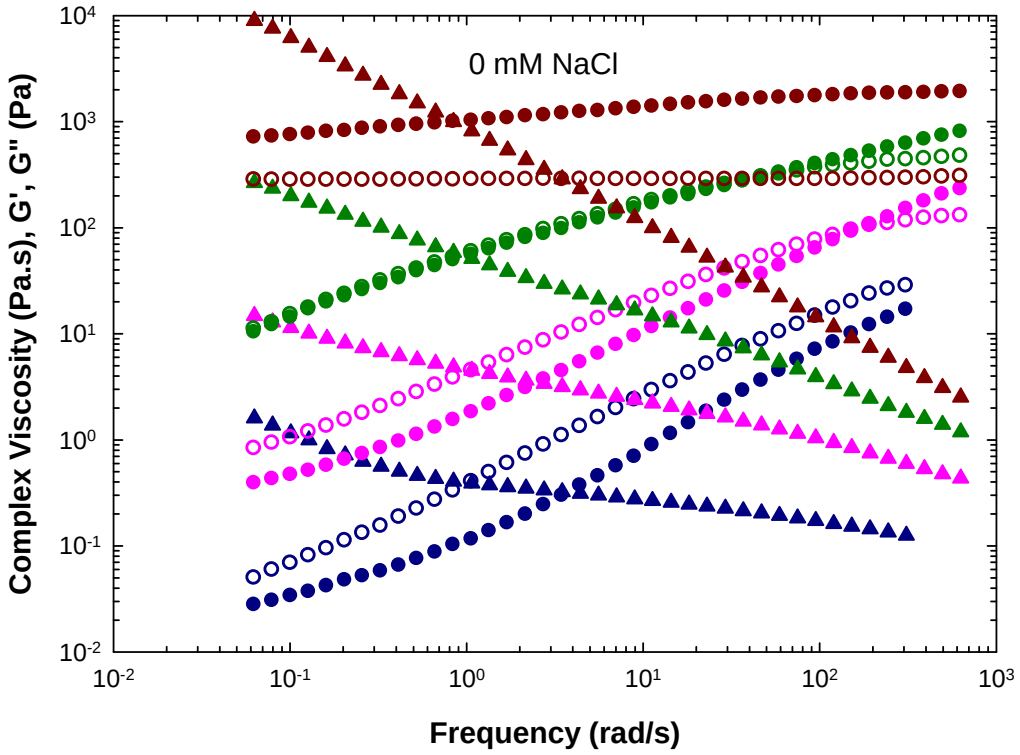

Figure A2: Complex viscosity (triangle), storage modulus, G' (filled circle), and loss modulus, G" (open circle), versus angular frequency, ω, for 7 wt.% (dark blue), 10 wt.% (pink). 12 wt.% (dark green), and 15 wt.% (dark red) CNC suspensions without NaCl.

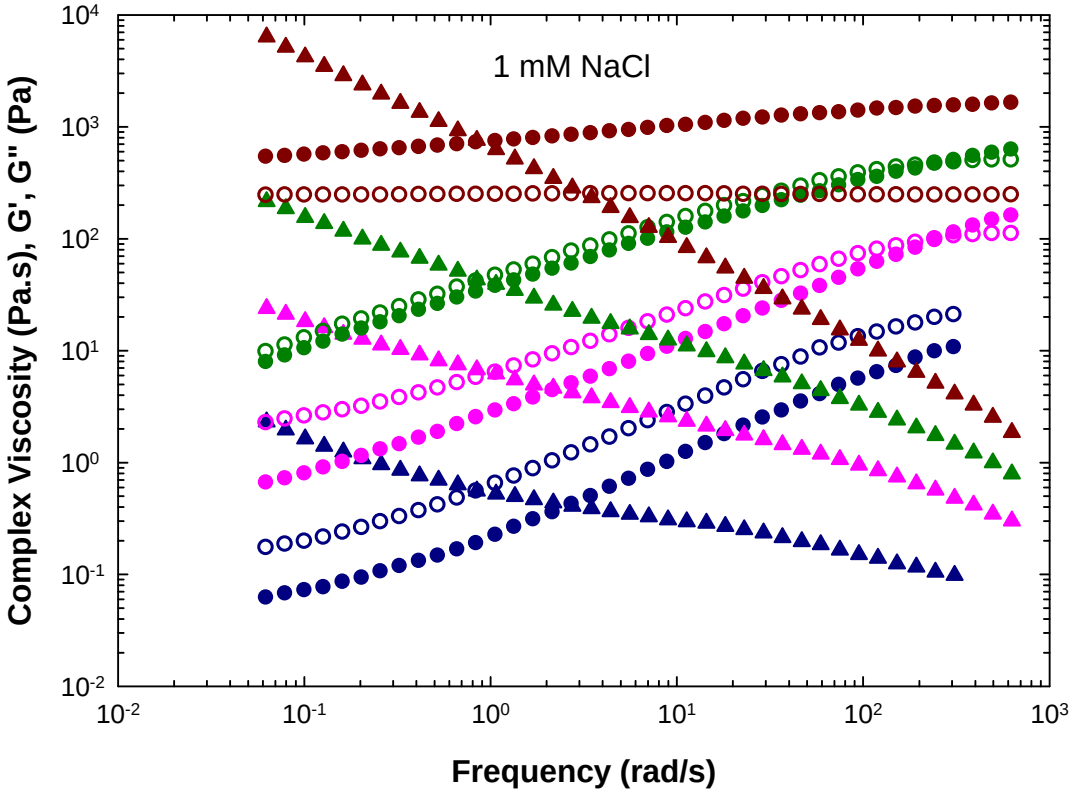

Figure A3: Complex viscosity (triangle), storage modulus, G' (filled circle), and loss modulus, G" (open circle), versus angular frequency, ω, for 7 wt.% (dark blue), 10 wt.% (pink). 12 wt.% (dark green), and 15 wt.% (dark red) CNC suspensions with 1 mM NaCl.

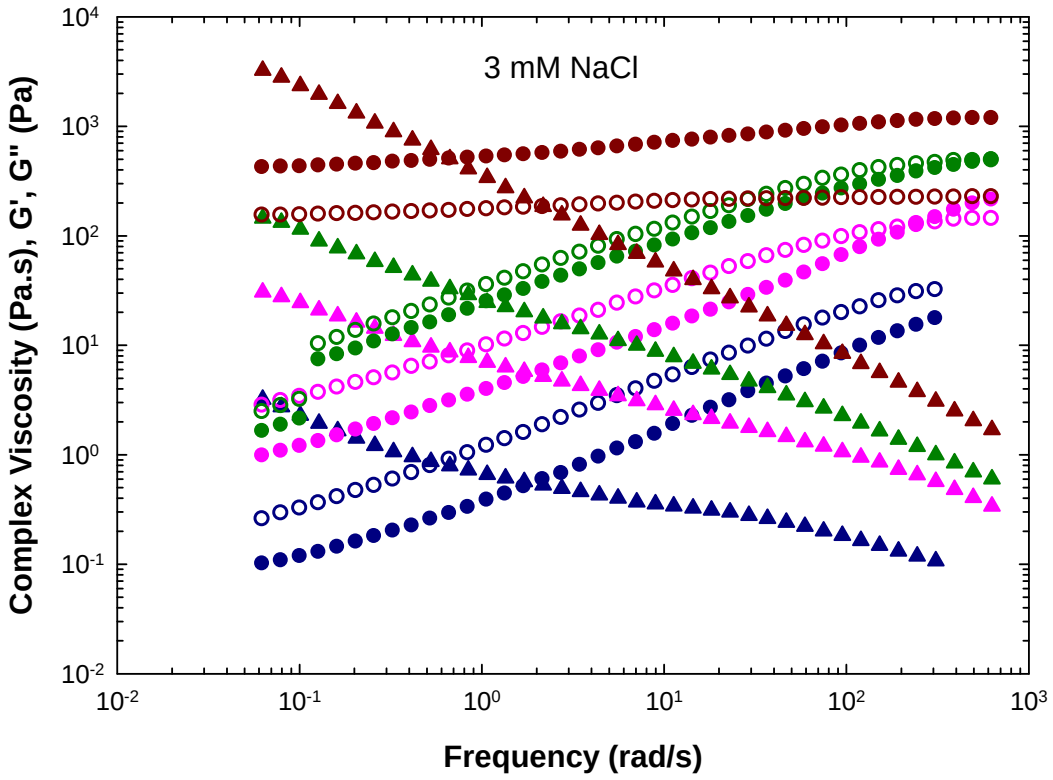

Figure A4: Complex viscosity (triangle), storage modulus, G' (filled circle), and loss modulus, G" (open circle), versus angular frequency, ω, for 7 wt.% (dark blue), 10 wt.% (pink). 12 wt.% (dark green), and 15 wt.% (dark red) CNC suspensions with 3 mM NaCl.

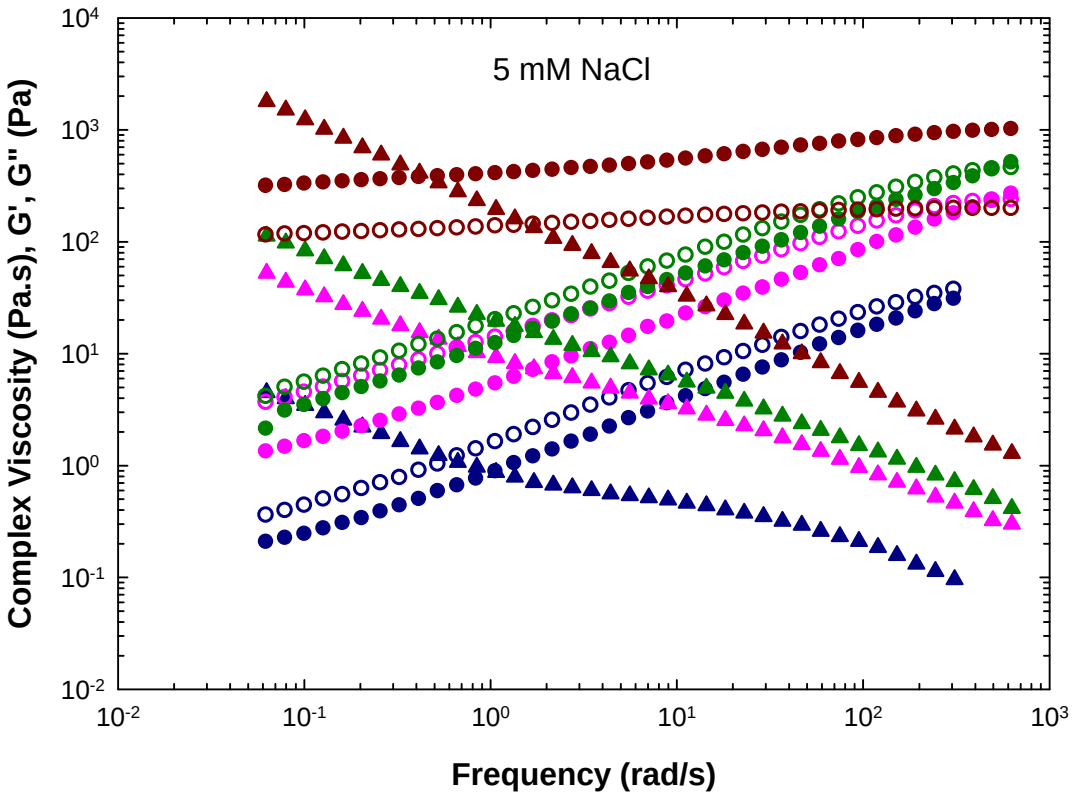

Figure A5: Complex viscosity (triangle), storage modulus, G' (filled circle), and loss modulus, G" (open circle), versus angular frequency, ω, for 7 wt.% (dark blue), 10 wt.% (pink). 12 wt.% (dark green), and 15 wt.% (dark red) CNC suspensions with 5 mM NaCl.

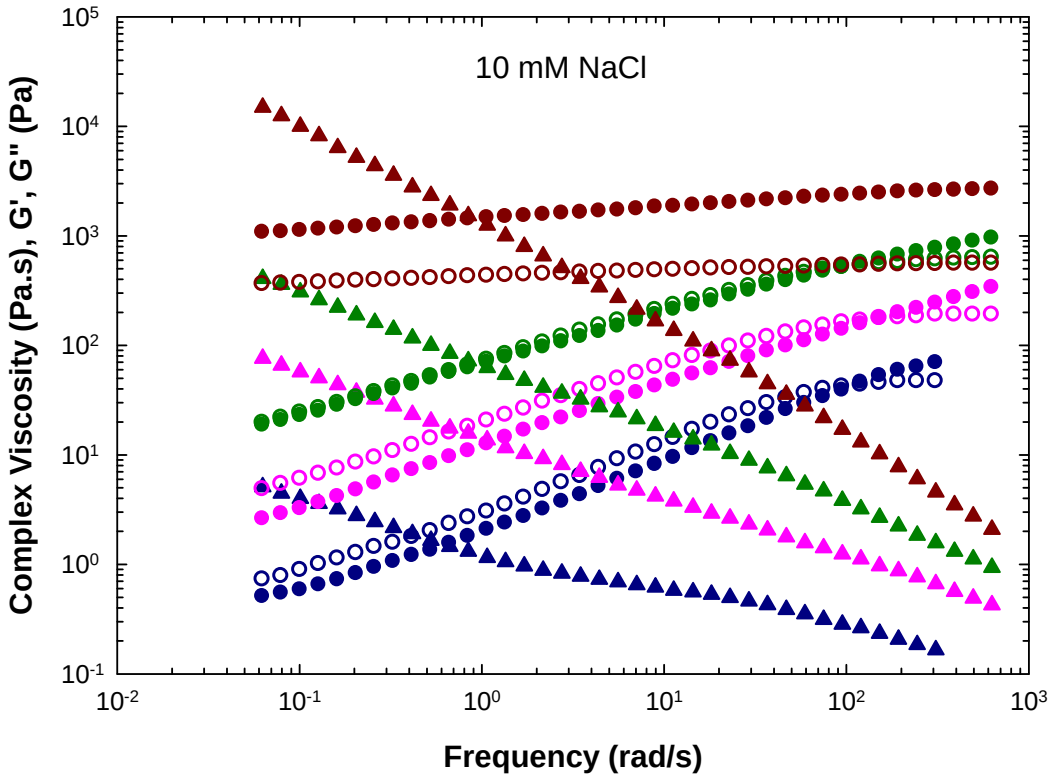

Figure A6: Complex viscosity (triangle), storage modulus, G' (filled circle), and loss modulus, G" (open circle), versus angular frequency, ω, for 7 wt.% (dark blue), 10 wt.% (pink). 12 wt.% (dark green), and 15 wt.% (dark red) CNC suspensions with 10 mM NaCl.

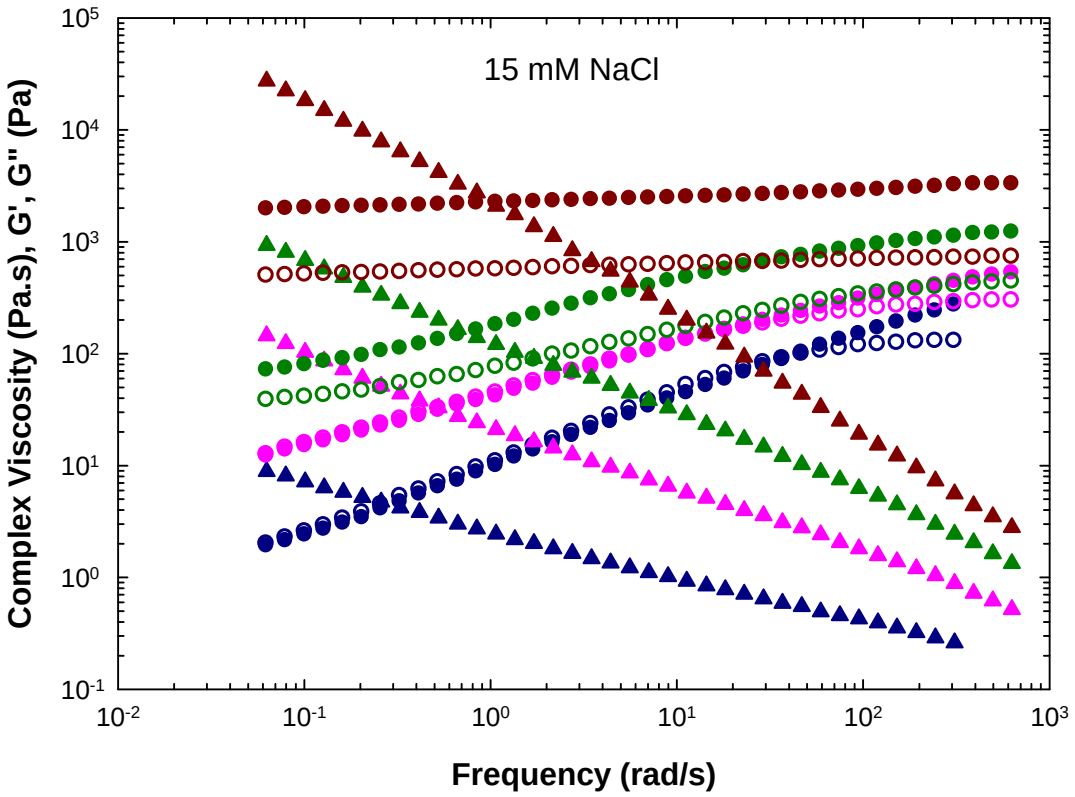

Figure A7: Complex viscosity (triangle), storage modulus, G' (filled circle), and loss modulus, G" (open circle), versus angular frequency, ω, for 7 wt.% (dark blue), 10 wt.% (pink). 12 wt.% (dark green), and 15 wt.% (dark red) CNC suspensions with 15 mM NaCl.

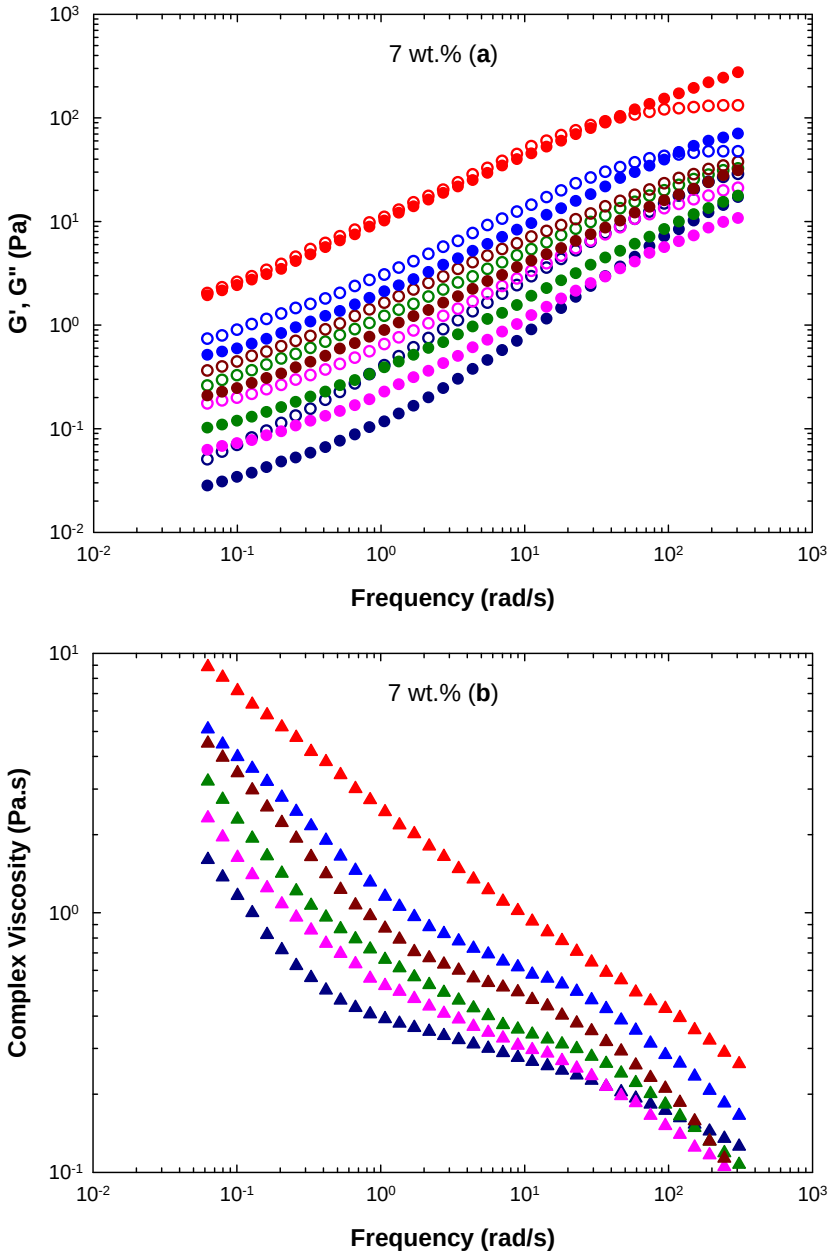

Figure A8: (a) Storage modulus, G' (filled circle), and loss modulus, G" (open circle) and (b) complex viscosity (triangle), versus angular frequency, ω, for 7 wt.% CNC suspension at 0 mM (dark blue), 1 mM (pink), 3 mM (dark green), 5 mM (dark red), 10 mM (blue), and 15 mM (red) NaCl concentrations.

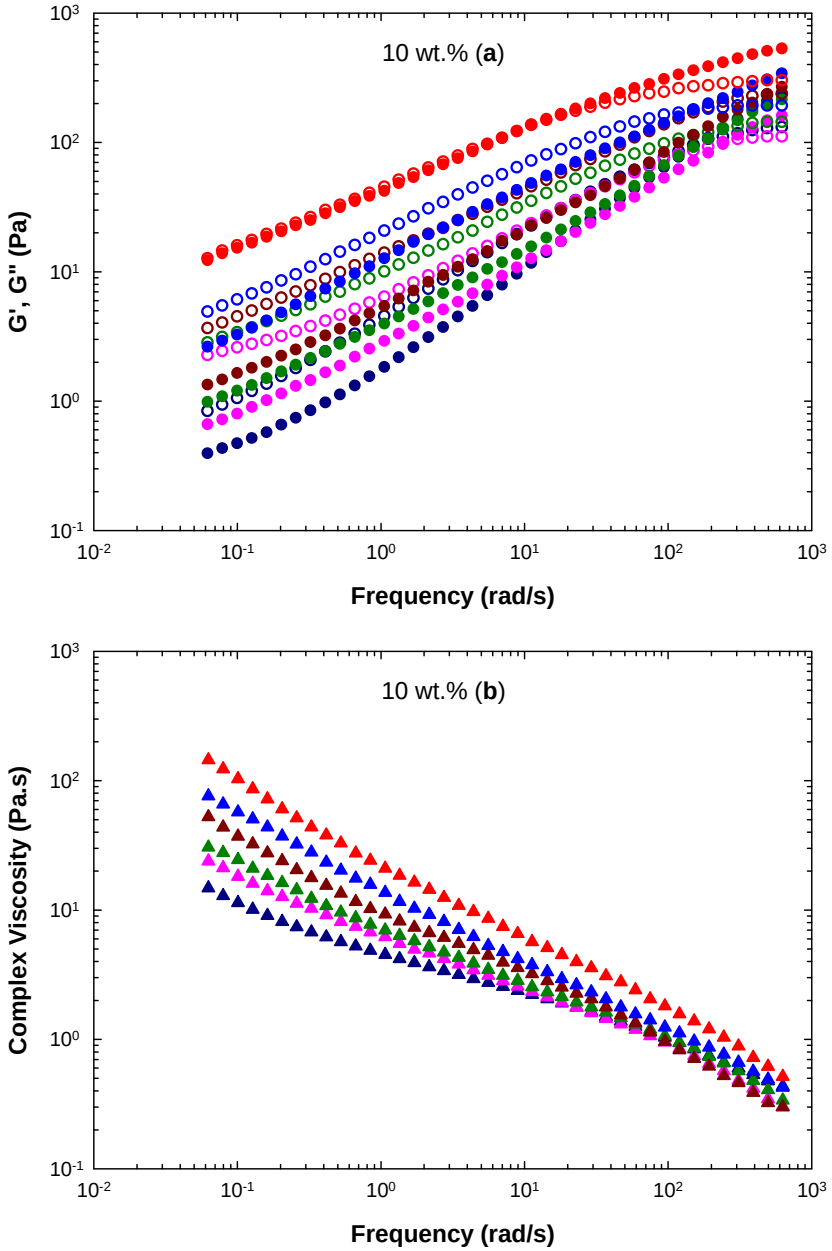

Figure A9: (a) Storage modulus, G' (filled circle), and loss modulus, G" (open circle) and (b) complex viscosity (triangle), versus angular frequency, ω, for 10 wt.% CNC suspension at 0 mM (dark blue), 1 mM (pink), 3 mM (dark green), 5 mM (dark red), 10 mM (blue), and 15 mM (red) NaCl concentrations.

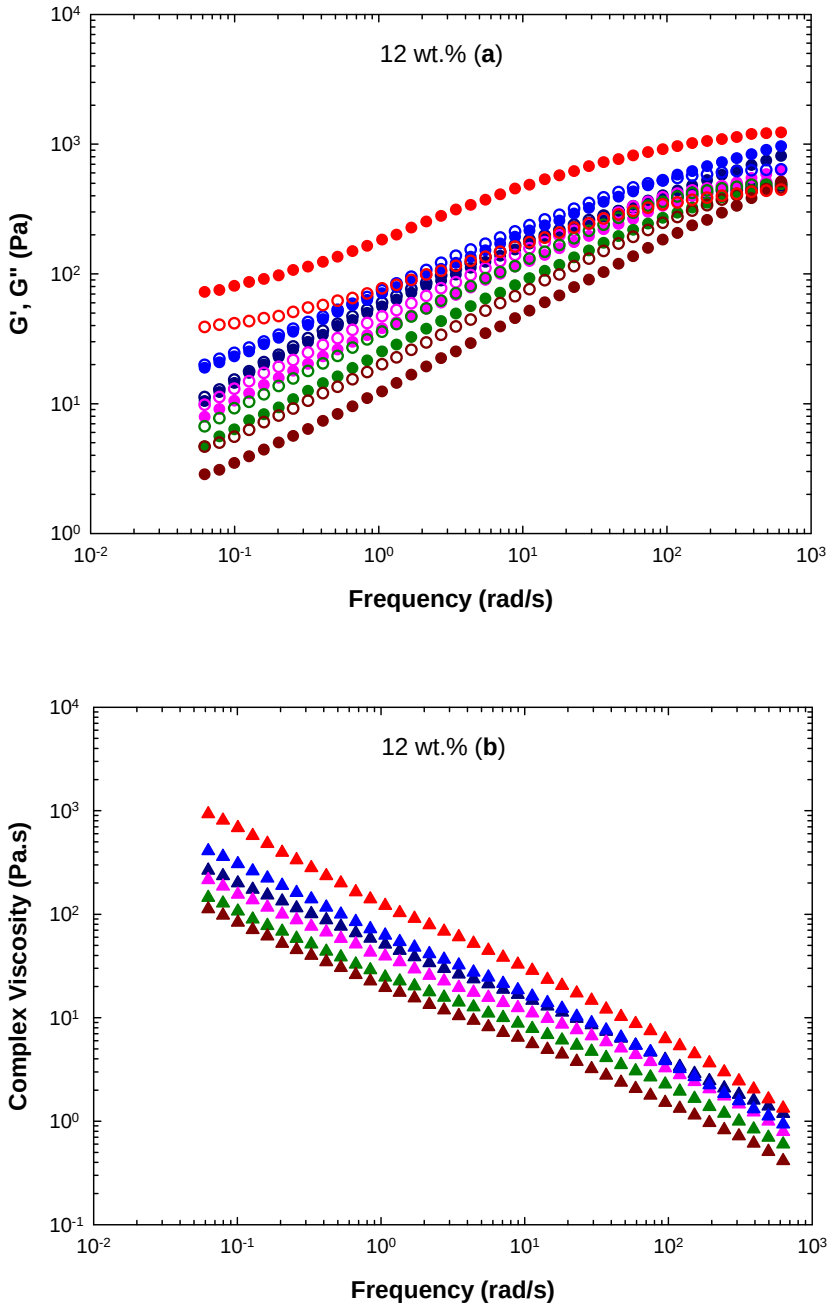

Figure A10: (a) Storage modulus, G' (filled circle), and loss modulus, G" (open circle) and (b) complex viscosity (triangle), versus angular frequency, ω, for 12 wt.% CNC suspension at 0 mM (dark blue), 1 mM (pink), 3 mM (dark green), 5 mM (dark red), 10 mM (blue), and 15 mM (red) NaCl concentrations.

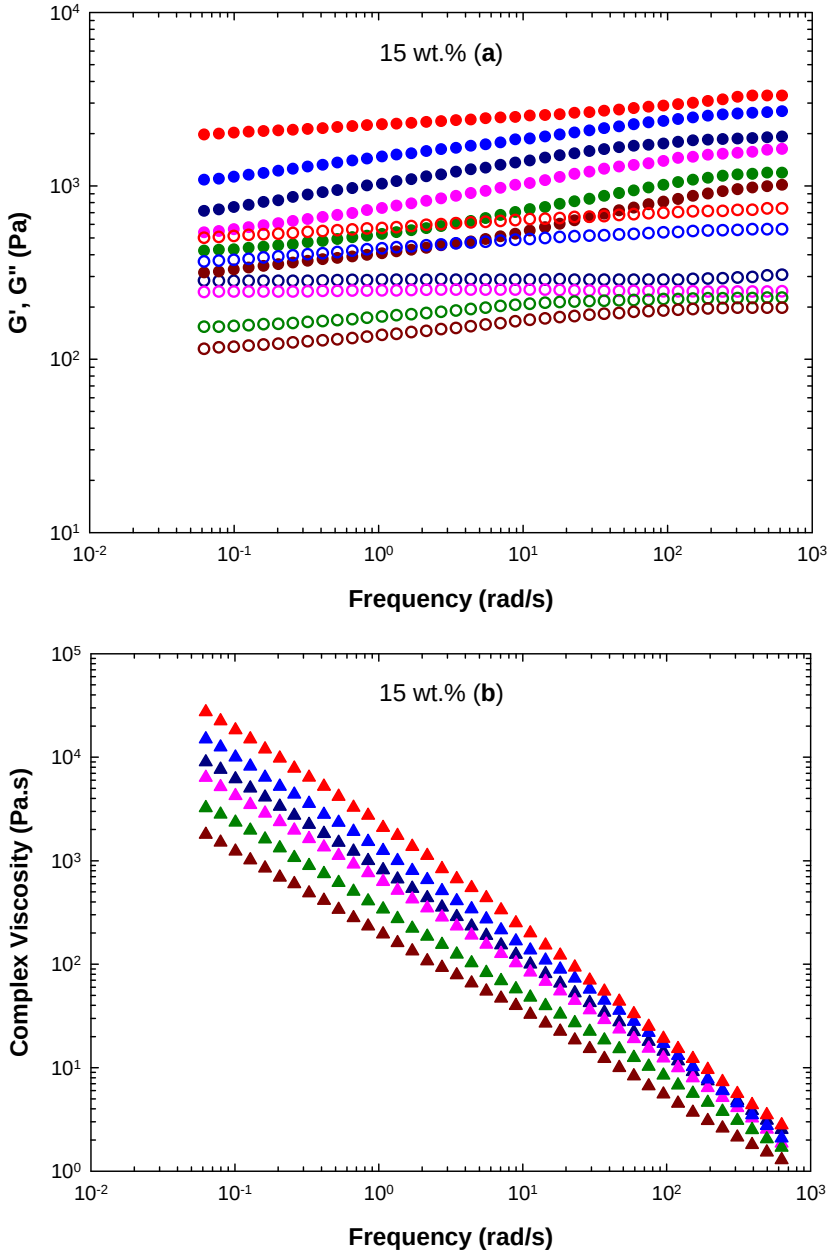

Figure A11: (a) Storage modulus, G' (filled circle), and loss modulus, G" (open circle) and (b) complex viscosity (triangle), versus angular frequency, ω, for 15 wt.% CNC suspension at 0 mM (dark blue), 1 mM (pink), 3 mM (dark green), 5 mM (dark red), 10 mM (blue), and 15 mM (red) NaCl concentrations.